Electrostatic forces for satellite swarm navigation and reconfiguration

Final Report

Authors: Lorenzo Pettazzi, Hans Krüger, Dr. Stephan Theil
Affiliation: ZARM, University of Bremen

ESA Research Fellow/Technical Officer: Dr. Dario Izzo

Contacts:

Lorenzo Pettazzi
Tel: +49(0)4212184786
Fax: +49(0)4212184356
e-mail: pettazzi@zarm.uni-bremen.de

Dario Izzo
Tel: +31(0)715653511
Fax: +31(0)715658018
e-mail: act@esa.int

Available on the ACT website
http://www.esa.int/act

Ariadna ID: 05/4107
Study Duration: 4 months
Contract Number: 9698/06/NL/HE

Contents

Abbreviations

ACT - Advanced Concepts Team

DE - Differential Evolution

EA - Electrostatic Actuation

ES- Equilibrium Shaping

ESA- European Space Agency

FEEP- Field Emission Electrostatic Propulsion

FF- Formation Flying

GEO- Geostationary Orbit

RIT- Radiofrequency Ion Thruster

SC - Spacecraft

SS - Satellitron Satellites

Executive Summary

In this work the concept of Satellitron Satellites, i.e. a swarm of satellites controlled by a hybrid thrusting electrostatic actuation system is assessed. The work described in this document is twofold.
On one side the propulsion system is investigated. To this end first a model of the interaction between plasma and a charged spacecraft is derived. On the basis of this result the requirements for the hybrid propulsion system are defined. A survey of the existing ion thrusting and spacecraft charge control technologies together with the derived specifications allowed to introduce an option for the hybrid propulsion system. The candidate propulsion system consists of the combined use of the Radiofrequency Ion Thruster engine (RIT) and an electron gun. A charge control tailored on this system has been derived and the performance analysis shows that the mass flow efficiency of the hybrid system is in advance to conventional ion thrusting for most of the intended force range.
In the second phase of the study the applicability of the electrostatic actuation for formation keeping and reconfiguration of swarms of satellites is considered. The highly coupled nature of the satellitron satellites dynamics leads to the choice of a decentralized navigation scheme to be considered to avoid a too high complexity. The recently developed equilibrium shaping navigation technique has been selected to control the maneuvers of the SS swarm following this idea.
First the formations that can be acquired autonomously relying upon the equilibrium shaping path-planning technique and then maintained at first order only relying upon the electrostatic actuation have been found. These formations enjoy both a high level of autonomy, ensured by the equilibrium shaping, and high fuel efficiency, provided by the electrostatic actuation. Exploiting the results on the compatibility the electrostatic interaction between the SC has been considered to increase the efficiency of acquisition or reconfiguration maneuvers. In particular it has been demonstrated that the electrostatic force can be used to reduce the fuel expenditure of the whole swarm associated to a given maneuver or to balance the fuel consumption between the SC in the formation. Different charging stategies have been developed. The most promising is the behavior based charge control that provides a solution for the minimum fuel consumption problem in the general case of an $N-$craft formation. This method allows an efficient exploitation of the electrostatic actuation and requires a minimum amount of inter SC communication. The developed charging strategy has been tested under different possible simulations and it has shown good performances in terms of reduction of Δv of the whole swarm.

1 Introduction

1.1 Scientific Motivation

The concept of formation control of groups of vehicles has been studied extensively in the literature for different applications. Many researchers in the past have faced the question whether it is possible or not to design systems in which clusters of vehicles autonomously behave in a coordinated manner performing high level tasks. There are several advantages of using formation of multiple vehicles such as increased feasibility, accuracy, robustness and thus probability of success of the mission. In the last years these advantages have also encouraged several aerospace researchers that are more and more considering a swarm of satellites as an attractive alternative to traditional large spacecraft [1, 2]. Some of the advanced exploration missions being proposed in the last years (such as ESA APIES [3] or NASA ANTS [4] mission) rely upon the use of a swarm of satellites. Various problems associated with coordination and control of multiple spacecraft in formation have also been considered for applications such as on orbit assembly of large structures and separated spacecraft interferometry. The design of a navigation scheme suitable for swarms of satellites can be faced in different ways. Many approaches have been tried to exploit optimal planning and control methodologies to drive the motion of satellite clusters. The approach introduced from Campbell in [5] can be considered as a typical example of that. It uses an optimal time-fuel solution for an individual satellite within the cluster as a basis, and builds a methodology to include collision avoidance, realistic dynamics and cluster optimality within the path planning technique. The resulting navigation scheme allows for efficient acquisition and reconfiguration maneuvers but requires a high level of pre-coordination in the system or a large number of inter spacecraft communications. Other approaches have considered the possibility of designing a highly decentralized path planning technique for swarms of vehicles [6]. In recent papers [7],[8], [9] one of the authors et al. introduce a distributed navigation technique to drive a swarm of satellites to acquire a certain target configuration in space. Such a method, called Equilibrium Shaping (ES), exploits a path planning algorithm that does not require any inter spacecraft communication and gives to each spacecraft belonging to the swarm the ability of autonomously decide which position it will take in the target formation. The methodology used to design the swarm navigation scheme is structured in two different phases. In the first one a behavior based approach is used to associate a desired velocity as a weighted sum of different behavioral contribu-

tions to each spacecraft in the swarm. In the second one a control feedback is introduced that allows each spacecraft to track the desired velocity field. The method proposed has proven to be reliable and requires a small amount of communications between the satellites. Therefore the resulting scheme is suitable for very large swarms of spacecraft. Introducing a very little inter-spacecraft communication, can allow to acquire complex shaped formations. So far the ES technique is not free from weak points. In particular the highly decentralized scheme results in the sub-optimality of the maneuvers pursued by each spacecraft. Moreover the behavior based desired velocity field can be affected by the problem of having alternative stationary stable configurations, different from the target one. Whenever the swarm acquires one of these configurations it gets stuck there with no chance of release. Even if this problem has been considered in many studies [10, 11], still a commonly accepted solution for it does not exist yet.
However, the technological challenges presented by the design and development of systems made of swarms of satellites working in a coordinated manner, are not only concerning the path planning area. In fact, constellation and formation of many and possibly small satellites will require propulsion systems capable to produce finely controlled impulse bits with a high specific impulse in order to maximize the system life time. Moreover for such missions the plume impingement problem represents a key concern. The plume of gas particles emitted by a thruster could in fact cause contamination, degradation or even serious damages to neighboring spacecraft leading to a complete mission failure.
For these reasons in 2002 King and Parker introduced and proved the concept of Coulomb satellites (CS) [12],[13]. There the relative dynamics of a swarm of satellites is controlled by the exploitation of the electrostatic forces. The interaction of the spacecraft with the ambient space plasma and an active emission of electric charge allow in fact to control the charge level of a satellite in space. A variation of the Coulomb charge of a spacecraft belonging to the swarm results in varied forces on all the other charged spacecraft. This inter-spacecraft force can be exploited to control the relative motion of the satellites formation with a very small fuel consumption. Even though the CS concept enjoys many advantages, it has also several drawbacks and its application is by far not straightforward. The dynamics of such a system are highly coupled and nonlinear since any change in charge or position of each spacecraft affects the forces acting upon every other charged satellite belonging to the swarm. Therefore it is not possible to design a control feedback able to stabilize the whole system using classical techniques. Moreover the plasma present in space environment tends to diminish the spacecraft's influence upon the other spacecraft of the swarm by masking its electric field. When an isolated charged body is placed in plasma in fact, it attracts charged particles of the opposite sign such that the effect of its charge is limited in extent. The Debye length gives reason of the length scale within which the interaction between the charged isolated body and space plasma is not negligible. So in a spherical region centered in the spacecraft center and with radius equal to the Debye length the electrostatic potential field due to

the charged spacecraft is approximately the one described by the simple Coulomb law. Outside this region the electrostatic potential drastically diminishes. Different Debye lengths are proper to different regions of the space around the earth. In some of these regions the plasma media is such that it is not possible to use electrostatic forces for control purposes. From the first study on, many researchers have been trying to get a better understanding of the dynamic properties of such a complex system. Berryman and Schaub [14, 15] have carried out an extensive study in order to find the static equilibrium positions of the electrostatic actuated satellites. When the swarm is in one of these configurations and each spacecraft has the prescribed level of charge, it is in a system equilibrium position. Ideally it can be kept there in formation without requiring any other actuation. Joe, Schaub et al. [16] and Schaub and Kim [17] have focused their attention on the analysis of the CS dynamical system, finding some general properties of the motion. Moreover Schaub [18] has shown how it is possible to use the Coulomb force in order to obtain bounded satellite formations and has proven his technique controlling the semi-major axis of a three spacecraft formation. Even if many promising results have already been obtained, many aspects of the CS concept have still to be studied and clarified. In particular the control techniques proposed so far (for example in [18]) are designed to stabilize at one moment in time only the motion of a single satellite relative to the remaining formation. Then a simple switched centralized strategy is considered that enables the whole system to control at each time only the spacecraft which has the largest position error. Moreover the collision avoidance has not yet been integrated in such a control scheme. Even if the electrostatic force is suitable for the control of relative positions between satellites of the swarm, it does not allow for controlling the center of mass of the formation since it can only produce inter-spacecraft forces.
The scenario outlined above allows to clearly understand which advantages could be triggered by integrating the concept of CS in the afore mentioned swarm navigation techniques. The resulting capabilities and the total system performance of such a hybrid actuated swarm of satellites could be significantly enhanced with respect to the classical actuated swarm of satellites.

1.2 Main contribution of the work and report structure

The present study aims at modelling and proving the concept of Satellitron Satellites (SS), i.e. a swarm of satellites controlled by a hybrid thrusting-electrostatic actuation system. In this work the assessment is carried out from two different perspectives. On one hand the concept of electrostatic actuation is assessed independently from the previous studies and a possible solution for the integration of this novel actuation concept with a conventional one is proposed. On the other hand the concept is evaluated from the perspective of the control and path planning subsystems. The main objective of this phase of the work is to integrate the CS concept into a swarm navigation technique in

order to enhance the performance of a swarm of satellites in terms of fuel consumption.

1.2.1 Hybrid propulsion system definition

Objective of this phase of the work is to find the most suitable thrusting and electrostatic actuation methods for being integrated into a hybrid propulsion system. Therefore it is necessary to get an understanding of the environmental effects in the earth orbit and their impacts on spacecraft and charge control. The findings lead to the preference of the GEO orbit for which a simplified model of the spacecraft plasma interaction is derived. Afterwards several methods for the prevention of natural space charging are assessed for their suitability to control the charge of a satellite. The result proposes the utilisation of an emission of positive and negative charges with a controllable energy for each one. Suitable devices are then selected and a control strategy is proposed. This chapter ends with the evaluation of the performance of the electric actuation system.

1.2.2 Path planning and Control of the SS swarm

In this work the ES is the selected navigation scheme to control the formation keeping and acquisition maneuvers of the SS swarm of satellites. The extreme simplicity of such a decentralized navigation scheme appears in fact to be particularly appropriate for the path planning and control of a complex and coupled system such as the SS one. Furthermore the ES technique can be considered as a two level approach being the path planning and the control feedback definition completely decoupled. Therefore the resulting navigation scheme appears particularly flexible for the integration of a different actuation technique. In the first phase of the work the compatibility of the two methods is assessed by studying for which target formations the two methods can be satisfactorily integrated. Then two different control feedback laws will be introduced in order to solve the problem of finding the optimal charging level of the spacecraft belonging to the formation during a general acquisition maneuver. A first charging strategy draws the inspiration from the work undertaken in the last years in literature[15, 18, 19]. For this case an analytical solution for the optimization problem is presented for the simple two spacecraft problem. The same approach is then extended to a three-craft problem. A second charging strategy is then introduced that allows to tackle the problem of steering a swarm of N satellites.

1.2.3 Report structure

This report is structured as follows. In chapter 2 the hybrid propulsion system definition and evaluation is presented. This chapter provides the theoretical basis for the definition of the electrostatic actuation and justifies the approach of exploiting the electrostatic force to control spacecraft relative positioning. At the end of the chapter an option for

a possible hybrid actuation scheme is presented and the main issues are discussed. In chapter 3 the first integration between the ES and the EA concept is considered. In particular the problem of finding the formation for which ES and EA are compatible is considered. For this reason in this chapter a mathematical background regarding the ES technique is included. In chapter 4 the general case of exploiting EA for a formation acquisition maneuver steered with the ES technique is presented and two different strategies to determine the charge level of the spacecraft during the maneuver are introduced. In chapter 5 the final considerations and recommendations are drawn.

2 Hybrid propulsion system definition and evaluation

2.1 Introduction

The general aim of this study is the exploitation of inter-spacecraft electrostatic forces to control the spacecrafts relative positions. Electrostatic forces act when a charged object is situated in an electric field **E**. The relation between the electric field **E**, applied from a pointcharge q_2 at the position $\mathbf{x_2}$ and the resulting electrostatic force on a pointcharge q_1 at the position $\mathbf{x_1}$ accounts to:

$$\mathbf{F_1} = \mathbf{E}q_1 \tag{2.1}$$

The electric field applied by q_2 at the position of q_1 is given by:

$$\mathbf{E} = \frac{k_c q_2}{|\mathbf{r_{12}}|^2} \frac{\mathbf{r_{12}}}{|\mathbf{r_{12}}|} \tag{2.2}$$

where $|\mathbf{r_{12}}| = |\mathbf{x_1} - \mathbf{x_2}|$ is the distance between the charges. k_c represents the Coulomb constant and is given by

$$k_c = \frac{1}{4\pi\varepsilon_0} \tag{2.3}$$

ε_0 is the permittivity of free space. Assuming a stationary electric field, it can be clearly seen, that $\vec{F_1}$ scales linearly with the value of charge q_1 and is squared inversely proportional with the distance $|\mathbf{r_{12}}|$ between the charges. In Figure 2.1 the value of q_1 is displayed, that is needed to achieve different electrostatic forces on q_1 in vacuum. The space around Earth is not a perfect vacuum, but characterized by the presence of particles. Depending on the altitude, the medium is neutral, partially ionized or a plasma. The plasma is described by the parameters of the number densities of electrons and ions and by their energies [20], [21], [22]. In Table 2.1 an overview is given for the plasma properties of different space regions. The parameters have a high variation between the different regions of the space around Earth. E.g. in the area of the Ionosphere there is, with $n = 1 \cdot 10^6/cm^3$, a relatively dense plasma. For higher space regions like the GEO orbit the particle density decreases. Also the composition varies for different heights. In LEO the space is composed of various ionized particles like oxygen, nitrogen and hydrogen, in GEO it reduces to mainly hydrogen.

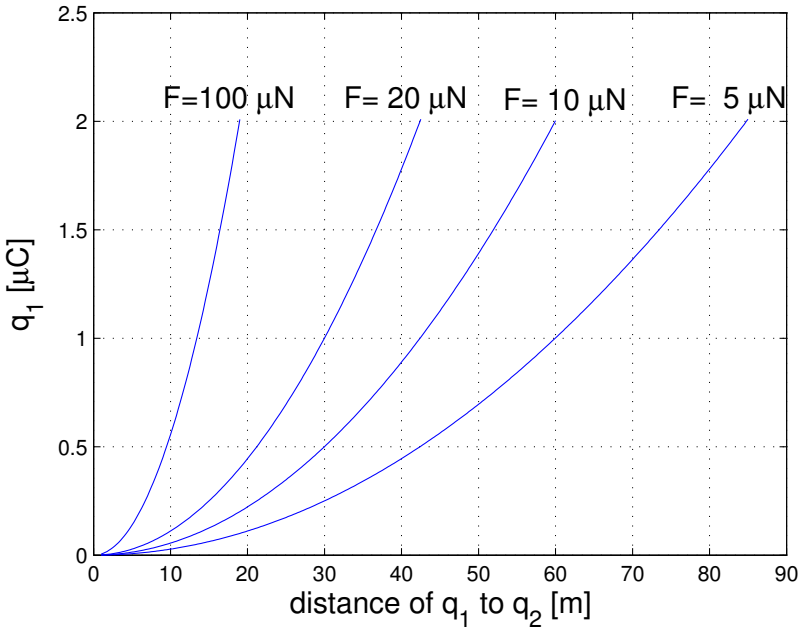

Figure 2.1: Value of pointcharge q_1 needed to apply specified electrostatic forces in vacuum, $q_2 = 2\mu C$, $q_{1_{max}} = 2\mu C$

Due to the presence of charged particles in the space plasma, the effect of Debye Shielding [20] has to be taken into account. When a charged body, e.g. a spacecraft is placed into a plasma it attracts oppositionally charged particles. The resulting ambient electric field diminishes the one of the satellite. Outside a specific volume around the spacecraft, resp. in a certain distance to the SC, the region appears as electrically neutral. Therefore charged bodies beyond this volume will not experience any electrostatic force from the electric field of the spacecraft inside that volume. Eq.(2.4) shows, how the distance to the center affects the force applied by the electric field.

$$\mathbf{F}_1 = \mathbf{E} q_1 exp(\frac{|\mathbf{x_1} - \mathbf{x_2}|}{\lambda_d}) \tag{2.4}$$

The Debye length λ_d gives the distance, at which the shielding effect has screened out around $\frac{2}{3}$ of the strength of the electric field.
As it will be shown in chapter 4, the accelerations demanded from the electric actuation system are in the order of 2 $\mu m/s^2$. For a SC of 50 kg this translates to an order of $F = 100\ \mu N$, which demands, by referring to Figure 2.1, the deployment of inter SC distances in the order of tens of meters. A further rise of the formations characteristic length would diminish the forces to a negligible order. Considering the information

region	plasma density $n\ [1/cm^3]$	electron energy $T_e\ [eV]$	ion energy $T_i\ [eV]$	debye length $\lambda_d\ [m]$
Plasmasphere	$10 - 10^3$	1	1	$0.25 - 2.5$
Plasmasheet	1	1000	6000	240
Solar Wind	6	15	10	12

Table 2.1: plasma properties in different space regions [22]

in Table 2.1 the upcoming studies will concentrate on the application of electrostatic actuation in GEO, as it is a region with a high Debye length.

2.2 Charging in the GEO environment

The GEO orbit is situated in the region of the magnetosphere. In this area, the movement of charged particles is dominated by the Earths magnetic field. Its shape forms due to the interaction of the magnetic field and the solar wind (see Figure 2.2). On the side facing the sun it has an almost dipole like shape, whereas on the night side it extends as the magnetotail several million kilometers far into the space. Thus the field lines and the particles which move along them, vary in their direction and density. Another source for changes of the plasma environment is the variability of the solar wind. During high solar activity the dayside of the Earths magnetic field is being compressed and also the magnetotail on the nightside changes. As a result the high energetic plasmasheet occasionally influences the GEO, giving this orbit changed plasma parameters. There are also other factors like the radiation belts and the ring current which may happen to change the plasma environment [23].

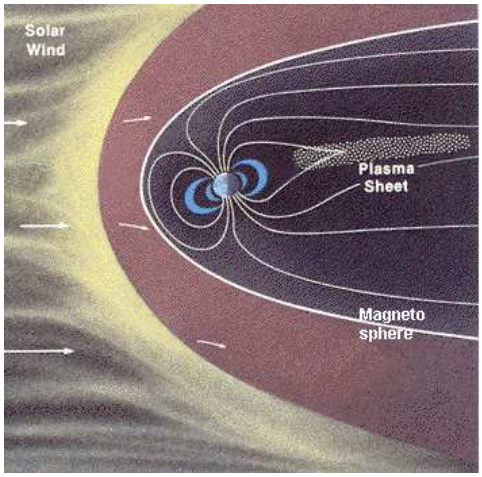

Figure 2.2: Magnetic field of Earth under influence of solar wind; (this Figure is a modified version from [23])

As mentioned in 2.1 the particle environment in GEO consists mainly of electrons and ions. Refering to [24] and [21], in the further work the ions are considered to be protons. Due to difference of their weight, the electrons move much faster than the protons. At thermal equilibrium this ratio accounts to

$$\frac{v_e}{v_p} = \sqrt{\frac{m_p}{m_e}} \approx 43 \tag{2.5}$$

Therefore at equal plasma properties the electrons hit the SC more often than protons. These fluxes of particles are the primary electron and the primary proton current. Besides these two incoming fluxes there exist the secondary electron emission from the SC. This is mainly caused by the impact of primary electrons. When they hit the SC surface within a certain material dependent energy range [25] (see Figure 2.3), electrons are expelled from the surface. The same happens by the impact of primary ions and backscattered secondary electrons. Beside the emission caused by the impact of matter, the photoelectron flux is a very important issue during sunlit periods. Also here the dimension of the flux is dependent on the material.

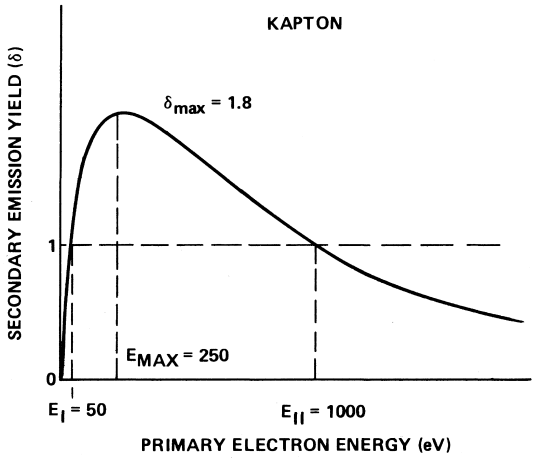

Figure 2.3: secondary electron yield for Kapton due to electron impact energy [25]

2.2.1 Model of Natural Space Charging

In the previous section, it was outlined, that the GEO orbit is a variable environment, which is causing a natural charging of SC surfaces with respect to the ambient plasma. An important task of the Hybrid Propulsion System is to apply a definite charge to the SC and to maintain it. Therefore it is important to evaluate the natural charging effects, to get an estimate of the required performance of the Hybrid propulsion system. To simplify the modeling process the following assumptions have been made. The plasma is considered to have a Maxwell-Boltzmann distribution for either the electrons and the protons. The SC body is spherical, perfectly conductive, uniformly charged and thus possessing an uniform electric field. In sunlight, half of the body is sunlit. The creation of secondary electrons is neglected for this study. Applying these simplifications the SC is receiving two natural currents and emitting one, namely the photoelectron current. Thus the total current, the SC receives, respectively emits, is described by:

$$I_{tot} = I_e + I_i + I_{photo} \tag{2.6}$$

where I_e is the electron current, I_i is the proton current and I_{photo} is the photoelectron current. If the total current is different from zero, the SC will change its voltage with respect to the plasma potential. For this study the SC is assumed to be a spherical capacitor with the outer shell having an infinite diameter. Thus the capacitance of a spherical satellite with a radius r_{SC} is given by:

$$C_{SC} = 4\pi\varepsilon_0 r_{SC}. \tag{2.7}$$

With the presence of a total current different from zero, the potential of the SC is therefore changed by:

$$\frac{dV_{SC}}{dt} = \frac{I_{tot}}{C_{SC}} \tag{2.8}$$

Depending on the sign of the total current the SC charges in negative or positive direction. The sign convention, used in this work is displayed in Table 2.2:

	sign multiplicator
current received from SC	+
current leaving SC	-
electron	-
ion	+

Table 2.2: particle flux sign convention

Following the rules given above, e.g. an electron current leaving the SC has a positive sign ($(-)\cdot(-) = (+)$), thus charging the SC in positive direction. The total current is determined by evaluating the single currents, giving them a sign according to Table 2.2 and summing them up. For the evaluation of the currents it is important, that they are not only dependent on the actual space weather, but also affected by the instantaneous potential V_{SC} of the SC. E.g. if the satellite is assuming a negative voltage, it attracts the ambient ions and thus increases I_i. At the same instant a part of the electrons is repelled resulting in a lower I_e. For a SC charging in positive direction the electron current increases and the ion current drops. The electron current densities are calculated for the two different charge states of the SC with the following equations [21]:

$$J_e = \begin{cases} J_{e0} \cdot exp(\frac{qV_{SC}}{kT_e}) & \mathrm{V_{SC}} < 0 \\ J_{e0} & \mathrm{V_{SC}} = 0 \\ J_{e0} \cdot (1 + \frac{qV_{SC}}{kT_e}) & \mathrm{V_{SC}} > 0 \end{cases} \tag{2.9}$$

$$\text{where} \qquad J_{e0} = (\frac{qn_e}{2})\sqrt{\frac{2kT_e}{\pi m_e}} \tag{2.10}$$

The proton current densities are given by [21]:

$$J_i = \begin{cases} J_{i0}(1 - (\frac{qV_{SC}}{kT_i}) & \mathrm{V_{SC}} < 0 \\ J_{i0} & \mathrm{V_{SC}} = 0 \\ J_{i0} exp(\frac{-qV_{SC}}{kT_i}) & \mathrm{V_{SC}} > 0 \end{cases} \tag{2.11}$$

$$\text{where} \qquad J_{i0} = (\frac{qn_i}{2})\sqrt{\frac{2kT_i}{\pi m_i}} \tag{2.12}$$

and where

k Boltzmann constant
q elementary charge

The outgoing current is caused by the photoemission of electrons. There the radiation of the sun excites electrons to leave the surface material. Assuming a constant solar radiation, the electron flux is material dependent. The values for some materials found in literature are presented in Table 2.3. As long as the potential of the SC is zero or negative, the photoelectron current is nearly a constant. When the satellite floats to a positive potential with respect to the ambient plasma, the photoemitted electrons are attracted back to the positive surface and the flux decreases. The energy of the emitted charges lies in the order of $T_{e_{ph}} = 1.5 - 4.5\ eV$, and therefore, the flux vanishes with higher positive potentials. To consider the highest charging disturbances, the surface

	$j_{e_{phs}}$ $[\mu A/m^2]$	$T_{e_{ph}}$ $[eV]$
stainless steel [22]	20	1.5
aluminium [22]	40	1.5
different materials [26]	10 - 80	1.5
different materials [12]	10	4.5

Table 2.3: photoelectron saturation current densities $j_{e_{phs}}$

properties of the satellites are assumed to have the highest values found in literature. Thus the photoemission capability is set to $j_{e_{phs}} = 80\ \frac{\mu A}{m^2}$ and the average electron temperature is set to $T_{e_{ph}} = 4.5\ eV$. The photoflux density is calculated via [26]:

$$J_{photo} = \begin{cases} J_{e_{ph0}} & \text{V}_{\text{SC}} \leq 0 \\ J_{e_{ph0}} exp(\frac{-qV_{SC}}{kT_{e_{ph}}}) & \text{V}_{\text{SC}} > 0 \end{cases} \tag{2.13}$$

After the determination of the current densities, the actual particle flux to the SC is calculated by multiplying them with the accompanied areas. The ambient ion and electron fluxes hit the SC on its whole area A_1, whereas the photoemission takes places only on the projected sunward surface A_2. Following that definition, the total natural current is gained by:

$$I_{total} = A_1(J_e + J_i) + A_2 J_{photo} \tag{2.14}$$

where

$A_1 = 4\pi r_{SC}^2$ whole SC area
$A_2 = \pi r_{SC}^2$ sunward SC area (projected)

2.2.2 Eclipse and sunlight charging

After the introduction of the model, two typical charging cases shall be explained. At first, consider the SC to be on the night side of the Earth. During geomagnetic storms the Earth's magnetic field is compressed by an intense solar wind and changes in the suns magnetic field. Due to this shape change, the plasma on the night side of the GEO is becoming more energetic. In Figure 2.4 two voltage-current-characteristics are displayed. The characteristics give an overview of the total current density, a spherical SC receives, when charged to different voltages. The charging behaviour shall be explained for a worst case scenario represented by the red line in this Figure. The plasma parameters in Table 2.4 describe these environments as single Maxwell-Boltzmann distributions for either the electrons and protons.
Assume the SC to be at a zero potential. With the lack of sunlight the SC is exposed to two currents, the ambient electron and the ambient proton flux. Due to the higher speed of the electrons, the SC receives a higher number of this species than from the protons. Thus it charges to a negative direction. While the SC floats to a negative charge, it is affecting the surrounding particles. Accordingly the electrons have to overcome a growing potential barrier, whereas the protons are attracted. The SC assumes an equilibrium charge, where both fluxes result in a zero total current. The potential of the SC at this point is the floating potential V_p. For high energetic environments this can be a very negative value, around $V_{f1} = -24\ kV$ for the red colored example.
The blue line represents the behaviour in a less energetic environment. Here the floating potential V_{f2} is located at $-5.6\ kV$.

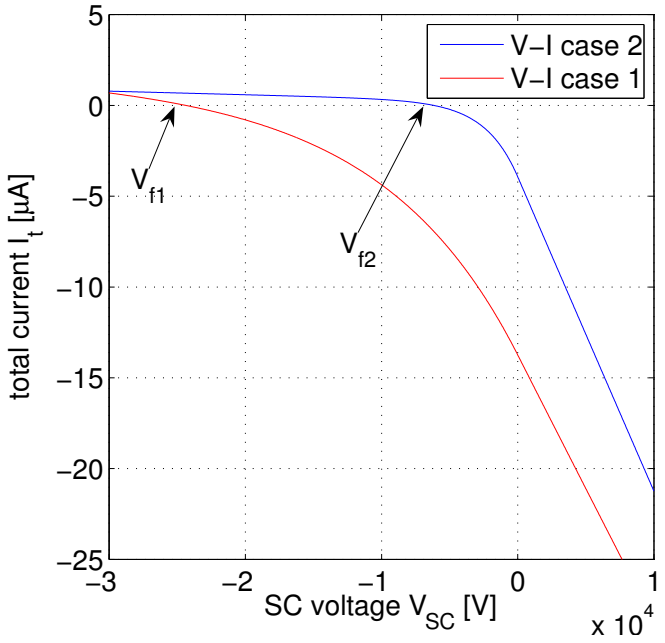

Figure 2.4: V-I-characteristics of GEO eclipse charging

	electrons	ions
case 1 (worst case)		
number density $[1/m^3]$	$1.12 \cdot 10^6$	$2.36 \cdot 10^5$
Temperature $[eV]$	$12 \cdot 10^3$	$23.5 \cdot 10^3$
case 2 (average)		
number density $[1/m^3]$	$1 \cdot 10^6$	$1 \cdot 10^6$
Temperature $[eV]$	$2.4 \cdot 10^3$	$10 \cdot 10^3$
case 3 (worst case)		
number density $[1/m^3]$	$1.7 \cdot 10^6$	$1.85 \cdot 10^6$
Temperature $[eV]$	$9.8 \cdot 10^3$	$14 \cdot 10^3$

Table 2.4: Plasma parameters for different GEO environment during eclipse; case 1: [21], cases 2,3:[20]

On the sunward side of the GEO orbit, the plasma environment is usually less energetic. The significant difference to the eclipse case is the emission of photoelectrons. In Figure 2.5(b) the voltage-current characteristic of a 1 m diameter spherical SC exposed to

sunlight is displayed. The plasma environment taken for this simulation is defined by the second set of parameters listed in Table 2.4. In its isolated representation in Figure 2.5(a) it can be clearly seen, that the photoflux outnumbers the other currents as long as the SC is at a negative potential. The emitted photoelectrons possess a low energy compared to the surrounding ambient plasma and are not able to escape a high surface potential. Therefore the ambient particle fluxes dominate the total current at positive SC voltages. In the case of Figure 2.5 the SC will assume a low positive voltage of 13 V.

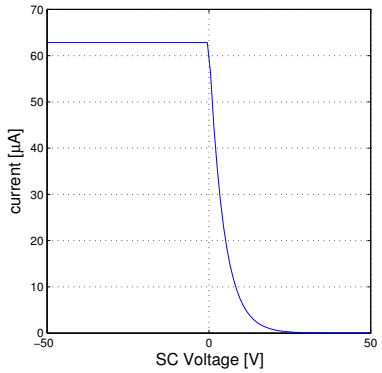

(a) photoelectron flux; $T_{e_{ph}} = 4.5\ eV$

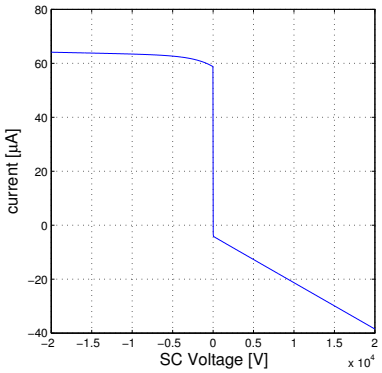

(b) total current in sunlight

Figure 2.5: V-I-characteristics for sunlight charging; case 2 of Table 2.4

2.2.3 Charge effects and review of mitigation methods

In the previous section it has been shown, that SC situated in GEO assume a floating potential which is strongly dependent on the actual space weather. Situated in eclipse with increased solar activity, the charging process can generate very high negative potentials. On the sunward side the presence of photoflux leads to a floating potential at low positive values. In the past there have been various reports about high level SC charging in GEO orbit. A very important side effect of these charging events is the occurrence of differential charging. This happens due to the different properties of the materials on a SC. Differential charging may e.g. happen between the conductive ground of a SC and insulators like mylar, kapton or astroquartz [22], [27]. One typical case is the approach of the SC from eclipse, where it has been highly negatively charged, to the sunlit part. The parts exposed to sunlight and the conductively connected SC ground on the shadowed side will be discharged. The insulators on the dark part will remain for much longer time on their high charge, because they have no possibility to conduct their excessive electrons to the sunlit part which floats positive. At high levels of differential charging, breakdowns may occur, which often disturb the electronics or even destroy parts of the hardware. Due to these dangers there has been a development of various

methods [28] to reduce or mitigate charging effects. These methods shall be evaluated here with regard to the ability to charge to definite values.

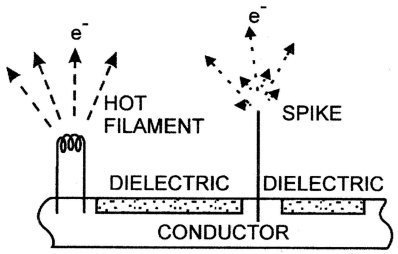

Figure 2.6: Discharge of SC surfaces by a sharp spike or a hot filament [28]

An easy applicable method is to place sharp spikes on conducting surfaces as shown in Figure 2.6. At the top of the spike a very high electric field is generated, which is dependent on the tips curvature radius. The presence of a high electric field is accompanied by the emission of electrons, which results in a reduction of charge of the connected conductive surfaces. An active way to emit electrons, is to use a heated filament. As long as the filament is below its melting point, only electrons are escaping. At temperatures above the melting point also ions leave the wire. In difference to the sharp spike the amount of excited electrons can be controlled via the temperature of the filament. The mutual drawback of both methods is the restriction to conductive grounds. Charged dielectrics will remain at their state and thus build up differential charge with respect to the spaceframe.
Another passive way to emit electrons is to use high secondary electron yield material. This creates a high outgoing flux of electrons for incoming electrons. According to Figure 2.3 the ratio between outgoing and incoming electrons is greater than unity for distinct energy ranges. There the ambient electron flux is effectively equalized. On the other hand, in the high energy environment of geomagnetic storms this method will not be effective.

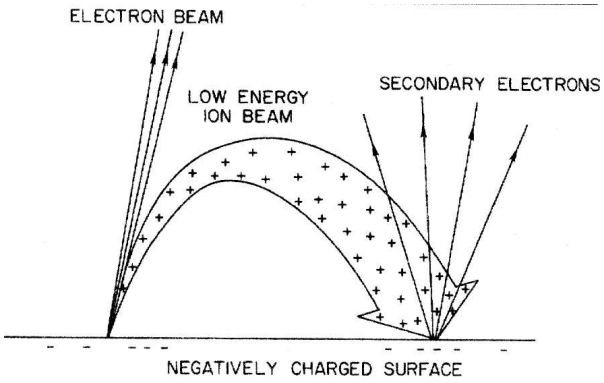

Figure 2.7: Discharge of SC surfaces by a emission of low energy plasma [28]

An interesting approach for discharging negative surfaces is the release of low energy plasma, which is having two effects. The plasma electrons are accelerated away from the SC and thus reducing the negative charge. The ions are, due to their low energy, attracted by the negative SC and accelerated to the most negatively charged areas. In that way the escaping electrons reduce the charge of the conducting ground and the ions decrease the charge of the insulators, which would otherwise remain charged.
Besides the utilisation of a plasma, also single species can be emitted. For the Cluster Mission positive potentials had to be mitigated, as the ambient plasma should be measured in the very low temperature component [26], [29]. During the sunward sections of the orbit, a liquid metal ion source was operated to emit positive indium ions and successfully lower the floating potential to a value near zero.
All the reviewed methods have in common, that they are made to drive the potential of the SC with respect to the ambient plasma ground to zero. None of them is capable to charge the SC to a certain value or to clamp it there. Thus another approach has to be chosen.

2.3 Definition of the Hybrid Propulsion System

In the previous sections it has been outlined, that the charge of a SC is object to frequent alterations as a consequence of variable environmental conditions. A review of charge control methods shown that there is a need for a an approach different to common techniques.

2.3.1 Requirements

The purpose of the study is the exploitation of electrostatic forces to minimize the fuel consumption of a satellite swarm during station keeping or acquisition maneuvers. It

will be shown in the following chapters, that the SS must be able to assume and to keep a broad range of voltages. For the control of the charge state of a SC it is necessary to control the current balance of the SC, which is stated in Eq.(2.6). With the presence of a control system Eq.(2.6) extends to:

$$I_{tot} = I_e + I_i + I_{photo} + I_{control} \tag{2.15}$$

When an electrically charged body with the voltage V_{SC} emits oppositionally charged particles, they need a certain energy to be able to escape the electric field. This energy amounts to: $E_{escape} = qV_{SC}$, when the ejected particle is charged with one elementary charge q. Thus the ejection mechanism has to provide at least an acceleration voltage which equals the maximum surface potential of V_{SC}. Assuming a 1 m diameter for the spherical SC and following:

$$V_{SC} = k_c \frac{q_{SC}}{r} \tag{2.16}$$

the charge range of $\pm 2\ \mu C$ demands acceleration voltages between $\pm$ 36 kV.
Besides the ability to create a flux of particles which can actually leave the SC, the amount of total current must be controllable. To achieve this, the emission system must be able to equalize the total natural current in any plasma environment and to output an additional flux which is used for the actual charging process.
On the other hand the current should not be higher as necessary to keep the mass flow as low as possible (more details in section 2.4.5). In Figure 2.8 the voltage-current characteristics for different plasma environments are displayed. The blue lines represent worst case plasma parameters in eclipse, while the red lines show the effect of photoemission during sunlit periods. It can be seen, that the highest natural currents occur, when the SC is at its maximum voltage levels either positive or negative. For a high positive V_{SC} in eclipse and substorm conditions, the total current assumes values of up to $-65\ \mu A$. In case of a negatively charged SC the sum of the natural currents falls to a lower negative value or changes or assumes a low positive amount. If the SC is situated on a sunward part of GEO, the photoelectrons represent the highest quantity for any negative charge state. The net current there is thus positive and amounts for this SC to 65 μA.

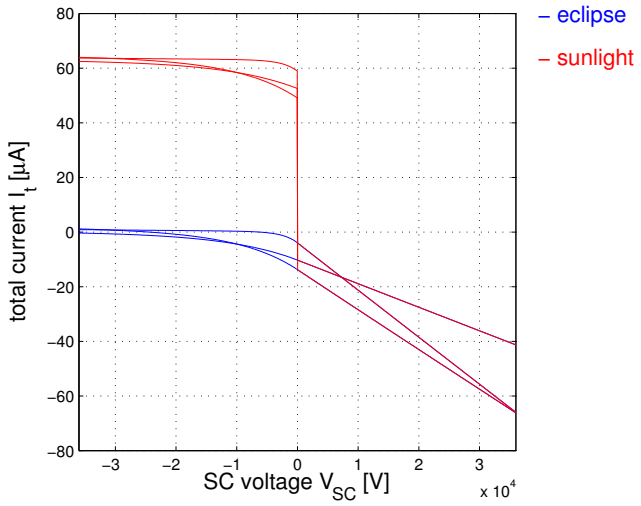

Figure 2.8: Natural currents at different SC voltage levels for plasma environment cases 1-3

While in a stationary formation the SS require smaller changes in the charge levels, there are higher demands during acquisition maneuvers. It will be shown, that the demand for the change of voltages can be in the order of $1-10\ s$. The additional actual charging current should therefore be able to provide a charging time of the SC in the before mentioned dimension. With reference to Eq.(2.8) and assuming a constant total current I_{total}, a charging time of $\Delta t_{charge} = 1\ s$ and $\Delta V_{SC} = 72000\ V$, the charging current is determined by:

$$I(\Delta t_{charge}) = I_{total} = C_{SC}\frac{\Delta V_{SC}}{\Delta t_{charge}} \approx 8\ \mu A \tag{2.17}$$

Given the maximum natural currents of $I_{nat} = [-65\ \mu A, +65\ \mu A]$ the control current has to have a minimum amount of $\approx 73\ \mu A$ to fulfill Eq.(2.17). The proposed control approach in section(2.4) demands the actuation system to emit a specified current at different acceleration voltages. The system should therefore be able to independently change the acceleration voltage and the amount of emitted current.
The requirements of the charge ejection system are summarized in Table 2.5. As the SC shall be charged in negative and positive direction the demands mentioned above are the same for an electron and for an ion ejection system. In the following section ion thrusters will be evaluated and one system selected from a compilation of commercially available or soon available devices.

- high range of acceleration voltage $V_{acc} = \pm$ 36 kV
- independent adjustability of $I_{control}$ and V_{acc}
- fast adjustability of $I_{control}$ and V_{acc} in less than 1 s
- provision of emission currents $I_{control}$ in the order of $\pm$ 73 μA

Table 2.5: Requirements to the Hybrid Propulsion System

2.3.2 Review of Ion Thrusters

As specified above, the current, the actuation system will be expected to emit, has the order of 100 μA. If this current is assumed to be realized by onefold charged ions, the massflow accounts to:

$$\dot{m}_I = I_{control}\rho_{q_{Ion}} \tag{2.18}$$

$$\rho_{q_{Ion}} = \frac{u_{Ion}}{q} \tag{2.19}$$

$\rho_{q_{Ion}}$ – mass of ions per one [C]
u_{Ion} – atomic mass of ion
q – elementary charge

For Ion thrusters the specific impulses are in the order of magnitude of $1 \cdot 10^3 s$. For this value and the use of propellants like Caesium, Indium or Xenon, the capabilities of the thrusting system should be in the order of μN

$$F = I_s \dot{m}_I g_0 \tag{2.20}$$

In [30] different μPropulsion thrusters are evaluated and will be summarized in the following. The Field Emission Electric Propulsion (FEEP) Systems extract ions out of a liquid metal source via an electric field. The thrust is generated via the acceleration of these ions with the help of the same electric field. Thus the scale of the emission current and its acceleration can not be controlled independently.
The colloid thrusters also extract charged material from a liquid source. For this application it is an organic substance, also called ionic fluid. The drawback in this method is the size of the charged particles. It ranges from single ions to clusters of atoms, which means, the massflow and the specific residual thrust of an electric current is much higher than one consisting of single ion charges. Another surveyed device is the Pulsed

Plasma Thruster (PPT) technology. In this system a discharge current between two capacitor plates ablates material from a teflon bar. A part of the material is ionized and accelerated by magnetic field of the discharge current. As the outgoing particles form a plasma, the released flux is electrically neutral and therefore not useable to charge the SC. Furthermore due to the discharge mechanism, the acceleration energy and the massflow are not independently adjustable.
The High efficiency Multistage Plasma (HEMP) system works with a combination of a static magetic field, realised via permanent magnets and an electric field applied with an anode-cathode configuration. The amount of ionised Xe atoms depends can be adjusted with the inlet flow rate of the neutral Xenon gas, whereas the acceleration can be independently controlled with the potential of the anode. The tested configurations however, are built for relatively high thrusts in the mN area and therefore produce too high currents for an application with SS. The cold gas resistojet thrusters mentioned in the end of the survey are not producing charged particles and are therefore not useful for this studys intention.
The Radio frequency Ion Thruster (RIT) is a very promising technique, which will be explained with more detail in the next section.

2.3.3 Radio Frequency Ion Thruster (RIT)

The RIT engine consists of two main parts. These are the ionisation tube equipped with an outer circumjacent RF coil and the gate electrodes. The engine works with Xenon gas which is brought in the ionisation via the inlet. In the tube the Xe is ionized by the 1 MHz radio frequency. After a buildup time in the order of ms [31] the stationary ionisation grade is reached. Due to the inlet velocity and the pressure difference to the ambient vacuum, the neutral Xe and mainly onefold ionized Xe^{+1} move in direction to the gate electrodes. Once the species have crossed the first grid, they are accelerated towards the second grid, which is at a low negative potential. It is utilised to prevent the movement of electrons from the neutraliser towards the first electrode. Recently there has been performed extensive research to downscale the existing RIT engines to μN capabilities [32]. During a test campaign with the RIT-4 engine, where the number 4 stands for the diameter of the tube in centimeters, the achieved thrusts ranged from around 25 μN to 125μN. While the ionizing RF power was adjusted, the flow rate was held at the lowest possible value of 0.08 sccm of Xe. During the campaign emission currents in the order of mA have been measured. While this current is still too high for the application in this study, with a new low flow controller also lower currents of about 250 μA are possible. Even better results promise the next downscaling steps towards the RIT-2 and RIT-1 engine. The lowest possible current feasible with a RIT-1 was estimated to be in the area of 100 μ A.
Besides the adjustability of the current with the amount of inlet Xenon, also the radio frequency power can be tuned. With a lower RF power the ionisation grade of the Xe gas

and thus the emission current is also lowered. As there is always a small residual thrust due to the escaping neutral Xe the preferred option of changing the amount of Xe^{+1} is to lower the incoming flow rate. By adjusting the potential between the acceleration grid and the ground, the energy of the Xe^{+1} can be tuned. The change of the grid voltages can be realized in the order of ms. Concerning the high demanded bandwith of grid voltages, the tests of the akin Dual Stage 4 Grid engine [33] have shown, that the application of acceleration voltages in the order of 30000 V is feasible.
After this survey, the RIT engine is the most promising device for the emission of positively charged particles in order to do SC charging with currents in the order of Table 2.5. The RIT-1 can fulfill the demands for a low current emission combined with high acceleration voltages. As a consequence of the separate generation of ions and their acceleration the value of the current and the acceleration voltage are independently controllable in a wide area.

2.3.4 Electron gun

The emission of negative charges will be realised with an electron gun. There is a wide selection of such devices commercially available e.g. at [34]. One selected e-gun provides emission energies of up to 50 keV which corresponds to an acceleration voltage of up to 50 kV. The electron flux can be adjusted between 1 nA and 5 mA. Both parameters are independently adjustable in the order of fractions of a second. Although the size of this e-gun is too large for satellite applications a downscaling should be possible, as comparable e-guns have been already operated in GEO. For example the device on SCATHA [35] was capable to provide currents between $1\mu\ A$ and 13 mA and V_{acc} between 50 V and 3 kV.

2.4 Control Strategy and performance evaluation

As shown in the previous sections, the environment in GEO leads to a natural SC charging. To charge a SC to definite values, the natural currents have to be balanced and an additional flux of charges has to be emitted. A survey of available μN ion thrusters shown, that the best suitable engine is the Radio Frequency Ion Thruster, as it can be operated with a high bandwidth of emission currents and acceleration voltages and is capable to adjust these two parameters independently. However with present techniques the emission has a lower boundary in the order of 250 μA for the RIT-4 and 100 μA for the RIT-1, available in future. In the following a control approach will be explained, which can work with the available device and possesses the ability to charge the SC to any given voltage and to keep it there in the scope of the requirements given in Table 2.5 .
The principle of the approach is to change the voltage-current characteristics of the SC-

plasma system in a way, that the floating potential assumes the value of the desired SC voltage. Having such a characteristic, the SC would always assume the desired value, no matter which initial value it possessed. This is done with the utilisation of a charging current I_{charge} and a stabilization current I_{st}.
At first the charging dynamics shall be explained with the charging current used exclusively.

2.4.1 Charging current

Consider the SC with zero charge and situated in GEO eclipse. The environment is defined to be low energetic following the plasma regime number 4 in Table 2.6. If the SC is left to float freely it would fast assume the floating potential $V_f = -1750\ V$ shown in Figure 2.9(a). To change the voltage of the SC to the desired value $V_{des} = -4000\ V$ the emission device is set to release a charging current with an acceleration voltage $|V_{acc}| = 4000\ V$. To let the SC achieve a more negative potential, it is set to emit positive ions. The magnitude of I_{charge} is set to $-250\mu A$, which is a feasible current for the RIT-4. This amount is sufficient to outnumber any environmental current and to leave an additional part for the actual charging. In Figure 2.9(b) the voltage-current characteristic which takes I_{charge} into account is displayed. Please note, that for clarity, $I_{ch} = -5\ \mu A$. In Figure 2.9(c) the V-I characteristic is calculated with $I_{ch} = -250\ \mu A$ and being displayed in true scale.

	electrons	ions
case 4		
number density $[1/m^3]$	$0.5 \cdot 10^6$	$1 \cdot 10^6$
Temperature $[eV]$	$1 \cdot 10^3$	$10 \cdot 10^3$
case 5		
number density $[1/m^3]$	$0.75 \cdot 10^6$	$1 \cdot 10^6$
Temperature $[eV]$	$2.4 \cdot 10^3$	$10 \cdot 10^3$

Table 2.6: Plasma parameters for low energy GEO environments; case 4,5: adapted from Table 2.4

With the SC at V_f, only I_{charge} is significant, as the natural fluxes balance each other. The energy of the ejected particles is sufficient to let them escape the influence of the electric field of the SC. At any V_{SC} the total current is determined from the sum

$$I_{total} = I_e + I_p + I_{charge}.$$

With the charge control system turned on, the V-I characteristic changes to the one in Figure 2.9(b) and the potential moves towards V_{des} accordant to Eq.(2.8). With

increasing negative potential the sum of the natural fluxes will assume a growing positive value, because I_e drops and I_p increases. Once the SC reaches V_{des} (which equals the acceleration voltage) the emitted Xe^{+1} Ions cannot escape the present electric field anymore. Thus the charging current decreases. The decay of the charge current depends on the energy distribution of its associated ions. In the case of the RIT engine the range of the energies lies between qV_{acc} and $q(V_{acc} + 20\ V)$ [31]. For this study a linear decay is assumed, with

$$\text{percentage of escaping ions}(\mathrm{I_{ch}}) \quad = \quad \begin{cases} 100\ \% & |\mathrm{V_{SC}}| \leq |\mathrm{V_{acc}}| \\ 0\ \% & |\mathrm{V_{SC}}| \geq |\mathrm{V_{acc}}| + 20\ \mathrm{V} \end{cases} \tag{2.21}$$

$$\text{for} \quad sign(I_{ch}) \quad = \quad sign(V_{SC})$$

The charging current will decrease until it balances the natural flux. At this point I_{total} is zero and the SC is at its floating potential, which will be situated between V_{acc} and $V_{acc} + 20\ V$. Figures 2.9(c) and 2.9(b) show, that the voltage state of the SC is fixed at a stable point. Starting from any initial voltage, the SC will be driven to the desired one.
For the case of charging the SC to a positive voltage, instead of the ion emission device the electron gun would be utilised. Besides the application of a differently charged species, the principle is the same. The application of I_{charge} changes the V-I characteristic of the SC-plasma system and puts the floating potential to the desired value. The electrone emission is set to $I_{charge} = 250\ \mu A$ and the acceleration voltage is set to V_{des}. Once the SC potential reaches the aimed value, an equilibrium with the natural fluxes will be achieved. Also here the precision depends on the energy distribution of the electrons. For simplification, in this study the shape of the distribution is assumed to be similar to the one of the RIT.

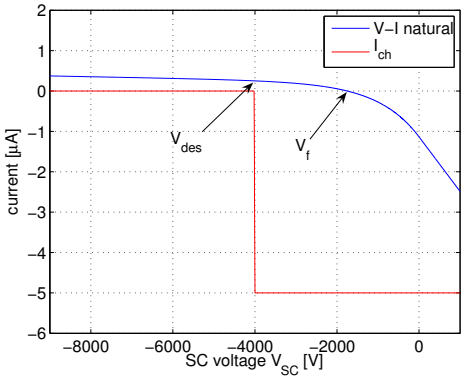

(a) V-I characteristic and charging current; for clarity $I_{ch} = 5\ \mu A$; plasma case 4

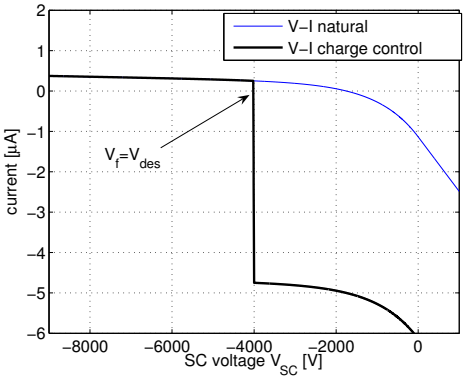

(b) V-I characteristic of combined natural and charging current; for clarity $I_{ch} = 5\ \mu A$; plasma case 4

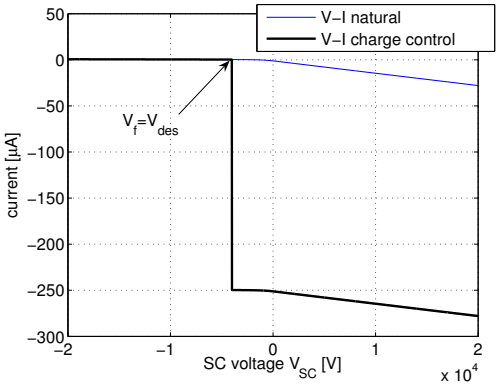

(c) V-I characteristic of combined natural and charging current in true scale; $I_{ch} = 250\ \mu A$; plasma case 4

Figure 2.9: charge control with the utilisation of charge current I_{ch} exclusively

2.4.2 Charging and stabilizing current

The utilisation of one current for the case described above is sufficient as long as the natural floating potential is below the desired potential. In other words, with this approach, the charging process cannot charge a SC below its floating potential. In general the desired voltage can not be achieved if:

$$\begin{array}{rcl} |V_{des}| & < & |V_f| \\ sign(V_{des}) & = & sign(V_f) \end{array} \tag{2.22}$$

In such a case the SC will be charged always to the floating potential. This shall be explained in the next paragraph.

Consider a change in the present plasma regime to case 5 in Table 2.6, which increases the energy and the number of electrons. In Figure 2.10(a) the V-I characteristics for both cases are displayed and show a move of V_f to a more negative value of -5550 V. The total current at $V_{des} = -4000\ V$ is now negative (Figure 2.10(b)) and will shift V_{SC} to the floating potential, even if the charging current is switched on. The problem arises from the property of the charging current, which is intended to fast decay and to find a balance with the natural currents, once the desired voltage is achieved. Considering the new environment the natural currents change in a way, that at the desired voltage there is still an incoming flux of electrons, driving the SC even more negative, while I_{charge} has already gone to zero, because no ion can escape anymore the SC potential.
To handle that, the stabilization current I_{st}, which posepossesses opposite sign of I_{ch} is introduced. It is intended to restore the V-I characteristic to the condition $V_f = V_{des}$. The properties of the two currents are determined following the relations in Eq.(2.23 - 2.24):

$$\begin{aligned} |V_{acc_{ch}}| &= |V_{des}| \\ |V_{acc_{st}}| &= \text{release energy} \end{aligned} \tag{2.23}$$

$$\begin{aligned} sign(I_{ch}) &= sign(V_{des}) \\ sign(I_{st}) &= sign(V_{des}) \cdot (-1) \end{aligned}$$

$$\begin{aligned} I_{st} + I_{nat} &= \Delta_1 \\ &\text{with} \quad \forall(V_{SC}) \quad \begin{cases} I_{st} > 0 & \Delta_1 \geq |I(\Delta t_{charge})| \\ I_{st} < 0 & \Delta_1 \leq |I(\Delta t_{charge})| \cdot (-1) \end{cases} \end{aligned} \tag{2.24}$$

$$\begin{aligned} I_{ch} + I_{st} + I_{nat} &= \Delta_2 \\ &\text{with} \quad \forall(V_{SC}) \quad \begin{cases} I_{ch} > 0 & \Delta_2 \geq |I(\Delta t_{charge})| \\ I_{ch} < 0 & \Delta_2 \leq |I(\Delta t_{charge})| \cdot (-1) \end{cases} \end{aligned}$$

There are two charging cases to be considered, the first one is a command to charge the SC to negative potential and the second is at $V_{des} > 0$.
If there were no technical restrictions, the control current parameters would follow Table 2.7. Utilising the RIT-4 engine, the minimum ion current amounts to $-250\ \mu A$, which results in the parameters given in Table 2.8. With the RIT-1 as device, the lowest emitable ion current amounts to $-100 \mu A$. This gives the possibility to change Δt_{charge} to 10 s and therefore drop $I(\Delta t_{charge})$ to $\approx 1\ \mu A$. The resulting control parameters are in Table 2.9. Please note, that these are the lowest values possible for the proposed control approach.
Following the example from section 2.4.1, $V_{des} = -4000\ V$. The charging current I_{charge} is set to $-250\ \mu A$ according to Table 2.8. The emission energy of the electron gun can

	$V_{des} < 0$	$V_{des} > 0$
I_{st}	$\geq +73\ \mu A$	$\leq -73\ \mu A$
$\lvert V_{acc}\rvert$	> 0 (release voltage)	> 0
I_{ch}	$\leq -146\ \mu A$	$\geq +146\ \mu A$
$\lvert V_{acc}\rvert$	V_{des}	V_{des}

Table 2.7: control current parameters (without the consideration of technical restrictions) for a given V_{des}, $\Delta t_{charge} = 1\ s$, $I(\Delta t_{charge}) = 8\ \mu A$, $I_{nat} = [-65\ \mu A, +65\ \mu A]$

be very low, as the current is only needed, when $sign(V_{SC}) \neq sign(I_{st})$. The particles, once released, will be accelerated by the electric field of the SC itself. For the case of an oppositional charged SC, all emitted particles of I_{st} will return, or I_{st} can be just switched off. A single application of I_{st} would drive the SC to a near zero potential. In combination with I_{ch} a very stable V-I characteristic around the desired voltage is created, shown in Figure 2.10(d). This is valid for any environment approaching in GEO, because with $I_{nat} = [-65\ \mu A, +65\ \mu A]$ the worst case natural fluxes have been considered. Summarizing the principle, the charging current is charging the SC in direction from zero to the desired voltage, whereas the stabilization current pulls the SC to a zero potential. Both currents balance with a 20 V precision around V_{des}, which corresponds to a charge precision of $2 \cdot 10^{-9} \mu C$. The position inside the 20 V window is determined by the natural fluxes, which have no further influence on the charging process.

	$V_{des} < 0$	$V_{des} > 0$
I_{st}	$\geq +73\ \mu A$	$\leq -250\ \mu A$
$\lvert V_{acc}\rvert$	> 0 (release voltage)	> 0
I_{ch}	$\leq -250\ \mu A$	$\geq +323\ \mu A$
$\lvert V_{acc}\rvert$	V_{des}	V_{des}

Table 2.8: control current parameters for using RIT-4 as ion emitting device for a given V_{des}; $\Delta t_{charge} = 1\ s$, $I(\Delta t_{charge}) = 8\ \mu A$, $I_{nat} = [-65\ \mu A, +65\ \mu A]$

	$V_{des} < 0$	$V_{des} > 0$
I_{st}	$\geq +66\ \mu A$	$\leq -100\ \mu A$
$\lvert V_{acc}\rvert$	> 0 (release voltage)	> 0
I_{ch}	$\leq -132\ \mu A$	$\geq +166\ \mu A$
$\lvert V_{acc}\rvert$	V_{des}	V_{des}

Table 2.9: control current parameters for using RIT-1 as ion emitting device for a given V_{des}; $\Delta t_{charge} = 10\ s$, $I(\Delta t_{charge}) \approx 1\ \mu A$, $I_{nat} = [-65\ \mu A, +65\ \mu A]$

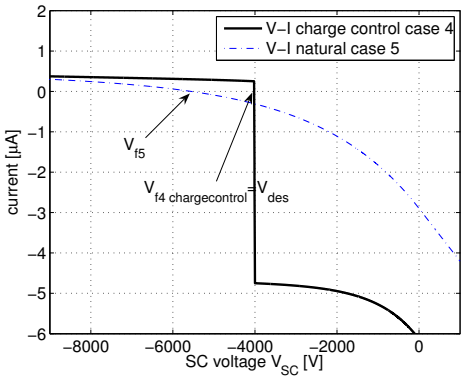

(a) change of V-I due to altered plasma parameters; plasma cases 4,5

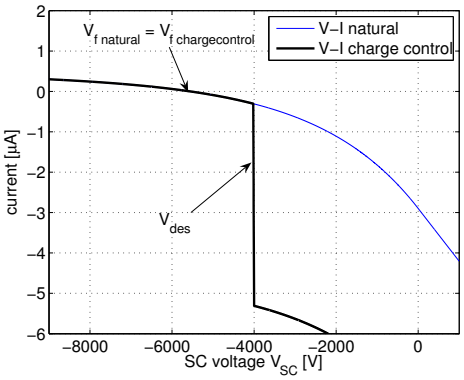

(b) drift of V_f to new position, charge control can not achieve V_{des}; for clarity $I_{ch} = -5\ \mu A$; plasma case 5

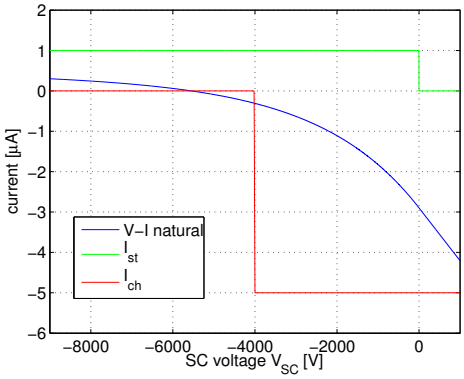

(c) Introduction of stabilisation current; for clarity $I_{ch} = -5\ \mu A$, $I_{st} = 1\ \mu A$; plasma case 5

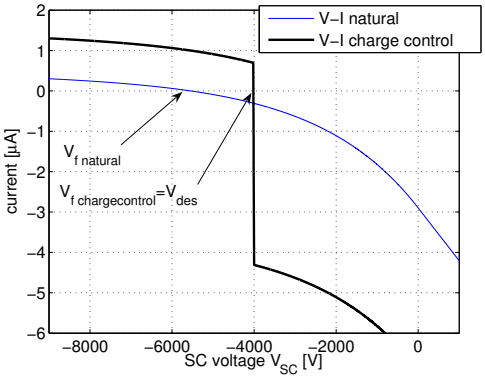

(d) V-I characteristic of combined natural and charging current; for clarity $I_{ch} = -5\ \mu A$, $I_{st} = 1\ \mu A$; plasma case 5

Figure 2.10: charge control via the combination of the charge current I_{ch} and the stabilisation current I_{st}

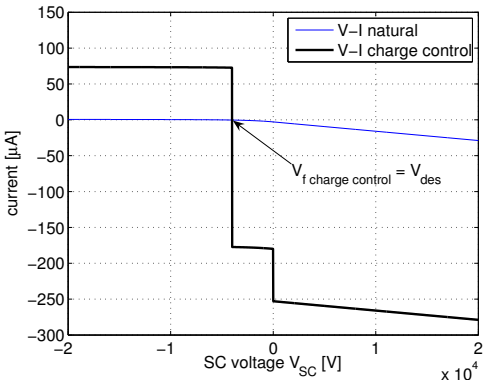

Figure 2.11: V-I characteristic of combined natural and charging current in true scale; $I_{ch} = -250\ \mu A$, $I_{st} = 73\ \mu A$, plasma case 5

Another example is displayed in Figure 2.12. Here two charging processes for the sunlit case are shown, where the SC desired potential is set to $-15\ kV$ and to $+20\ kV$. Due to photoemission the natural negative flux is outnumbered for the whole negative SC potential area. Without charge control the SC would assume a low positive potential, at a voltage where the decaying photoelectrons and the natural flux balance. According to the control scheme and considering technical limits the parameters in Table 2.10 are used.

	$V_{des} = -15000\ V$	$V_{des} = 20000\ V$
I_{st}	$+73\ \mu A$	$-250\ \mu A$
$\lvert V_{acc}\rvert$	> 0	> 0
I_{ch}	$-250\ \mu A$	$+323\ \mu A$
$\lvert V_{acc}\rvert$	$15000\ V$	$> 20000\ V$

Table 2.10: control current parameters for using RIT-4; $\Delta t_{charge} = 1\ s$, $I(\Delta t_{charge}) = 8\ \mu A$, $I_{nat} = [-65\ \mu A, +65\ \mu A]$

In Figure 2.12(a) the control currents are shown for $V_{des} = -15000\ V$, whereas Figure 2.12(b) shows the resulting V-I characteristic, which leads the SC potential from any initial voltage to $-15\ kV$. In Figure 2.12(c) the scheme is displayed for $V_{des} = 20000\ V$. The charging current and the stabilization current change their signs each and create a V-I characteristic for the SC-plasma system, which leads the potential of the SC from any initial voltage towards the desired 20 kV (Figure 2.12(d)).

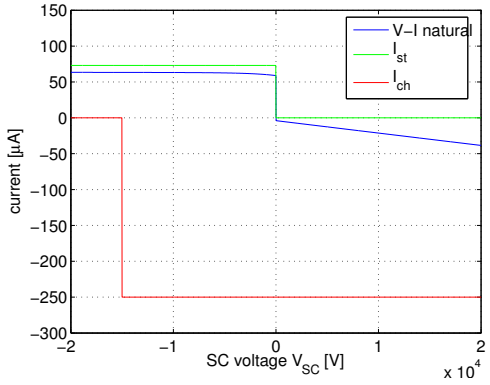

(a) V-I of natural fluxes and control currents; $V_{des} = -15\ kV$, $I_{st} = +73\ \mu A$, $I_{ch} = -250\ \mu A$; plasma case 2

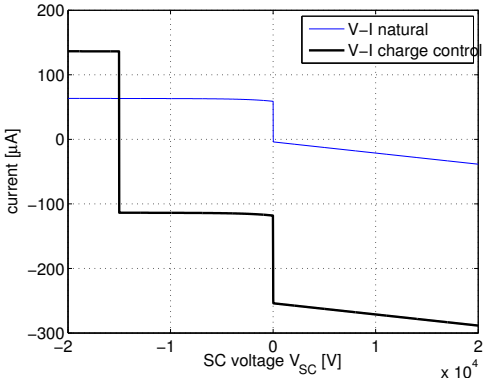

(b) resulting V-I for applied control currents

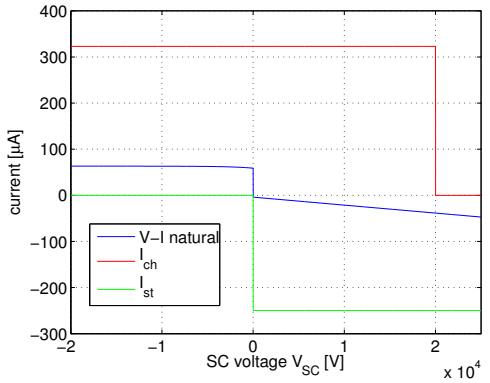

(c) V-I of natural fluxes and control currents; $V_{des} = +20\ kV$, $I_{st} = -250\ \mu A$, $I_{ch} = +323\ \mu A$, plasma case 2

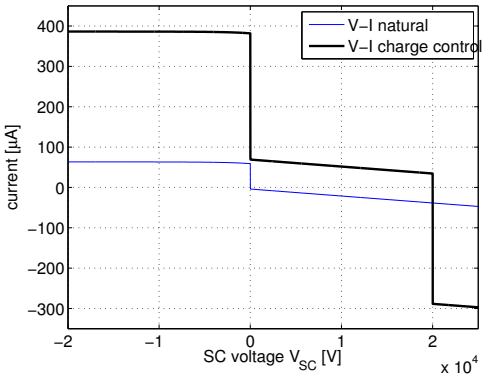

(d) resulting V-I for applied control currents

Figure 2.12: charge control via the combination of the charge current I_{ch} and the stabilisation current I_{st}, plasma environment 2 and photoemission

The stabilisation current has been introduced to avoid problems which happen in the case of Eq.(2.22). In GEO, this problem mainly affects the negative range of desired voltages. In the positive direction problems of this kind only occur, if a very low positive voltage is desired. On the other hand, a disclaimer of I_{st} would create a dependence on the natural currents. If a SC is e.g. ordered to go from $+20\ kV$ to $+2\ kV$ it would rely only on the attraction of ambient electrons to charge in direction to zero. Assuming a low electron flux in a moderate plasma environment, the charging may need more time than demanded in Table 2.5. The utilisation of the stabilisation current allows to stay in the requirements (please refer next section 2.4.3). With the proposed control scheme

any charge in the range of the requirements can be achieved. According to its design it does not need fast measurements of the SC voltage or the analysis of the surrounding plasma.
Another possibility for a control scheme would be to use only one current, to go from the initial voltage to the desired one. Once at V_{des} the current is changed to exactly balance the natural fluxes and thus fix the SC charge. This method would use lower currents than the two current approach, but needs a feed back control. This would require fast ($t_{measure} < \Delta t_{charge}$) measurements of the plasma environment and the SC voltage. In the trade off of simplicity and available technology, this approach is not foreseen in this study.

2.4.3 Evaluation of duration of the charging process

In this section the speed of the charging process shall be evaluated. This is done via calculating the charge cases in which the highest charging times are expected. Therefore the control system is ordered to switch between the limits of the SC voltages, mentioned in Table 2.5. Furthermore the charging time is dependent on the amount of natural fluxes. Thus the worst case plasma environments of case 1 and case 3 from Table 2.4 are chosen, as well as the average plasma regime of case 2 from the same Table. While the worst case environments provide very high negative natural fluxes, the sunlit part of the orbit has also to be taken into account. Following this test setup, the control system is ordered to calculate the charging durations in three plasma regimes, situated once in sunlight and once in eclipse, switching from $-36\ kV$ to $+36\ kV$ and vice versa. The magnitudes of the control currents have been taken from the general parameters of Table 2.8. Despite the individual acceleration voltages, the magnitudes for the currents are suitable for each charging situation, taking also into account the technical circumstance of the proposed devices. The resulting 12 cases are plotted in Figure 2.13. It can be seen that the highest charging time is not greater than 100 ms. The sharp bend in the curves, located at zero voltage for each one is due to the sudden appearance the stabilisation current. Due to the charging dynamics explained in 2.4.2, it is necessary to pull the SC potential in direction to zero, when $sign(V_{SC}) = sign(V_{des})$.

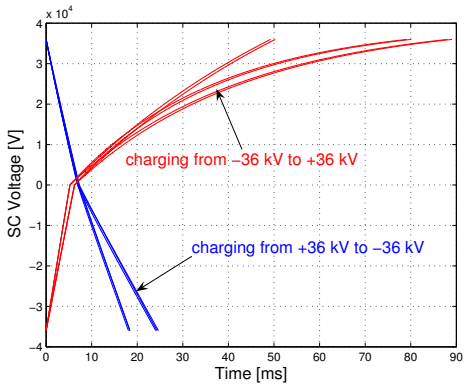

Figure 2.13: Charging durations for the plasma cases 1-3 in Table 2.4 for different charging situations; control current parameters from Table 2.8

2.4.4 Residual forces analysis

The acquisition of a certain potential demands the ejection of charged particles of different species. While it is intended to exploit the electrostatic effects between the charged SC, also the actual emission of the particles creates a force. For the proposed devices these are electrons and Xenon ions or protons. This force will probably show in an unsuitable direction and is therefore being considered as completely residual.
Using a convenient alignment of two simultaneously operated devices, the repulsion forces could be canceled. However, for the case of design restrictions or the failure of a device it is important to be aware of the order of magnitude of the expected disturbances.
At conventional ion thrusting, the repulsion force is dependent on the acceleration voltage of the device. Considering EA, also the potential of the SC itself has to be taken into account. Depending on the magnitude of the SC potential and its sign, it is additionally accelerating or decelerating the particle. The final exhaust velocity is dependent on the remaining energy, that an ejected particle still possesses, after it leaves the influence of the SC. Considering an emitted current $I_{emission}$, with a remaining energy of ΔE for each charge carrier and the charge-mass $\rho_{q_{species}}$ (please refer Eq.(2.18)) , the residual force accounts to:

$$F_{res} = \dot{m}_{species} c_e = I_{emission} \rho_{q_{species}} \sqrt{\frac{2\Delta E}{m_{species}}} \tag{2.25}$$

Residual forces due to ΔE are caused from both the charging current and the stabilisation current. The determination of ΔE is shown in Eq.(2.26).

$$\begin{aligned} \Delta E \quad = \quad & \begin{cases} I_{charge} & : \quad |qV_{des}| + qV_{SC} \cdot sign(q_{species}) \\ I_{stabilize} & : \quad \text{release energy} + qV_{SC} \cdot sign(q_{species}) \end{cases} \\ \text{where} \quad & \begin{aligned} \text{sign(Xenon)} &= +1 \\ \text{sign(electron)} &= -1 \\ \Delta E = 0 \quad & \text{if} \quad \Delta E \leq 0 \end{aligned} \end{aligned} \tag{2.26}$$

At first the residual forces at an established formation shall be considered, where the SC charges vary only in small ranges. With the SC at its desired voltage, a part of the charging current is leaving the SC to balance the sum of I_{st} and the natural fluxes. It is possessing a low excessive energy in the range of $0 - 20\ V$, as described in 2.4.2. The highest expected force due to the leaving part of I_{ch} will occur for a negative desired voltage in the sunlit part of the orbit. There the stabilization current and the natural current sum to $I_{ion} = 73\ \mu A + 65\ \mu A = +138 \mu A$, which are balanced by an leaving I_{ch} of $-138 \mu A$. The resulting force is in the order of 1 μN.
The forces due to the stabilisation current are negligible, when caused by electrons. For positive desired SC voltages, where I_{st} would consist of Ions, the current can be switched off, as there is no environmental current pulling the SC to higher positive potentials, except in the range between zero and a few tens of Volts. The contribution of the stabilisation current in achieved formations can thus be neglected for all species.
Higher force have to be expected during acquisition maneuvers, where the desired voltage is frequently changing. Also here the high residual forces are caused by the emission of ions, building either I_{ch} or I_{st}. The highest values are experienced, when the SC is told to change its voltage from $+36\ kV$ to $-36\ kV$. In this situation the ions are accelerated twice, once by the ion thruster and once by the highly positive charged SC itself. For an I_{ch} of $-250\ \mu A$ the force (Xenon ions) will amount to 110 μN at $+36\ kV$, and fast decrease during the approach to the desired voltage. For the complimentary case of charging from $-36\ kV$ to $+36\ kV$, I_{ch} will consist of electrons and create a small force in the sub-μN-area (please refer Table 2.11).
Forces due to the stabilisation current are considerable for a positive desired voltage. Due to the low release energy the contribution of the thruster system is low, but the particles will be accelerated by the electric field of the SC itself. The force increases for higher positive potentials and will possess a highest value of 58 μN at a SC voltage of $+20\ kV$.
The second source for residual forces is the working principle of the RIT itself. Depending on the ionisation rate, there is always an amount ($2 - 5\ \frac{\mu g}{s}$ [31]) of neutral gas leaving the ionisation tube into space. Considering a neutral flow of around 5 $\frac{\mu g}{s}$ and a gas release temperature T_{Xe} of 500 K, the residual force is in the order of $1 - 2\ \mu N$.
Refering to Table 2.11, the residual forces during the formation keeping, where the

	worst case formation keeping V_{des} is varying in small range	worst case acquisition V_{des} may change rapidly	neutral gas release
Xe^{+1}	0.72 μN constant (I_{ch})	110 μN short period (I_{ch})	1.25 μN
	-	78 μN constant (I_{st})	
H^+	$\ll 1$ μN constant (I_{ch})	10 μN short period (I_{ch})	< 1 μN
	-	6.8 μN constant (I_{st})	
electrons	$\ll 1$ μN constant (I_{ch})	0.3 μN short period (I_{ch})	-
	$\ll 1$ μN constant (I_{st})	$\ll 1$ μN constant (I_{st})	

Table 2.11: worst case residual forces for electric actuation; RIT-4 as ion delivering device; control current parameters from Table 2.8

charges have to be kept constant have a maximum order of 1 μN (Xenon). During acquisition maneuvers the residual forces might be much higher, depending on the gradient of the desired voltage. In the following study (see chapter 4), $V_{des}(t)$ possesses low gradients for most of the maneuvers, thus the appearance of such high forces is unlikely. A problem of more importance is represented by the stabilisation current at very high SC voltages, which are e.g. probable during long distance periods in the course of an acquisition maneuver or in certain formations.
An interesting approach would be the substitution of the ion-delivering gas with Hydrogen, as it is the species with the lowest achieveable weight per charge. H^+ ions consist only of one proton. Refering to [31] the utilisation of Hydrogen in a RIT engine has already been proven to be feasible. With a further reduction of the size of the thruster from RIT-4 to RIT-1 the lower limit of the emitted currents could be reduced to a value of 100 μA. For an acquisition maneuver this would decrease the highest possible force caused by I_{st} to 2.7 μN.

	worst case formation keeping V_{des} is varying in small range	worst case acquisition V_{des} may change rapidly
H^+	$\ll 1$ μN constant (I_{ch})	5 μN short period (I_{ch})
	-	2.7 μN constant (I_{st})
electrons	$\ll 1$ μN constant (I_{ch})	0.1 μN short period (I_{ch})
	$\ll 1$ μN constant (I_{st})	$\ll 1$ μN constant (I_{st})

Table 2.12: worst case residual forces for electric actuation; RIT-1 engine as ion delivering device; control current parameters of Table 2.9

It could even be further reduced by generally not using a stabilisation current for pos-

itive V_{des} and thus relying on the natural currents to get from higher to lower positive charges. If the charging durations Δt_{charge} would be too long, another way would be to introduce a specialized device for the release of low energy protons in the range of $0-10\ \mu A$ (depending on Δt_{charge}). Doing that, the lower current limit of the RIT could be overcome and the residual forces would fall below the sub-μN area.

2.4.5 Comparison between Coulomb thrusting and repulsion forces

In this section the mass flows needed to apply the electric actuation shall be compared with the ones needed for conventional ion thrusting. When the electric actuation system is utilised, a current of charged particles is emitted to bring the SC to a certain charge level and to maintain it. The mass flow due to a current I amounts to (please refer Eq.(2.18))

$$\dot{m} = I\rho_{q_{species}}$$

The ion delivering species considered in this report are Xenon and Hydrogen, while the mass flow of electrons will be neglected. In the following, different control setups, listed in Table 2.13 are evaluated. Setup 1 is utilising the present technology device RIT-4 and the electron gun. It is evaluated with the parameters from Table 2.10. By changing to the RIT-1 engine in setup 2, lower currents in the order of 100 μA become feasible. Exploiting this limit, Δt_{charge} can be set to a less demanding value of 10 s. Following Eq.(2.24) the highest mass flow relevant ion current amounts to $-132\ \mu A$. Setup 3 is a change from the robust control evaluated in this study to a different method, mentioned in the end of section 2.4.2. Following that scheme, the environmental currents are exactly balanced to maintain a charge. Furthermore an amount of $-1\mu A$ (the negative sign is due to the exclusive consideration of Ions) ensuring $\Delta t_{charge} = 10\ s$ at each V_{SC} is added. This approach is included to get an impression, what could be gained from further developments in terms of mass flow efficiency. The highest natural currents which have to be balanced using Ions occur at negative desired voltage due to the photoflux in sunlight. Refering to Figure 2.8 these currents will be in the order of 65 μN. It should be noted that for scheme 3, which requires feedback control, a continuous measurement of the SC potential level and the plasma parameters is needed.
The evaluation has been carried out for two SC, making the following assumptions:

- SC charges $q_1 = q_2$
- SC radius $r_{SC} = 0.5\ m$
- charge level $|q_i| \leq 2\ \mu C \Rightarrow |V_{SC_i}| \leq 36\ kV$
- 100 % ionisation rate (no neutral gas emission)

setup	control parameters	Ion control current (negative)
1 (robust approach)	RIT-4 & electron gun; $\Delta t_{charge} = 1\ s$, $I(\Delta t_{charge}) = 8\mu A$	$-250\ \mu A$
2 (robust approach)	RIT-1 & electron gun; $\Delta t_{charge} = 10\ s$ $I(\Delta t_{charge}) \approx 1\ \mu A$	$-132\ \mu A$
3 (feed-back control)	low emission device; $\Delta t_{charge} = 10\ s$ $I(\Delta t_{charge}) \approx 1\ \mu A$	$I_{nat}(V_{SC}) - 1\mu A$

Table 2.13: Ion current parameters for the evaluation of mass flows

With these conditions the mass flows have been calculated to realise electrostatic forces between 0 μN and 100 μN. The calculations had been carried out for different distances r_{12} between the satellites.
The ion thruster utilised for EA could also be used to do conventional ion thrusting. Therefore it is interesting to calculate the mass flows needed to generate the same force range of $F = 0 - 100\ \mu N$. The acceleration voltage of the thruster is set to the highest one of the charge actuation system. Thus the mass flow is determined by:

$$\dot{m} = \frac{F}{c_e} = F \cdot \sqrt{\frac{m_{species}}{2qV_{acc}}} \tag{2.27}$$

$$\text{with} \qquad V_{acc} = 36\ kV$$

Without any technical limitations, especially in the near zero thrust area the conventional ion thrusting mass flow is represented as a straight line in Figure 2.14(a), which is naturally independent of the distance between the SC. The robust control schemes can be seen as straight lines, which are caused by the constant emission currents. The crosses on the lines mark the maximum force, which can be achieved in that particular distance r_{12}. Higher forces for each r_{12} would only be possible via increasing the SC charge over the limit of 2 μC. The red coloured curves in the lower part of Figure 2.14(a) represent the adaptive approach of setup 3. Due to the scheme, the emitted currents are dependent on the natural fluxes. With increasing demanded forces, also the SC charges increase. Higher charges cause growing natural fluxes, and thus the mass flow to balance the system assumes greater values.
It can be seen, that for the application of Xenon ions, the robust approaches have a higher massflow than conventional thrusting for force values lower than 75 μN (setup 1) or 40 μN (setup 2). Furthermore these forces are only achieveable in distances lower

than 30 m (setup 1) or $\approx$ 20 m (setup 2). The conventional system is in advance, because the robust control approaches emit always the same current. In the case of adaptive application, the preference of the conventional system drops to a thrust value of $\approx 20_{\mu}N$ for a inter SC distance of less than 40 m.
A clear improvement in terms of applicability of the EA is achieved, when substituting the ion delivering species from Xenon to Hydrogen. This is displayed in the Figures 2.14(b) to 2.14(d). Here the robust control approaches are in advance already at 3.5 μN or 7 μN. The adaptive approach is to be preferred for forces higher than 1.5 μN with an applicability for distances less than $\approx$ 100 m. The utilisation of EA with hydrogen as ion delivering gas is a promising approach, which has clear advances in terms of mass flow for most of the force range. The limits of application are given by the distance in the upper force range and by the mass flow efficiency in the lower force region.

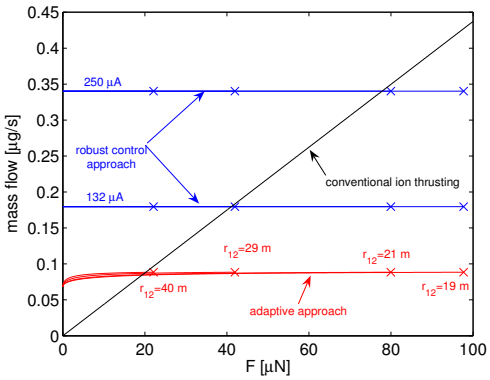

(a) mass flows with Xenon as ion delivering gas

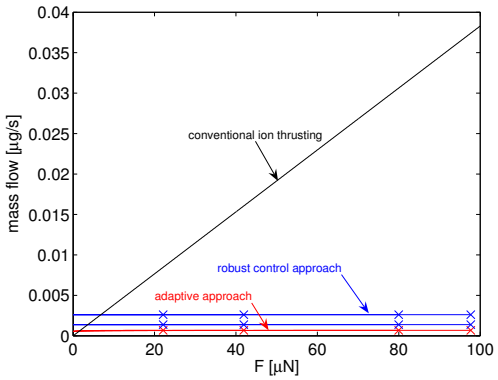

(b) mass flows with Hydrogen as ion delivering gas

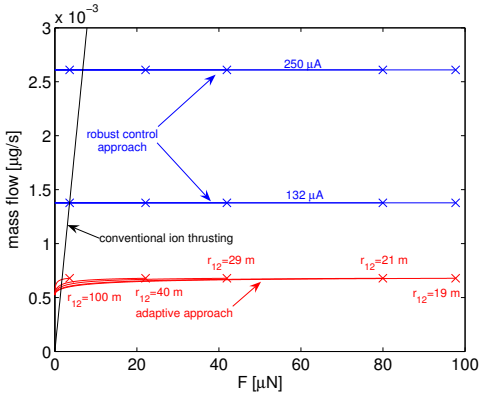

(c) zoom into Figure 2.14(b)

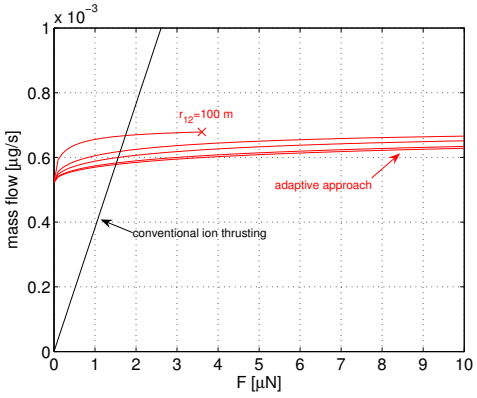

(d) zoom into mass flow values of adaptive approach

Figure 2.14: Comparison of mass flows between electrostatic actuation and conventional ion thrusting

2.5 Conclusion

In this chapter a scheme for a possible Hybrid Propulsion System has been developed. The best suitable environment for the application of electric fields is the GEO orbit because it possesses a high Debye length. Due to environmental effects in this space region the potential of a non charge controlled SC is subject to continuous changes. After a survey of existing technology and the consideration of technical limits a system consisting of the RIT-4 or RIT-1 engine and an electron gun has been chosen. With the application of Hydrogen as ion-delivering gas, the mass flow efficiency is in advance to conventional ion thrusting for most of the intended force range. The devices are operated

simultaneously for the emission of two fluxes, the charging current and the stabilisation current. Their sign and magnitude are determined, depending on the actual desired SC voltage. The combination of the two currents creates a voltage current charateristic of the SC plasma system, which drives the SC from any voltage to the desired one and keeps it there. This is valid also for the worst case environmental conditions expected at GEO. The approach has been chosen in a trade off of simplicity and applicability. All requirements of Table 2.5 are fulfilled and thus a fast and robust control of the individual SC charges is provided.

3 Verification of the level of compatibility of the ES and the CS concepts

3.1 Mathematical background

In this section a brief introduction to the mathematical modelling used for both the ES and the CS concept will be presented in order to highlight which problems exist concerning the integration of the two concepts and to better introduce the solution approaches that will be explained in the forthcoming sections.

3.1.1 Equilibrium Shaping

The ES technique aims at steering a swarm of N homogeneous satellites to acquire a target formation in orbit in a way such that each spacecraft belonging to the swarm can autonomously decide which position it will take in the final configuration. This method draws its inspiration from behavior based techniques and designs a desired velocity field as a sum of different behavioral contributions acting at different length scales. For each spacecraft three velocity vectors are considered each of them taking over one of the tasks that each spacecraft at any time has, to gather with the rest of the group, to avoid any collision and to dock in the final target configuration. The resulting expression for the desired velocity of the $i-$th spacecraft is

$$\mathbf{v}_{d_i} = \mathbf{v}_i^{Gather} + \mathbf{v}_i^{Avoid} + \mathbf{v}_i^{Dock} \tag{3.1}$$

where each velocity vector in Eq.(3.1) is relative to the velocity of the target formation center of mass. The $\mathbf{v}_i^{Avoid}$,$\mathbf{v}_i^{Dock}$ and $\mathbf{v}_i^{Gather}$ vectors are themselves sums of different contributions and their main characteristics are listed below:

- **Gather behavior:** This behavior introduces N different global attractors towards the N targets belonging to the formation to be acquired. The $\mathbf{v}_i^{Gather}$ vector is the weighted sum of all these N attractive contributions with weighting parameters $c_1.....c_N$.

$$\mathbf{v}_i^{Gather} = \sum_j c_j \psi_G(\|\boldsymbol{\xi}_j - \mathbf{x}_i\|)(\boldsymbol{\xi}_j - \mathbf{x}_i)$$

- **Avoid behavior:** This local behavior drives the spacecraft away from each other when they are in a dangerous condition of close proximity.

$$\mathbf{v}_i^{Avoid} = \sum_j b\psi_A(\|\mathbf{x}_i - \mathbf{x}_j\|, k_A)(\mathbf{x}_i - \mathbf{x}_j)$$

- **Dock behavior:** This behavior introduces N different local attractors towards the N targets belonging to the formation to be acquired. Also in this case the $\mathbf{v}_i^{Dock}$ vector is a weighted sum of all these N contributions with weighting parameters $d_1.....d_N$.

$$\mathbf{v}_i^{Dock} = \sum_j d_j\psi_D(\|\boldsymbol{\xi}_j - \mathbf{x}_i\|, k_D)(\boldsymbol{\xi}_j - \mathbf{x}_i)$$

At any time the desired velocity vector is the sum of all these contributions and therefore it depends linearly on the weighting parameters c_j,d_j. If we want the target configuration to be achieved and kept, whenever the swarm of satellites acquires the final formation, the desired velocity vector associated to each spacecraft must be zero

$$\begin{aligned} &\mathbf{v}_{d_i} = \mathbf{v}_i^{Avoid} + \mathbf{v}_i^{Dock}(d_j) + \mathbf{v}_i^{Gather}(c_j) = 0 \\ &i = 1.....N, j = 1.....N. \end{aligned} \tag{3.2}$$

This condition results in a set of linear scalar equations

$$\mathbf{A}\left[c_1, .., c_N, d_1, .., d_N\right]^T = \mathbf{g} \tag{3.3}$$

The matrix $\mathbf{A}$ and the vector $\mathbf{g}$ depend on the functions ψ chosen to represent the various behaviors and on the target positions. A typical acquisition maneuver steered by means of the ES technique is displayed in Figure 3.1. Eq.(3.3) represents, for each target disposition and for each choice of the parameters k_D, k_A and b, a linear set of equations in the $2N$ unknowns c_j, d_j. Depending on the spatial distribution of the target points we might be able to find solutions. Therefore not all possible formations can be acquired using this technique. Conditions of compatibility of a target formation with the ES technique have been derived in [8]. If the formations to be achieved have particular properties of symmetry (see again [8] for a detailed analysis) then the number of independent equations reduces and the system eventually becomes solvable.
In Table 3.1 some formations are listed with its number of independent equations and unknowns in the associated inverse dynamic calculation. In Figure 3.2 some of these formations are shown. All the formations for which the number of unknowns is larger than the number of equations can be acquired using the ES technique. The ES technique imposes on the target formation only a constraint on the relative positioning between the SC. It does not require any special attention to the orientation of the formation with respect to any reference frame. On the other hand also the characteristic length of

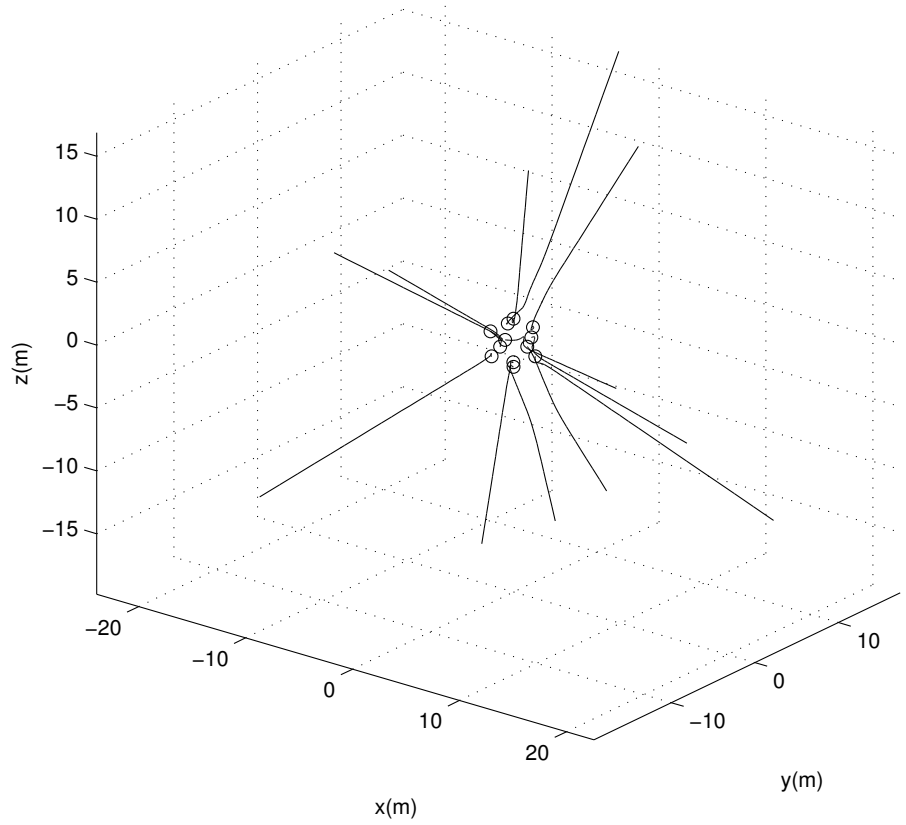

Figure 3.1: Swarm of 12 satellites acquiring an icosahedron shaped formation.

the target formation can vary freely and is constrained only by the sphere of influence characterized by the position sensors mounted on board the SC. Therefore every formation that can be acquired using the ES technique actually identifies an entire set of ∞^4 different configurations in the reference frame.

3.1.2 Coulomb Satellites

The CS system consists of a group of satellites in an orbital environment each of them with a particular value of electric charge. A sketch of a Coulomb satellite formation is given in Figure 3.3. The force acting on each charged spacecraft belonging to the formation can be split in two different contributions. The first one comes from the inertial and gravity force and the second one comes from the electrostatic interaction between different spacecraft influenced by the ambient plasma media. In particular the latest effect can be modelled using the Coulomb expression scaled with an exponential

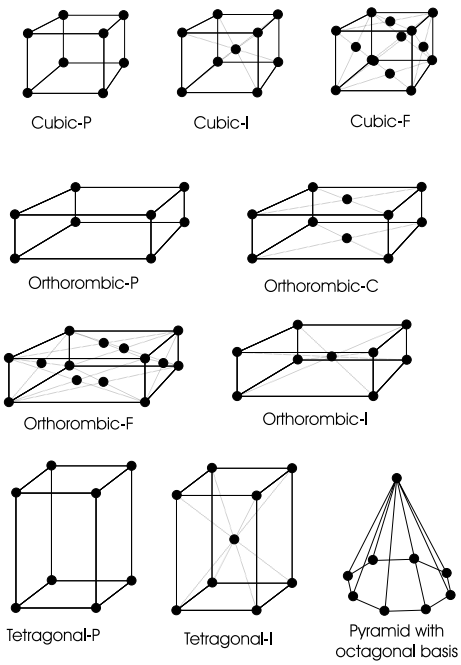

Figure 3.2: Formation shapes that can be acquired by means of the ES technique.

term depending on the Debye length λ_d [12]

$$\begin{aligned} &\mathbf{u}_{el} = \frac{\kappa_c}{m_i} q_i \sum_{j=1}^{N} q_j \frac{\mathbf{r}_{ij}}{|\mathbf{r}_{ij}|^3} e^{-\frac{|\mathbf{r}_{ij}|}{\lambda_d}} \\ &i \neq j \end{aligned} \tag{3.4}$$

In Eq.(3.4) $\mathbf{r}_{ij} = \mathbf{r}_i - \mathbf{r}_j$ is the relative position vector between the $i-$th and the $j-$th spacecraft, κ_c represents the Coulomb constant, q_i and q_j are the charging levels of the $i-$th and $j-$th satellite respectively and m_i is the $i-$th spacecraft mass. Using this expression and under the assumption that the center of the CS formation is on a circular orbit, the inertial and gravity gradient induced accelerations can be expressed using the Clohessy-Wiltshire equations

$$\begin{cases} \ddot{x}_i - 2n\dot{y}_i - 3n^2 x_i = \mathbf{u}_{el_i} \cdot \hat{\mathbf{i}}_H \\ \ddot{y}_i + 2n\dot{x}_i = \mathbf{u}_{el_i} \cdot \hat{\mathbf{j}}_H \\ \ddot{z}_i + n^2 z_i = \mathbf{u}_{el_i} \cdot \hat{\mathbf{k}}_H. \end{cases} \tag{3.5}$$

In Eq.(3.5) n is the orbital mean motion of the Hill's frame, $[x_i, y_i, z_i]^T$ represent the coordinates of the $i-$th spacecraft and $[u_{el_x}, u_{el_y}, u_{el_z}]^T$ is the electrostatic induced specific force, both projected in the Hill's reference frame of unit vectors $[\hat{\mathbf{i}}_H, \hat{\mathbf{j}}_H, \hat{\mathbf{k}}_H]$(see Figure 3.3). Writing Eq.(3.5) for each satellite belonging to the swarm yields a set of $3N$ scalar

Formation shape	Number of equations	Number of unknowns
All regular solids	1	2
All regular polygons	1	2
Pyramids with a regular basis	3	4
Cubic-P	1	2
Cubic-I	1	4
Cubic-F	2	4
Tetragonal-P	2	2
Tetragonal-I	2	4
Orthorhombic-P	3	2
Orthorhombic-I	3	4
Orthorhombic-C	4	4
Orthorhombic-F	6	4
Hexagonal-P	3	4

Table 3.1: Count of the equations and the unknowns for different formations.

coupled equations describing the dynamics of the whole CS system. In [13],[14],[15] an analysis aimed at finding the static equilibrium positions for the system in Eq.(3.5) has been performed. In particular in [13] a first study has been performed on some simple configurations for which an entire set of static solutions has been found. Moreover the static solution with the minimum charge level associated to the SC in the formation has been computed. In [14] an analogous analysis has been performed without imposing any constraint on the shape of the formation. The static solution of Eq.(3.5) have been computed by means of a Genetic Algorithm (GA) optimization technique. In [15] an analytical approach has been used in order to solve the same problem for simple regularly shaped two-three SC formations.

3.2 Equilibrium position selection: problem definition

The set of equations describing the motion of SS can be easily derived from Eq.(3.5) by adding the specific force due to the conventional (thrusting) actuation system

$$\begin{cases} \ddot{x}_i - 2n\dot{y}_i - 3n^2 x_i = (\mathbf{u}_{el_i} + \mathbf{u}_{th_i}) \cdot \hat{\mathbf{i}}_H \\ \ddot{y}_i + 2n\dot{x}_i = (\mathbf{u}_{el_i} + \mathbf{u}_{th_i}) \cdot \hat{\mathbf{j}}_H \qquad , i = 1, .., N \\ \ddot{z}_i + n^2 z_i = (\mathbf{u}_{el_i} + \mathbf{u}_{th_i}) \cdot \hat{\mathbf{k}}_H. \end{cases} \tag{3.6}$$

where the expression for $\mathbf{u}_{el}$ is given in Eq.(3.4).

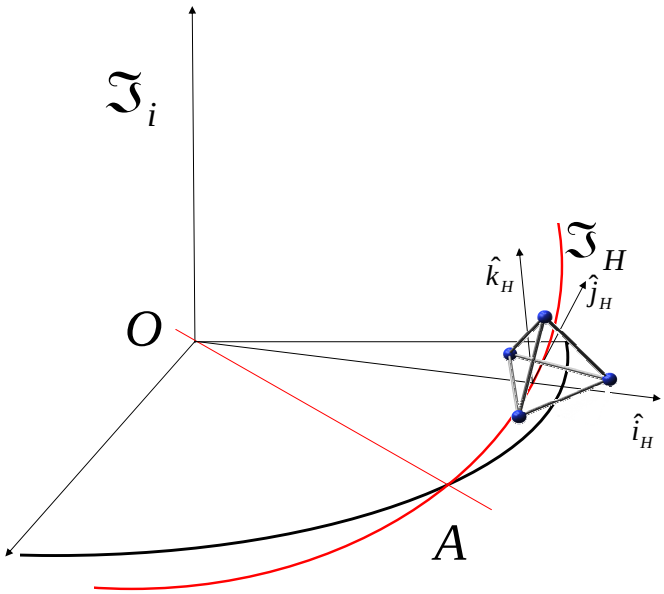

Figure 3.3: Satellitron Satellite formation baseline. $\mathcal{F}_i$ represents the inertial reference frame. $\mathcal{F}_\mathcal{H}$ represents the Hill's reference frame (LHLV).

The compatibility between the two concepts is defined as follows:
Definition: The ES and the EA concepts are said to be compatible for a given formation if:

- *the formation can be acquired using the ES path planning technique*
- *the formation is an equilibrium position for the system of equations in Eq.(3.6) with* $||\mathbf{u}_{th_i}|| = 0, \forall i = 1, .., N$.

It is interesting to remark that if the second condition in the definition above is satisfied the electrostatic forces balance perfectly the inertial ones. Therefore if the non-Keplerian contributions are neglected the formation can be maintained just relying upon the electrostatic forces.
In this work we propose a numerical approach based on a Differential Evolution (DE) optimization algorithm. The static equilibrium configuration for the system describing the motion of SS can be found by solving Eq.(3.7) for the charging values and for the

positions of each SC:

$$\begin{cases} -3n^2 x_i = (\mathbf{u}_{el_i} + \mathbf{u}_{th_i}) \cdot \hat{\mathbf{i}}_H \\ 0 = (\mathbf{u}_{el_i} + \mathbf{u}_{th_i}) \cdot \hat{\mathbf{j}}_H \qquad , i = 1, ..., N. \\ n^2 z_i = (\mathbf{u}_{el_i} + \mathbf{u}_{th_i}) \cdot \hat{\mathbf{k}}_H \end{cases} \tag{3.7}$$

Eq.(3.7) can be easily obtained by dropping in Eq.(3.6) all the terms where velocity or acceleration appear. For a swarm of N SC Eq.(3.7) is a set of $3N$ coupled nonlinear equation. Following the definition of compatibility given above, the searching strategy is aimed at finding among all the possible formations that can be acquired by means of the ES technique and that are solutions of Eq.(3.7) the one for which $||\mathbf{u}_{th_i}|| = 0$, $\forall i = 1, .., N$.
With this intention the selected search strategy starts from a possible target configuration that can be acquired by means of the ES technique. As already remarked a configuration solution of the ES formula corresponds to a set of formations in the Hill's frame. Once the inter-SC relative geometry is fixed the searching procedure tries to find among all the possible solutions of Eq.(3.7):

- the orientation of the formation with respect to the Hill's reference frame
- the characteristic length of the formation
- the spacecraft charging levels

such that $||\mathbf{u}_{th_i}|| = 0$, $\forall i = 1, .., N$. According to this strategy the parameter vector $\mathbf{p}$ for a swarm of N spacecraft contains $N + 4$ variables

- q_i- charge level of the i-th SC
- $[\phi, \theta, \psi]$- Euler angles identifying the orientation of the formation in the Hill reference frame
- r- characteristic length of the formation.

Note that this is a reduced search space with respect to the approach used in [14] since the formation we are searching are constrained to belong to the set of formations acquirable by means of the ES technique, i.e. the inter-SC relative geopmetry is held fixed. Moreover some inequality constraint have been included in order to take into account the physical limitations connected with EA concept. In particular the maximum value of the characteristic length of the spacecraft formation has been bounded such that the average distance between the satellites is below the Debye length. In this way the masking exponential factor in Eq.(3.4) can be neglected. The issues concerning these simplifications will be addressed in section 3.6. In [15] it has been observed that a general

formation that is a static equilibrium configuration of Eq.(3.5) must have its center of mass on the $\hat{\mathbf{j}}_H$ axis of the Hill's reference frame. Moreover the formation principal inertia axes must be aligned with the Hill's reference frame axes. Whereas the first condition is automatically ensured in our setting by the definition of the search space the second one is not. In particular introducing the second condition in our strategy would mean constrain the Euler angles to take only some values in their range. This has not been applied directly in the search strategy used in this work since the optimization algorithm requires in input continuous ranges of variations for the variables in the search space rather than discontinuous ones.

3.3 Cost function definition

In this section the cost function used in order to find the equilibrium position of Eq.(3.5) is introduced. The first step in order to successfully apply an optimization algorithm to this problem is to rescale the variables of the problem. In this way the variables belonging to the search space will have the same order of magnitude and numerical problems will be mitigated. Following the approach proposed in [14] the following definitions are set:

$$\tilde{\mathbf{u}} = \frac{\mathbf{u}}{n^2} \tag{3.8}$$

$$\tilde{q}_i = q_i \frac{\sqrt{\kappa_c}}{n}. \tag{3.9}$$

where $\mathbf{u}$ is a generic specific force acting on the SC. Substituting these definitions into Eq.(3.7) yields the following set of equation for $i = 1, ., N$:

$$\begin{cases} 3x_i + \frac{\tilde{q}_i}{m_i} \sum_{j=1}^{N} \tilde{q}_j \frac{x_i - x_j}{|\mathbf{r}_i - \mathbf{r}_j|^3} = \tilde{\mathbf{u}}_{thr_i} \cdot \hat{\mathbf{i}}_H \\ \frac{\tilde{q}_i}{m_i} \sum_{j=1}^{N} \tilde{q}_j \frac{y_i - y_j}{|\mathbf{r}_i - \mathbf{r}_j|^3} = \tilde{\mathbf{u}}_{thr_i} \cdot \hat{\mathbf{j}}_H \\ -z_i + \frac{\tilde{q}_i}{m_i} \sum_{j=1}^{N} \tilde{q}_j \frac{z_i - z_j}{|\mathbf{r}_i - \mathbf{r}_j|^3} = \tilde{\mathbf{u}}_{thr_i} \cdot \hat{\mathbf{k}}_H. \end{cases} \tag{3.10}$$

Since the purpose of the search procedure is to find the static equilibrium position of the system for which $||\tilde{\mathbf{u}}_{thr_i}|| = 0$, $\forall i = 1, .., N$ then the first cost function used to solve Eq.(3.10) is simply

$$C_1(q_1, .., q_N, \phi, \theta, \psi, r) = C_1(\mathbf{p}) = \frac{\sum_{i=1}^{N} ||\tilde{\mathbf{u}}_{thr_i}||}{N} \tag{3.11}$$

In this study in order to render the search procedure easier all the SC are supposed to have the same mass set to $m_i = 1kg$. The cost function defined in Eq.(3.11) does not encounter the problems described in [14] (i.e. always converging to the solution with all the SC aligned on the $\hat{\mathbf{j}}_H$ axis) because the relative formation geometry is held fixed

here during the search. On the other hand the solution obtained with the cost function in Eq.(3.11) is often a boundary solution in the r variable. A different approach to the search of the equilibrium position has therefore been introduced. In particular the analysis is changed to find among all the possible formations that can be acquired by means of the ES path planning technique those that have the lowest portion of specific force to be provided by means of the thrusting actuation system. In this case the search strategy aims at finding those formations that minimize the average rate between the specific force required from the thrusting system and the required total specific force, i.e.

$$C_2(\mathbf{p}) = \frac{1}{N}\sum_{i=1}^{N}\frac{||\tilde{\mathbf{u}}_{thr_i}||}{||\tilde{\mathbf{a}}_{g_i}||}. \tag{3.12}$$

In Eq.(3.12) $\tilde{\mathbf{a}}_{g_i}$ denotes the gravitational acceleration (specific force) acting on the $i-$th SC. The solution of this problem will find those formations in space for which it is highest the advantage of using EA given a certain relative geometry. A possible application for such formations can be self assembly of large structures in space. For such applications it may be only needed to acquire a certain formation in space no matter of its orientation in the Hill reference frame or its characteristic length (to a certain extent). When this cost function is considered different solutions have been found. Moreover the optimizer does not always converge to the lower bound of the parameter r.

3.4 Differential Evolution optimization algorithm

In this section a brief review of the optimization algorithm used to solve the problem outlined in section 3.3 is introduced. The algorithm proposed is the Differential Evolution (DE) introduced by Storn et.al.[36]. This technique is a very simple population based, stochastic function minimizer which is very powerful at the same time. A simple sketch explaining the way in which the algorithm is working is displayed in Figure 3.4. This technique utilizes at each iteration a pre-defined number NP of parameters vectors called population. Each member $\mathbf{p}_i$ of the population is a possible solution of the optimization problem i.e. it is possible to associate to each member of the population a value of the objective function. In our case for a swarm of N spacecraft each population vector contains $N+4$ parameters $\mathbf{p}_i = [p_i^i, ..., p_{N+4}^i]$. The initial population is chosen randomly. At each iteration to each member of the population $\mathbf{p}_i$ a trial vector is associated. The trial vector is produced by adding the weighted difference vector between two population members to a third member

$$\mathbf{v} = \mathbf{p}_{r1} + F(\mathbf{p}_{r2} - \mathbf{p}_{r3}).$$

where F is a parameter to be chosen from the user and $r1, r2$ and $r3$ are randomly chosen integer numbers smaller than NP. If the resulting trial vector yields a lower objective

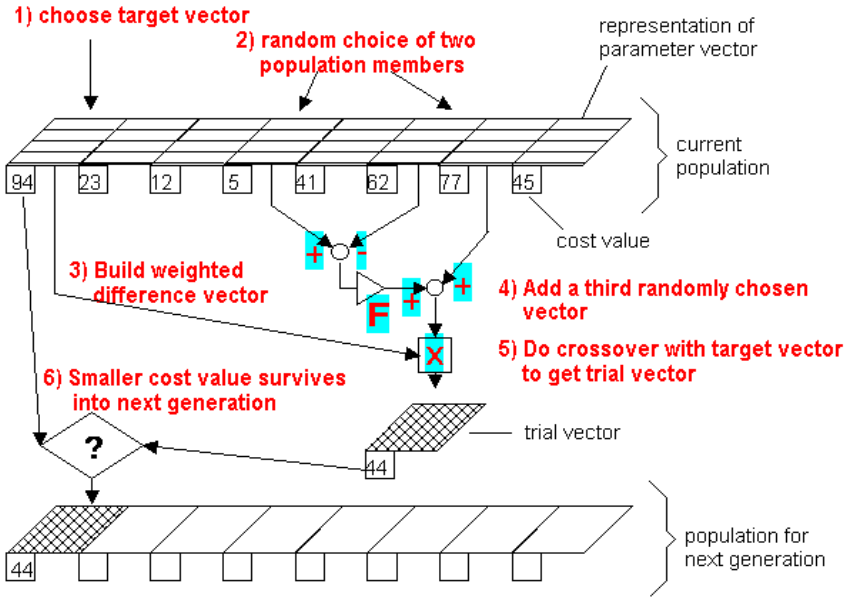

Figure 3.4: Sketch of the DE algorithm.

function it replaces the one with which it was compared. The comparison vector itself can be part of the trial vector generation process. Moreover for each generation the best parameter vector is evaluated in order to keep track of the progress in the overall optimization process. A mutation scheme is also included into the algorithm so that the DE is more capable of escaping the eventual local minima. The mutation process is similar to what is called crossover in the GA framework. This process simply changes some randomly chosen elements of the trial vector keeping them equal to the ones of the comparison vector. Therefore for a given comparison vector $\mathbf{p}_i$ the final trial vector $\mathbf{u}$ after mutation becomes

$$u_j = \begin{cases} u_j = v_j \quad if \quad j < L \cup j > L + M \\ u_j = p_i^j \quad if \quad j > L \cup j < L + M \end{cases}$$

where L and M are randomly chosen positive integer numbers whose sum, in our case, is$\leq N + 4$. As for all the Evolutionary algorithms this method offers several advantages over the most traditional optimization methods. In particular the DE algorithm does not need an initial guess and allows to search the solution in the parameter space in a more global manner. By combining together the different vectors of each population by means of the differential scheme or using the mutation the search space is in fact spanned in a more complete way and a more global solution may be found. The DE algorithm is

therefore an attractive alternative for the solution of the optimization problem defined in the previous sections that involves the solution of an highly coupled nonlinear set of equations.

3.5 Compatibility test outcome for GEO environment

In this section the solution of the compatibility test will be presented. When the GEO environment is considered the variables belonging to $\mathbf{p}$ are set to vary in the following ranges:

- $\tilde{q}_i \in [-400, 400]$
- $\phi \in [0, \pi]$
- $\theta \in [-2\pi, 2\pi]$
- $\psi \in [-2\pi, 2\pi]$
- $r \in [5, 100]$.

In particular the selected maximum value of the nondimensional charge has been selected according to the following ideas. Let the swarm being made of spherical SC with $D = 1m$ diameter. Then it is possible to simply relate the charge on the surface of the SC with the $i-$th SC potential V_i

$$V_i = \frac{q_i \kappa_c}{R}.$$

In [13] it has been demonstrated that with a 200 mW power supply available on board it is possible to charge in GEO a $D = 1\ m$ diameter spherical SC of 6 kV in 8 $msec$. Such a voltage can be easily related to the corresponding value of the non-dimensional charge

$$\tilde{q}_i = \frac{V_i D}{2n\sqrt{\kappa_c}} = 435.32\sqrt{N}m.$$

On the other hand the bounds on the characteristic length of the formation have been selected to be less than the corresponding Debye length evaluated for the selected operation orbit (GEO orbit). A Matlab tool has been developed that allows to find the solution for such a problem and to provide a visualization of the final formation achieved. Some examples of the results obtained with this tool are displayed below.
In Table 3.2 the best values of C_1 and C_2 over 20 runs of the DE algorithm are presented. These values have been divided by the number of spacecraft in the formation so that both can give an indication of the average absolute and relative non dimensional residual acceleration acting on each spacecraft. Moreover in Table 3.2 also the average cost function ($\overline{C}_i$) and the standard deviation (σ_{C_i}) computed over the runs of the optimizer

are included. These values give reason of the optimizer different behavior with respect to the optimization problems in Eq.(3.11) and in Eq.(3.12).

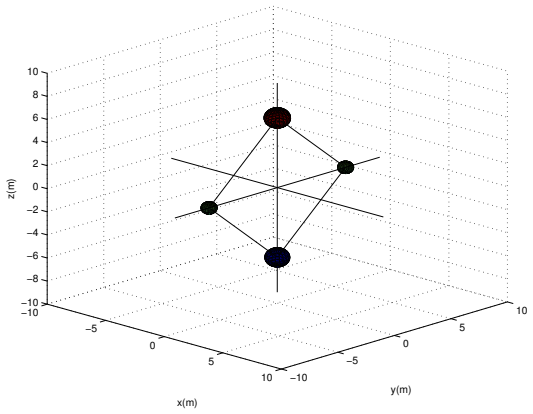

(a) Four spacecraft equilibrium formation C_1.

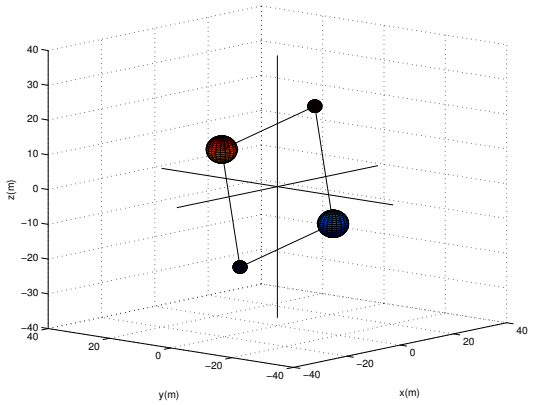

(b) Four spacecraft equilibrium formation C_2.

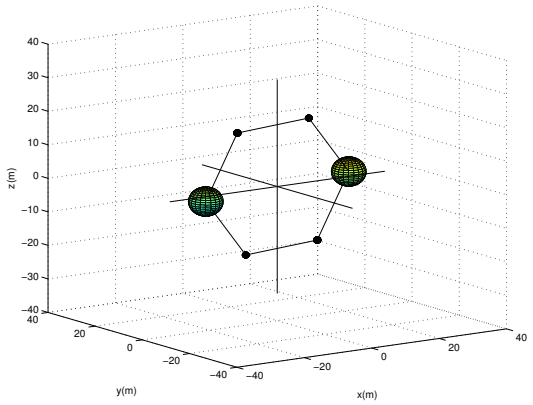

(c) Six spacecraft equilibrium formation C_1.

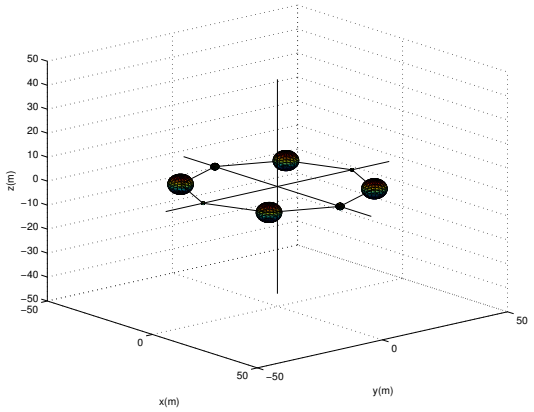

(d) Eight spacecraft equilibrium formation C_2.

Figure 3.5: Polygonal equilibrium formations.

The most interesting polygonal formations are shown in Figure 3.5. Both the two square formation reach very low values of the cost functions and therefore represent the most suitable configurations to be acquired using the ES technique and to be maintained at first order using only electrostatic actuation. These configurations are shown in Figure 3.5(a) and 3.5(b) where the spacecraft are represented as spheres whose radius has been set to be proportional to the charging level. Note that according to the performed literature review the formation in Figure 3.5(b) has not been found so far. On the other hand the hexagonal and octagonal formations displayed in Figure 3.5(c) and 3.5(d) are particularly interesting because yield an average fuel consume in terms of specific

force that is respectively 73% and 82% smaller with respect to the case in which no electrostatic actuation is used for formation maintenance.

Regular Polygon Formation

N	C_1/N(m)	$(\overline{C}_1 \pm \sigma_{C_1})/N$(m)	C_2/N	$(\overline{C}_2 \pm \sigma_{C_2})/N$
4	$5.3 \cdot 10^{-7}$	$(8.0 \cdot \pm 1.3) \cdot 10^{-7}$	$5.9 \cdot 10^{-7}$	$(8.6 \pm 1.0) \cdot 10^{-7}$
5	1.1	(1.13 ± 0.05)	$5.3 \cdot 10^{-2}$	$(8.9 \pm 2.5) \cdot 10^{-2}$
6	1.3	(1.41 ± 0.03)	$9.1 \cdot 10^{-2}$	$(1.8 \pm 1.1) \cdot 10^{-2}$
7	1.9	(1.97 ± 0.02)	$2.7 \cdot 10^{-1}$	$(3.1 \pm 0.8) \cdot 10^{-1}$
8	2.0	(2.01 ± 0.03)	$1.8 \cdot 10^{-1}$	$(4.6 \pm 0.7) \cdot 10^{-1}$
9	2.3	(2.28 ± 0.01)	$2.7 \cdot 10^{-1}$	$(3.8 \pm 1.1) \cdot 10^{-1}$
10	2.2	(2.19 ± 0.01)	$4.9 \cdot 10^{-1}$	$(5.6 \pm 0.3) \cdot 10^{-1}$
11	2.3	(2.27 ± 0.01)	$3.2 \cdot 10^{-1}$	$(4.7 \pm 1.2) \cdot 10^{-1}$
12	2.2	(2.23 ± 0.02)	$4.6 \cdot 10^{-1}$	$(6.3 \pm 0.5) \cdot 10^{-1}$

Regular Solid Formation

N	C_1/N(m)	$(\overline{C}_1 \pm \sigma_{C_1})/N$(m)	C_2/N	$(\overline{C}_2 \pm \sigma_{C_2})/N$
4	$6.3 \cdot 10^{-7}$	$(9.21 \pm 1.31) \cdot 10^{-7}$	0.14	$(1.41 \pm 0.02) \cdot 10^{-1}$
6	$1.1 \cdot 10^{-3}$	(0.53 ± 0.33)	$9.9 \cdot 10^{-7}$	$(2.82 \pm 0.08) \cdot 10^{-4}$
12	14.2	(15.02 ± 1.72)	$5.7 \cdot 10^{-1}$	$(5.7 \pm 0.2) \cdot 10^{-1}$

Bravais Lattice Formations

N	C_1/N(m)	$(\overline{C}_1 \pm \sigma_{C_1})/N$(m)	C_2/N	$(\overline{C}_2 \pm \sigma_{C_2})/N$
9 (BCC*)	4.1	(4.07 ± 0.01)	$2.2 \cdot 10^{-1}$	$(2.5 \pm 0.1) \cdot 10^{-1}$
14 (FCC*)	1.5	(2.97 ± 1.05)	$2.6 \cdot 10^{-1}$	$(2.6 \pm 0.1) \cdot 10^{-1}$

*BCC Body Centered Cubic Lattice, FCC Face Centered Cubic Lattice.

Table 3.2: List of the cost function values for some formations that can be acquired by means of the ES technique. In this table N represents the number of spacecraft in the formation.

In Figure 3.6 some regular solid formations are shown together with some formation forming the well known Bravais lattice shapes. From the values of the cost function it is possible to infer that tetrahedron and octahedron formations are configurations for which EA and ES are perfectly compatible. In Figure 3.6(c) and 3.6(d) some Bravais like formations are displayed that still yield a saving in terms of fuel consumption of

75% and 78% with respect to the case in which no electrostatic actuation is used for formation maintenance.

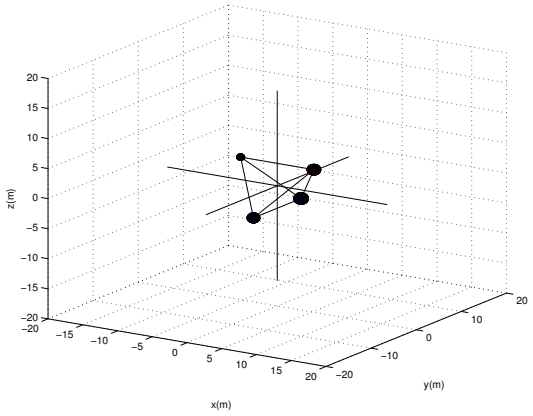

(a) Four spacecraft equilibrium formation C_1.

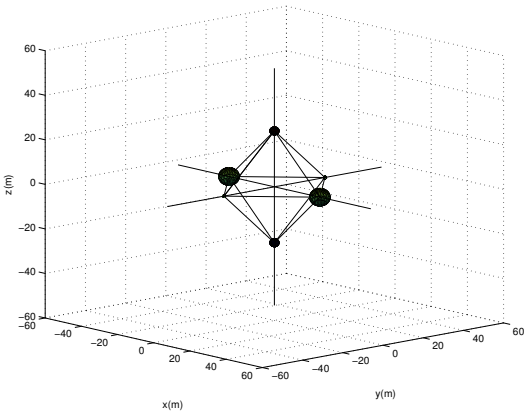

(b) Six spacecraft equilibrium formation C_2.

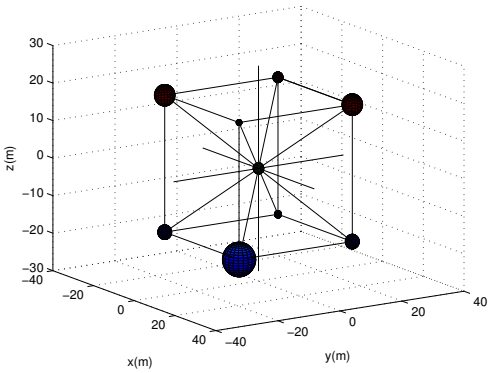

(c) Bravais BCC equilibrium formation C_1.

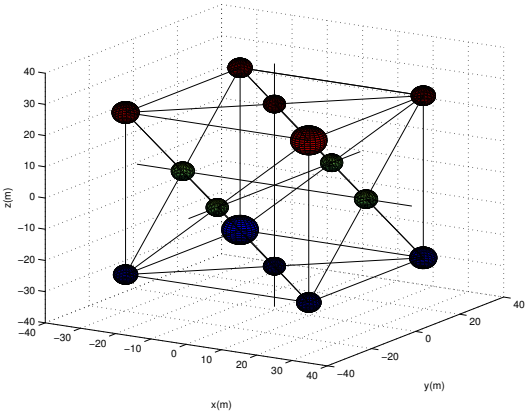

(d) Bravais FCC equilibrium formation C_1.

Figure 3.6: Solid equilibrium formations.

3.6 Compatibility test outcome for Earth-Sun L1 environment

The same analysis has been performed for a formation of satellites in the $L1$ Earth-Sun Lagrangian point. The equation of motion of the SS in this environment is different with respect to the ones in Eq.(3.6) because in this case the influence of both Sun and Earth gravity field is non negligible. Following the line of the derivation in [37] let us consider the circularly restricted three body problem where the two massive bodies are

the Sun and the Earth. Moreover let us consider a reference frame $[\hat{\mathbf{i}}_I, \hat{\mathbf{j}}_I, \hat{\mathbf{k}}_I]$ located in the center of mass of the Earth-Sun system and with the $\hat{\mathbf{i}}_I$ direction always aligned with the line connecting the two massive bodies (see Figure 3.7). In this setting the third mass in Figure 3.7 represents a satellite or a general third body with a mass much smaller with respect to the other two masses. With the given assumptions the equation

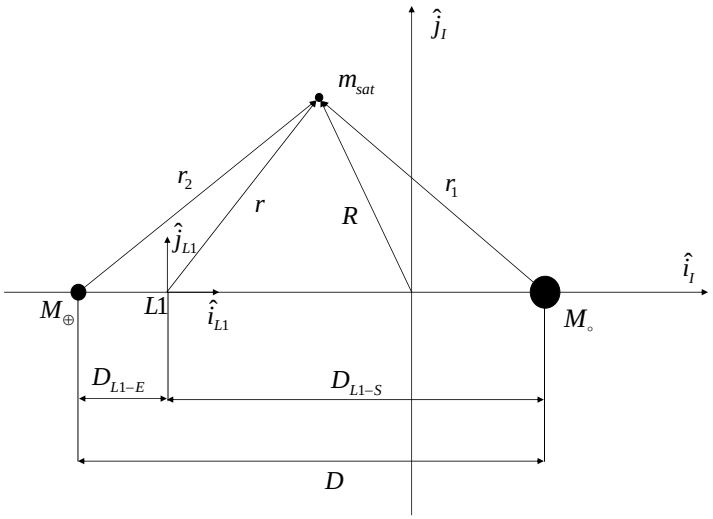

Figure 3.7: Circularly restricted three body problem.

of motion of the third mass is:

$$\begin{cases} \ddot{X} - 2n\dot{Y} - n^2 X = -\frac{\mu_\odot (X-D)}{{r_1}^3} - \frac{\mu_\oplus (X+D)}{{r_2}^3} \\ \ddot{Y} + 2n\dot{X} - n^2 Y = -\frac{\mu_\odot (Y)}{{r_1}^3} - \frac{\mu_\oplus (Y)}{{r_2}^3} \qquad , i = 1, .., N \\ \ddot{Z} = -\frac{\mu_\odot (Z)}{{r_1}^3} - \frac{\mu_\oplus (Z)}{{r_2}^3}. \end{cases} \tag{3.13}$$

where the following definitions are set

- $\mu_\oplus = 398601 km^3/s^2$
- $\mu_\odot = 1.3271 \cdot 10^{11} km^3/s^2$
- D is the Earth-Sun distance
- $\mathbf{R} = [X, Y, Z]$ position of the SC in the $[\hat{\mathbf{i}}_I, \hat{\mathbf{j}}_I, \hat{\mathbf{k}}_I]$ reference frame
- $n = \sqrt{(\mu_\odot + \mu_\oplus)/D^3}$

The Lagrangian points are the well known equilibrium points of the system in Eq.(3.13) and can be found setting to zero all the derivatives in Eq.(3.13) and solving for X, Y, Z. The interesting point for our analysis is the so called L1 point, the collinear point that lies on the line connecting the Earth and the Sun (see again Figure 3.7). Let us identify the position of the L1 point in the $[\hat{\mathbf{i}}_I, \hat{\mathbf{j}}_I, \hat{\mathbf{k}}_I]$ reference frame with $[X_0, Y_0, Z_0]$ and let us express the position of the m_3 body with respect to the reference frame $[\hat{\mathbf{i}}_{L1}, \hat{\mathbf{j}}_{L1}, \hat{\mathbf{k}}_{L1}]$ centered in $L1$ with $\mathbf{r} = [x, y, z]$ then:

$$X = X_0 + x, \quad Y = Y_0 + y, \quad Z = Z_0 + z$$

Substituting this definitions in Eq.(3.13) and expanding the right hand side of the obtained equation exploiting the binomial theorem it is possible to derive the linearized equation of motion of a body around the $L1$ point (see [37] for more details regarding the derivation). This is given by

$$\begin{cases} \ddot{x} - 2n\dot{y} - (2\sigma + 1)x = 0 \\ \ddot{y} + 2n\dot{x} + (\sigma - 1)y = 0 \\ \ddot{z} + \sigma z = 0. \end{cases} \tag{3.14}$$

where σ is defined as follows

$$\sigma = \left(\frac{\mu_\odot}{D^3_{L1-S}} + \frac{\mu_\oplus}{D^3_{L1-E}}\right)$$

and D_{L1-S} and D_{L1-E} are the distances of the $L1$ point with respect to the sun and the earth. From this set of equation the equation of motion of the SS formation around the $L1$ point can be easily derived including the specific forces coming from EA and conventional actuation.

$$\begin{cases} \ddot{x}_i - 2n\dot{y}_i - (2\sigma + 1)x_i = (\mathbf{u}_{el_i} + \mathbf{u}_{th_i}) \cdot \hat{\mathbf{i}}_{L1} \\ \ddot{y}_i + 2n\dot{x}_i + (\sigma - 1)y_i = (\mathbf{u}_{el_i} + \mathbf{u}_{th_i}) \cdot \hat{\mathbf{j}}_{L1} \qquad , i = 1, .., N \\ \ddot{z}_i + \sigma z_i = (\mathbf{u}_{el_i} + \mathbf{u}_{th_i}) \cdot \hat{\mathbf{k}}_{L1}. \end{cases} \tag{3.15}$$

Following the derivation of the previous section in this case the optimization problem aims at finding among all the possible solutions of Eq.(3.16)

$$\begin{cases} -(2\sigma + 1)x_i = (\mathbf{u}_{el_i} + \mathbf{u}_{th_i}) \cdot \hat{\mathbf{i}}_{L1} \\ (\sigma - 1)y_i = (\mathbf{u}_{el_i} + \mathbf{u}_{th_i}) \cdot \hat{\mathbf{j}}_{L1} \qquad , i = 1, .., N \\ \sigma z_i = (\mathbf{u}_{el_i} + \mathbf{u}_{th_i}) \cdot \hat{\mathbf{k}}_{L1}. \end{cases} \tag{3.16}$$

the one for which $||\mathbf{u}_{th_i}|| = 0$, $\forall i = 1, .., N$. Also in the L1 environment both the two cost function in Eq.(3.11) and in Eq.(3.12) are considered including the new expression of the inertial and gravitational specific force. As outlined in chapter the Debye length in the interplanetary space is much smaller with respect to the one in GEO environment (maximum value of approx. $27m$). For this reason the maximum possible formation charachteristic length is constrained so that the Debye exponential term in Eq.(3.4) can still be neglected. The resulting bounds on the variables belonging to $\mathbf{p}$ are therefore in L1:

- $\tilde{q}_i \in [-400, 400]$
- $\phi \in [0, \pi]$
- $\theta \in [-2\pi, 2\pi]$
- $\psi \in [-2\pi, 2\pi]$
- $r \in [2, 10]$.

In order to validate the last assumption the analysis has been repeated removing the constraint on the characteristic length and including in the expression of $\mathbf{u}_{el}$ also the Debye length. The results for some polygonal formations are shown in Table(3.3).

Without Debye Length

N	C_1/N(m)	$(\overline{C}_1 \pm \sigma_{C_1})/N$(m)	C_2/N	$(\overline{C}_2 \pm \sigma_{C_2})/N$
4	$5.7 \cdot 10^{-7}$	$(8.81 \cdot \pm 1.2) \cdot 10^{-7}$	$6.8 \cdot 10^{-7}$	$(8.7 \pm 1.0) \cdot 10^{-7}$
5	0.9	(0.94 ± 0.01)	$1.3 \cdot 10^{-1}$	$(1.3 \pm 0.1) \cdot 10^{-2}$
6	1.1	(1.21 ± 0.09)	$1.1 \cdot 10^{-1}$	$(1.1 \pm 0.2) \cdot 10^{-2}$
7	0.9	(0.91 ± 0.01)	$1.3 \cdot 10^{-1}$	$(1.1 \pm 0.8) \cdot 10^{-1}$
8	0.8	(1.21 ± 0.53)	$1.0 \cdot 10^{-1}$	$(1.0 \pm 0.1) \cdot 10^{-1}$

With Debye Length

N	C_1/N(m)	$(\overline{C}_1 \pm \sigma_{C_1})/N$(m)	C_2/N	$(\overline{C}_2 \pm \sigma_{C_2})/N$
4	$6.3 \cdot 10^{-7}$	$(9.21 \pm 1.31) \cdot 10^{-7}$	0.14	$(1.41 \pm 0.02) \cdot 10^{-1}$
6	$1.1 \cdot 10^{-3}$	(0.53 ± 0.33)	$9.9 \cdot 10^{-7}$	$(2.82 \pm 0.08) \cdot 10^{-4}$
12	14.2	(15.02 ± 1.72)	$5.7 \cdot 10^{-1}$	$(5.7 \pm 0.2) \cdot 10^{-1}$

Table 3.3: List of the cost function values for some formations that can be acquired by means of the ES technique. In this table N represents the number of spacecraft in the formation.

Despite the low value of the Debye length in $L1$ there are more formations for which high savings are obtained with respect to the analysis performed in the GEO environment. This is mainly due to the fact that the specific force field induced by the gravity gradient has an higher degree of symmetry in $L1$. This means that in the $y-z$ plane for example the gravity gradient static forces are all working as positive stiffness forces.

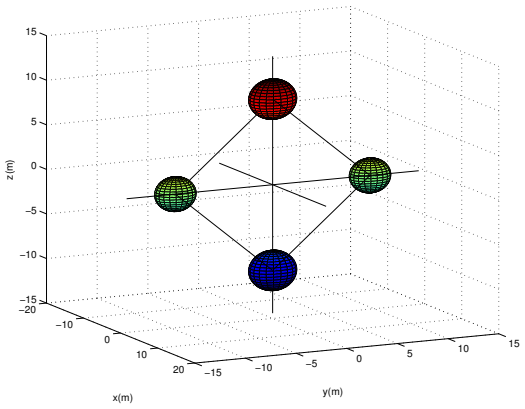

(a) Four spacecraft equilibrium formation C_1.

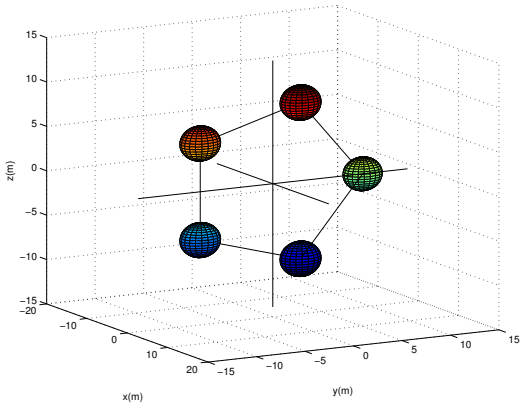

(b) Five spacecraft equilibrium formation C_2.

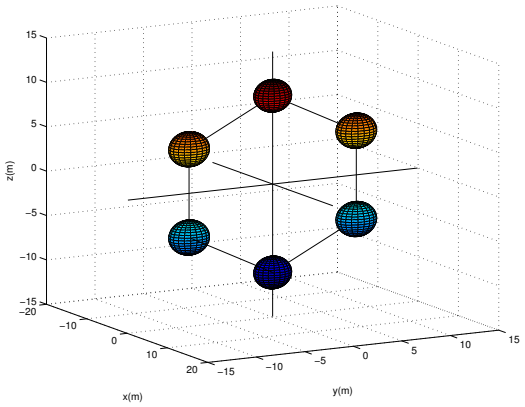

(c) Six spacecraft equilibrium formation C_2.

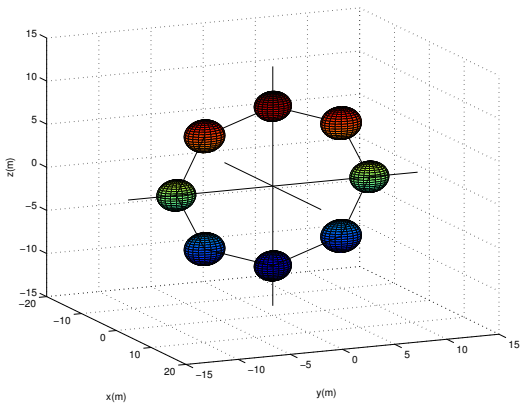

(d) Eight spacecraft equilibrium formation C_2.

Figure 3.8: Equilibrium formation in L1. No Debye length is considered in the equation of motion.

Some of these formations are shown in Figure 3.8. The value of the cost function for the square formation shows that for such a configuration the ES and EA are perfectly compatible. This formation is displayed in Figure 3.8(a). Moreover the pentagonal, hexagonal and octagonal formations shown in Figures 3.8(b) to 3.8(d) are all yielding savings in terms of fuel consumption of almost 90%. In Figure 3.9 the results of the

same analysis performed considering the Debye length exponential term are displayed. It is possible to see that the formations displayed in Figure 3.8 have the same shape of the ones displayed in Figure 3.8 and just the charachteristic length and the spacecraft charging values are changed. Therefore the analysis performed neglecting the Debye exponential term is still valid in order to find the equilibrium formations of Eq.(3.16). As a final remark it is interesting to point out that the the hexagonal configuration in the $y - z$ plane has a non-negligible interest because it is one of the proposed baseline configuration for the Darwin mission.

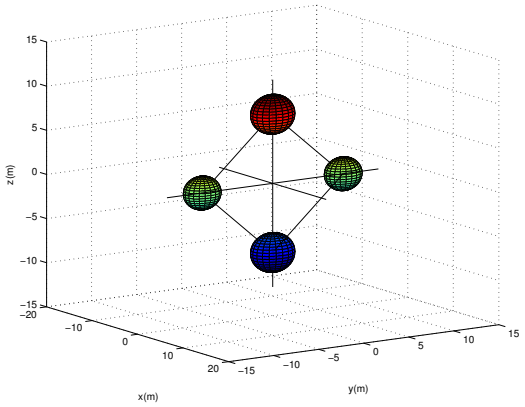

(a) Four spacecraft equilibrium formation C_1.

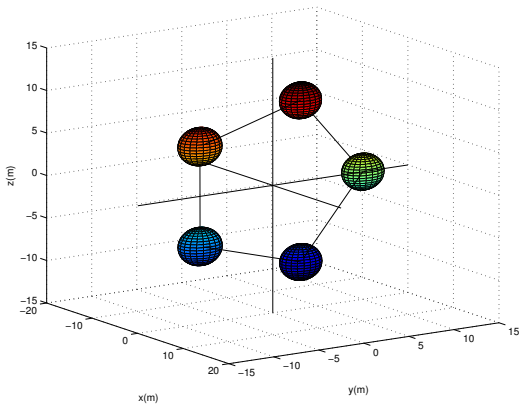

(b) Five spacecraft equilibrium formation C_2.

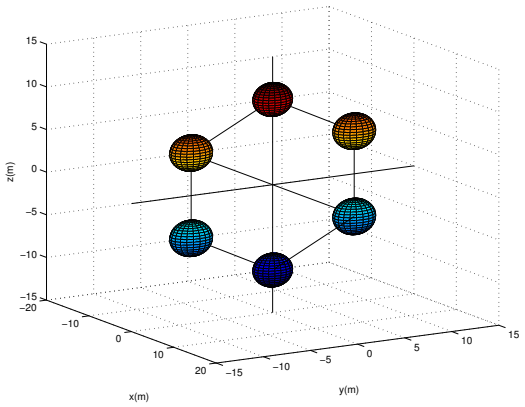

(c) Six spacecraft equilibrium formation C_2.

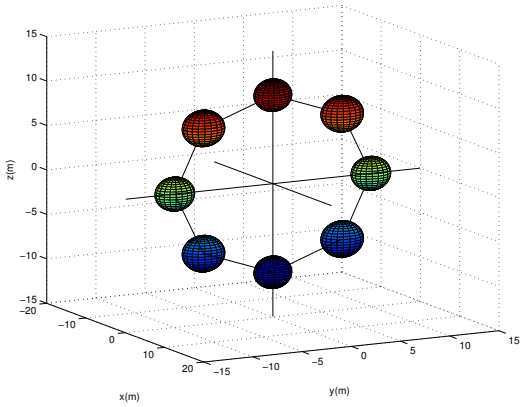

(d) Eight spacecraft equilibrium formation C_2.

Figure 3.9: Equilibrium formation in L1. The Debye length is considered in the equation of motion.

3.7 Stand-by formation

The technique used so far for solving Eq.(3.7) is aimed at finding the formations for which the level of residual specific force acting on the SC is negligible. Therefore in this approach the formation orientation and characteristic length in the Hill's reference frame are left free to vary. On the other hand typically a mission requires a group of satellites to achieve a precise formation with a predetermined shape and orientation in the Hill's reference frame. Moreover in general a formation flying mission (or even a mission involving a whole swarm of satellites) may require the swarm of satellites to keep the predesigned relative positioning only during a fraction of the orbit. In this case the formation exploiting the EA would represent an attractive possibility for the design of stand-by formations. In figure (3.10) this possibility is explored for a formation of 6 satellites in a GEO environment. The target formation (i.e. the one chosen from the design of the mission) is an hexagonal formation in the Hill's $y-z$ plane (drawn in green in Figure 3.10). The ES technique is used in order to navigate the swarm towards the acquisition of the stand-by formation (drawn in blue in Figure 3.10). In this simulation the stand-by formation acquired is an octahedron formation with four SC in the $y-z$ Hill's plane disposed as in Figure 3.6(b) and two spacecraft along the $\hat{\mathbf{j}}_H$ axis. The black lines represent the SC trajectories towards the final stand-by configuration. Since the acquisition of the stand-by formation is performed by means of the ES technique each agent autonomously decides which position it will have in the final formation. Different strategies for the swarm navigation during the reconfiguration maneuver could decrease the level of autonomy of the system increasing the optimality in terms of acquisition time or fuel consumption. The example displayed in Figure 3.10 gives the motivation for the introduction of a different optimization technique that allows to find, for a given target formation, the best possible stand by configuration. The new cost function is made up of two different terms, the first one penalizes all the formations that have an high value of residual acceleration, whereas the second one penalizes the solutions far from the target formation.

$$C_3(\mathbf{p}') = \sum_{i=1}^{N} [||\mathbf{u}_{thr_i}|| + w \cdot (||\mathbf{r}_i^d - \mathbf{r}_i^s||)] \tag{3.17}$$

This cost function is defined in Eq.(3.17) where $\mathbf{r}_i^d$ denotes the position of the $i-$th SC in the design formation and $\mathbf{r}_i^s$ denotes the position of the $i-$th SC in the stand-by formation. The parameter w in Eq.(3.17) can be used to weight the importance of the two different contributions in C_3. For this problem a new search space is defined since also the inter-SC distances can vary.

$$\begin{aligned} \mathbf{p}' &= [\tilde{q}_i, \mathbf{r}_i] \\ i &= 1, .., N. \end{aligned} \tag{3.18}$$

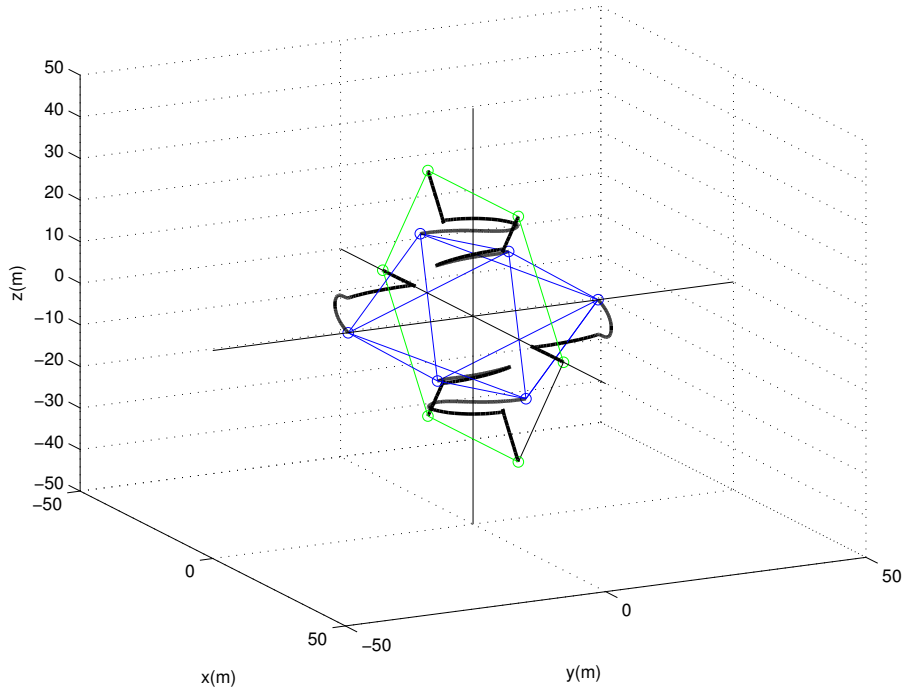

Figure 3.10: Switch maneuver between the design 6 SC formation and the stand-by one.

In Figure 3.11 an example of the results that can be obtained from this analysis is presented. The design target formation is a regular octagonal formation in the Hill's $y-z$ plane and it is drawn in red line in Figure 3.11. On the other hand some characteristics of the acquired and design formation are listed in Table 3.4. In particular for this simulation two different search procedures have been performed. The first one for the design case aimed at finding the charging values for the SC in order to minimize the residual specific force on that configuration. The result of the average thrusting specific force is given in $\overline{||\mathbf{u}^d_{thr_i}||}$. The second search procedure has been performed considering an optimization problem with C_3 cost function and $\mathbf{p}'$ search space. The average level of the thrusting specific force acting on the SC in this case is given in $\overline{||\mathbf{u}^s_{thr_i}||}$. It is possible to see by comparing these two values the advantage of introducing a stand-by configuration for formation keeping.

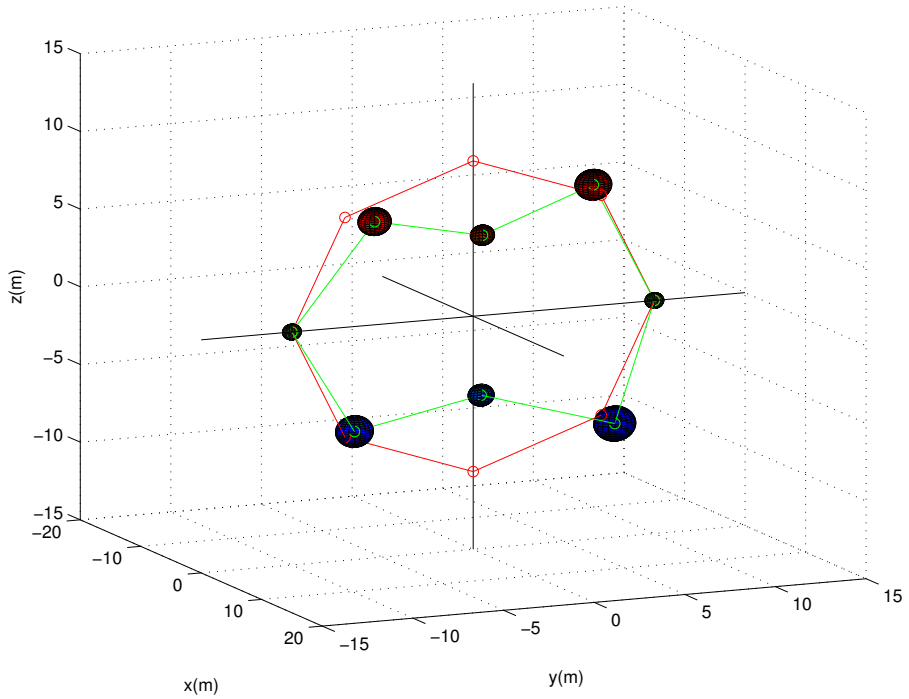

Figure 3.11: Optimized 8 SC stand by formation and design one.

Formation Characteristic	Numerical value
$\overline{\|\|\mathbf{u}^d_{thr_i}\|\|}$	12.314
$\overline{\|\|\mathbf{u}^s_{thr_i}\|\|}$	0.002
$\|\|\mathbf{r}^s_i - \mathbf{r}^d_i\|\|$	$[4.894, 0.975, 0.001, 0.845, 4.861, 1.691, 0.003, 0.611]m$

Table 3.4: Stand-by vs. design formation characteristics.

3.8 Conclusions

In this section the compatibility between the ES path planning technique and the EA concept has been investigated. With this intention the formations that can be acquired autonomously relying upon the ES path-planning technique and then maintained with high efficiency only relying upon the EA have been found. For these formations the integration between the two concepts is already satisfactory because the resulting system enjoys a high level of autonomy (ensured by the ES path planning technique), and is also fuel efficient. Two different approaches have been used in this chapter to find the compatible formations. Both the two approaches rely upon the same search strategy but

they differ in the definition of the function expressing the objective of the search. In the first case the objective of the search is to find the formation for which is minimum the force to be given by the thrusting actuation system. The second approach instead aims at finding those formations that minimize the average rate between the specific force required to the thrusting system and the required total specific force. The different approaches have been used to search the compatible formations in a GEO environment and around the Earth-Sun L1 Lagrangian point. The results showed that there exist particular formations (square-, tetrahedron- octahedron-shaped) for which the ES and EA are fully compatible. Moreover some other formations have been found that yield a considerable amount of fuel savings such as the hexagon-shaped one in GEO and the hexagon-,octagon-shaped ones in L1. At the end of the chapter a possible application of these formations as stand-by configurations has been considered and a simple search has been designed to find the best possible stand-by configuration associated to a given design formation.

4 Integration of EA and ES for acquisition maneuvers

4.1 Introduction

In the previous chapter it has been shown that for certain formations the ES approach can be satisfactorily integrated with the EA by using the EA for high efficiency formation keeping and the ES for autonomous formation acquisition. In principle inter-SC electrostatic interaction can be used also during acquisition or reconfiguration maneuver. If the EA system is present on board the satellite in fact, we may think to use it in order to steer the spacecraft to acquire the desired position with higher efficiency.
In recent literature the EA concept has been considered mainly for formation keeping. In particular in [18] a stabilizing spacecraft charging control law has been investigated. This technique uses the orbital element difference formulation to describe the relative motion of the satellites and defines a charging strategy to control any set of orbit element differences relative to the formation center of mass motion. In [38] the problem of the stabilization of a Coulomb virtual tether formation is addressed and a solution based on the combined exploitation of the electrostatic forces and the gravity gradient effect is proposed. In [39] the same problem is considered for a three spacecraft virtual tether formation and a stabilizing feedback is proposed exploiting the Lyapunov theory and an optimization search routine method. The first attempt to use the electrostatic force also for formation reconfiguration is in [40]. In this work the problem is to steer the reconfiguration of a two-spacecraft virtual tether formation. The maneuver considered there is a tether separation distance variation and the main aim is to perform it only by means of EA. The Rosembrock stability proof for linear time-varying systems is then used to find limits of the tether expansion and contraction rates. The bounds on the tether length variation rates define a set of linearly stable maneuvers that can be performed only relying upon the EA. In [41] a completely different approach is considered. There a chief spacecraft deploys deputy crafts to specified positions. The chief is supposed to be able to use multiple charge surfaces, i.e. to control in an active way the charge of different parts of its body. A simple linear control design is then used to control the deployment of formations of multiple spacecraft.
As highlighted in this introduction in the past work the main task was to develop a charging control law able to stabilize the motion of a formation of satellites or to steer

reconfiguration maneuvers only by means of the EA system. Only in a recent paper [41] an hybrid approach has been considered where a chief satellite can control its position by trusters and in the meantime exploit the charge control to deploy a group of deputy satellites.
In this work a completely different approach is introduced in which every spacecraft is equipped with both electrostatic and conventional actuation system. This new perspective allows to tackle the problem of the design of a EA based feedback law from a completely different point of view. Following this idea the problem is not anymore to find a formation that can be stabilized or a maneuver that can be steered only relying upon the inter-SC electrostatic interaction. Rather the proposed approach tries, for a general maneuver, to find the spacecraft charge levels that minimize the residual force to be provided by the thrusting actuation system.
In the remaining of this chapter it is shown how this new approach, used in connection with the ES path planning scheme, can allow to drive a swarm of spacecraft to perform acquisition and reconfiguration maneuvers in an autonomous and highly efficient manner.

4.2 General Problem Formulation

Let us consider a swarm of N SC performing a given maneuver. According to the particular control scheme implemented on board, the $i-$th SC will evaluate at any instant a control signal $\mathbf{u}_{des_i}$ that, if provided, will allow it to achieve its control objective. Whenever an electrostatic actuator is mounted on board the SC, it can provide part of the required control force exploiting the Coulomb force:

$$\mathbf{u}_{des_i} = \mathbf{u}_{el_i} + \mathbf{u}_{th_i} \tag{4.1}$$

where $\mathbf{u}_{el_i}$ and $\mathbf{u}_{th_i}$ represent the control acceleration given with the electrostatic and thrusting devices respectively. The general problem is sketched in Figure 4.2 for a swarm of four spacecraft.
When the electrostatic force is exploited to provide part of the required control force, a coordination algorithm needs to be implemented because the dynamics of the SC become highly coupled, i.e. a charge variation on the $i-$th SC generates a variation in the forces acting on the other charged SC. Moreover such a coordination scheme should take into account that the electrostatic actuation can be used to reach different objectives. The SC coordination problem can be recast into an optimization one and then the definition of an objective function is obviously a crucial point. Different objective functions will reflect different tasks that the swarm of satellites have to accomplish using the EA. A simple example involving just two SC is depicted in Figure 4.2.
The objective function can take into account as a primary figure of merit the total fuel consumption required to the whole swarm during the maneuver i.e.

$$\forall t, \quad \min_{\mathbf{q}}(J(\mathbf{q})) = \min_{\mathbf{q}}(\textstyle\sum_{i=1}^{N} \parallel \mathbf{u}_{th_i} \parallel_2) \tag{4.2}$$

where $\mathbf{q} = [q_1, .., q_N]$ is a vector containing the charge value of all the SC. This is shown in Figure 4.2(a).

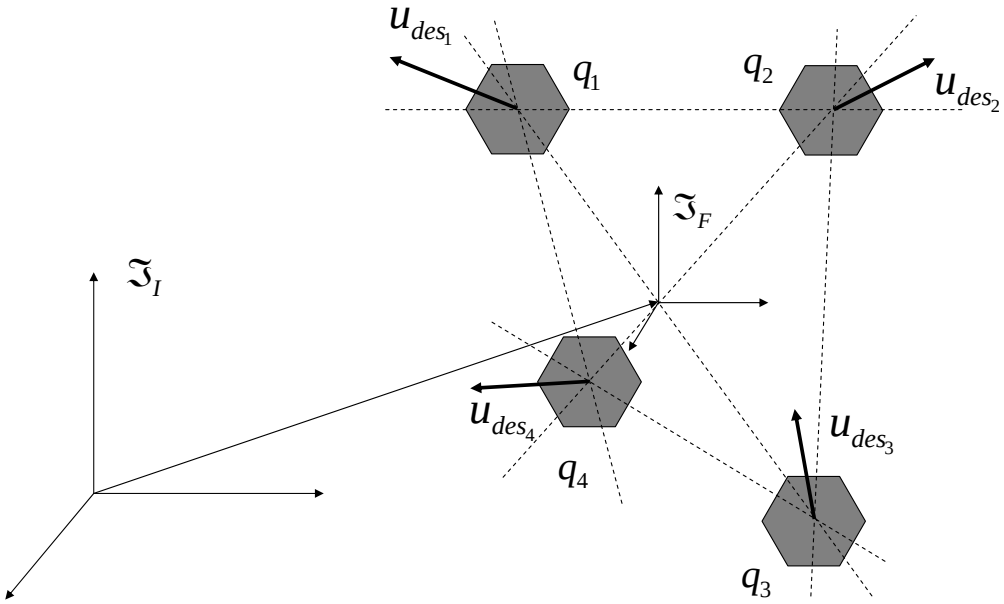

Figure 4.1: Simple sketch of a the general problem.

Other figures of merit could also be introduced in the cost function. For example the SC balanced fuel consumption represents also a key objective in swarm navigation. In order to explain how this objective could be achieved relying upon the electrostatic actuation system, a simple example is sketched in Figure 4.2(b). In this situation only the SC 2 could take advantage from the exploitation of the electrostatic actuation whereas an eventual electrostatic force acting upon SC 1 will be seen as a disturbance. Therefore in this case the electrostatic force can not produce any advantage in terms of fuel consumption of the cluster formed by the two satellites. If only the total fuel consumption of the whole swarm is considered in the cost function, the use of EA will not be recommended.

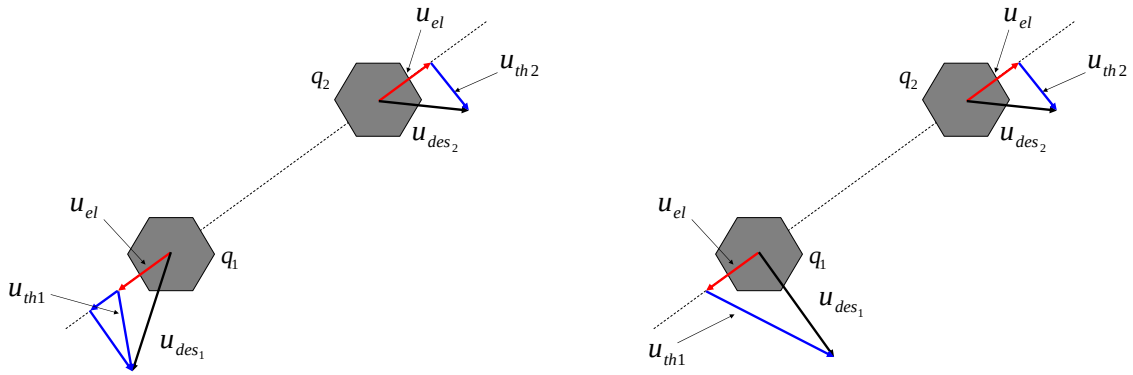

(a) Two SC case, minimization of total fuel consumption.

(b) Two SC case, balanced fuel consumption.

Figure 4.2: Two SC formation simple scheme, minimum fuel consumption, balanced fuel consumption strategies.

Even if the electrostatic actuation is not effective to reduce the total fuel consumption, it could be used to redistribute the control force in order to achieve a better fuel consumption distribution among the SC belonging to the swarm. Let us admit that the SC 2 in Figure 4.2(b) has already exploited more of its resources with respect to the SC 1. In this case the exploitation of EA for the control of the two SC will allow SC 2 to perform a maneuver employing a small amount of propellant at the price of increasing the cost of the maneuver performed by SC 1. For such a problem the cost function can be defined as:

$$\begin{aligned} &\forall t \quad \min_{\mathbf{q}}(\| \mathbf{u}_{th_i} \|_2) \\ &with \quad i : \min_{i\in[1,..,N]}(\Delta v_i(t)). \end{aligned} \tag{4.3}$$

Both these two ideas are considered in the remaining of the chapter and a solution to the optimization problems in Eq.(4.2) and in Eq.(4.3) is proposed in the forthcoming sections.

4.3 ES technique: definition of the desired control force

The exploitation of the EA proposed in Eq.(4.1) does not impose any constraint to the satellite control law, i.e. Eq.(4.1) applies to a general $\mathbf{u}_{des}$ signal. In this work the EA will be integrated in the ES swarm navigation technique. For this reason the way in which the signal $\mathbf{u}_{des}$ is obtained in the ES framework is here briefly recalled.

As already mentioned in the previous chapters the ES technique is structured in two different levels:

- First, for each target disposition and each agent neighborhood configuration, each SC defines a desired velocity vector as a sum of different weighted contributions named "behaviors".
- Then, a control feedback is considered that allows each spacecraft to track the desired kinematical field.

In this way the control design is completely independent from the design of the desired velocity field and may be faced separately.
The basic procedure followed to define the desired kinematical field has been outlined in chapter 3. The expression of the desired velocity field is given in Eq.(3.1) where the parameters b, c_j, d_j for a given target formation are found solving Eq.(3.2) for each SC in the formation. Once the desired velocity vector is defined, a control feedback must be designed in order to enforce the SC to follow the path planned by the ES technique. The feedback considered here is the one introduced in [8] inspired by the Q-guidance steering law introduced formally by Battin [42] for rocket guidance. It is based on the definition of the "velocity to be gained" vector $\mathbf{v}_{g_i}$ that represents, in our case, the instantaneous difference between each agent's actual $\mathbf{v}_i$ and desired velocity $\mathbf{v}_{d_i}$. The objective of the control system is to drive the velocity to be gained vector to zero. From now on each quantity will be related to each agent but, in order to simplify the notation the subscript will be omitted. Let us define, for each agent, the following function:

$$V = \frac{1}{2}\mathbf{v}_g \cdot \mathbf{v}_g$$

the velocity to be gained vector decreases along the trajectories followed by each agent if and only if:

$$\dot{V} = \mathbf{v}_g \cdot \dot{\mathbf{v}}_g < 0. \tag{4.4}$$

The time derivative of $\mathbf{v}_g$ during the motion has the expression $\dot{\mathbf{v}}_g = \dot{\mathbf{v}}_d - \dot{\mathbf{v}}$. Substituting the momentum balance of each spacecraft written in the LHLV frame into this relation one obtains:

$$\dot{\mathbf{v}} = \mathbf{a}_{in} + \mathbf{u}_{des}$$

where $\mathbf{a}_{in}$ are the external specific inertial forces and $\mathbf{u}_{des}$ is the control vector. The following expression is obtained:

$$\dot{\mathbf{v}}_g = \dot{\mathbf{v}}_d - \mathbf{a}_{in} - \mathbf{u}_{des}.$$

Using the chain rule the desired velocity derivative can be written as:

$$\dot{\mathbf{v}}_d = \frac{\partial \mathbf{v}_d}{\partial t} + \frac{\partial \mathbf{v}_d}{\partial \mathbf{x}}\mathbf{v} = \frac{\partial \mathbf{v}_d}{\partial t} + \frac{\partial \mathbf{v}_d}{\partial \mathbf{x}}(\mathbf{v}_d - \mathbf{v}_g)$$

The various terms can be found by deriving Eq.(3.1) and taking into account the expressions chosen for the different behaviors. To make $\dot{V} < 0$ the following feedback is introduced:

$$\mathbf{u}_{des} = \kappa \mathbf{v}_g - \dot{\mathbf{v}}_d - \mathbf{a}_{in} \tag{4.5}$$

in which $\kappa > 0$ is a positive real parameter whose choice will be discussed below. The resulting espression for $\dot{V}$ is:

$$\dot{V} = -\kappa \mathbf{v}_g \cdot \mathbf{v}_g$$

that assures the global stability of this controller. In real cases the agents will have an upper limit to the thrust magnitude, therefore a saturation level must be introduced for the defined above feedback. As soon as a saturation level is introduced the mathematical result on the feedback global stability is lost, but the controller is still able to drive the velocity to be gained to zero as confirmed by numerical simulations. In particular it is possible to note how the geometrical interpretation of the saturated feedback shown in Figure 4.3 allows to rederive, for particular choices of the positive parameter κ the analogous to known steering laws based on the Q-guidance (see Battin [42]).

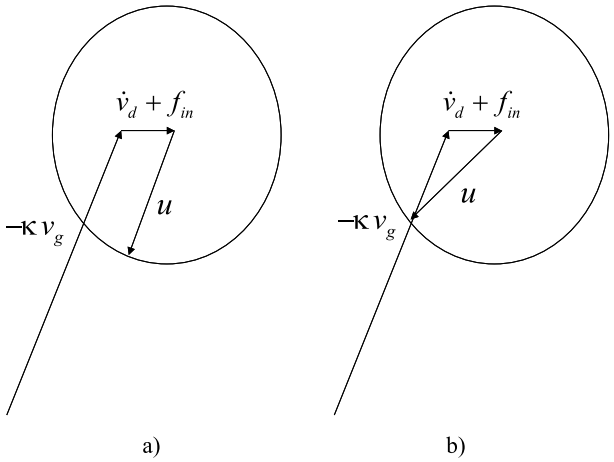

Figure 4.3: Vectorial diagrams representing different control strategies.

If $\kappa \to \infty$ the control strategy is to thrust in the direction of the velocity to be gained vector regardless of the contribution to the $\dot{\mathbf{v}}_g$ due to the uncontrollable terms $\dot{\mathbf{v}}_d$ and $\mathbf{a}_{in}$. A different strategy can be achieved if the thrust direction is chosen in order to try aligning the time derivative of the velocity to be gained vector to the $\mathbf{v}_g$ vector itself, as expressed by the following relation:

$$\dot{\mathbf{v}}_g \times \mathbf{v}_g = 0. \tag{4.6}$$

The feedback coming from Eq.(4.6) is the known cross product steering that, in this notation, may be implemented by finding that value of κ for which (see Figure 4.3):

$$(\dot{\mathbf{v}}_d + \kappa \mathbf{v}_g) \cdot (\dot{\mathbf{v}}_d + \kappa \mathbf{v}_g) = u_{sat}$$

where u_{sat} is the saturation considered for the thrust vector modulus.

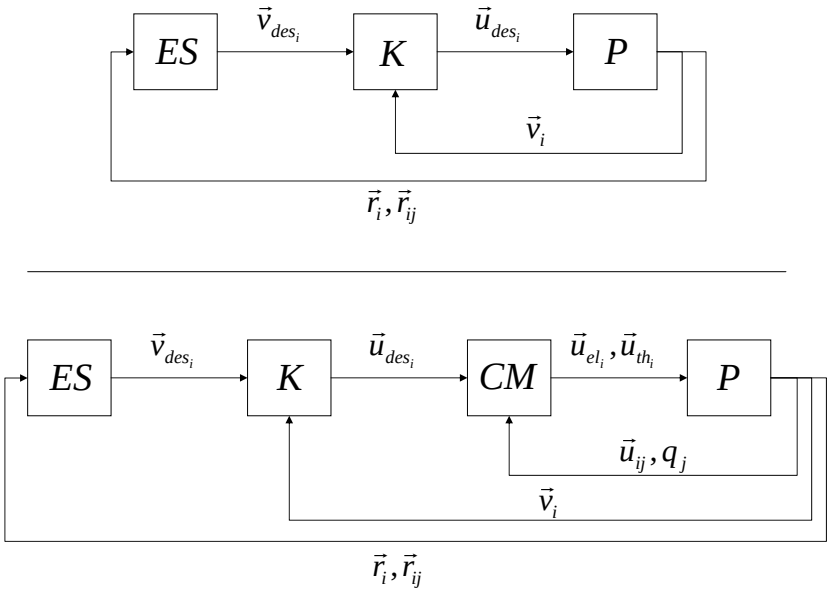

Figure 4.4: Block diagram showing the control system structure with and without EA.

In the remaining of this work the feedback considered is the one in Eq.(4.5) with a fixed value of $\kappa = 0.7s^{-1}$.
Besides the introduction of the EA device itself the actuation strategy in Eq.(4.1) requires the introduction of a subsystem called charging management unit (CM) between the controller and the plant. This subsystem gets in input the desired control force commanded by the control system, processes it with measurements fed back from the plant, and provides the force to be given by the thrusters and the desired charge. In Figure 4.3 a simple block diagram explains the new structure of the control and actuation system. In this figure also the signals fed back from the plant to the different subsystems are included.

4.4 Charge product approach

In this section the so called charge product charging strategy is introduced. This approach draws the inspiration from the work described in [18]. The motion of a formation of charged satellites in an orbital environment is described by Eq.(3.6) where the expression of the electrostatic forces is the one in Eq.(3.4). The instantaneous acceleration

experienced by the $i-$th satellite due to the Coulomb force is

$$\mathbf{u}_{el_i} = \frac{q_i}{m_i}\kappa_c \left(q_1 \frac{\mathbf{r}_{1i}}{\| \mathbf{r}_{1i} \|^3} + .. + q_N \frac{\mathbf{r}_{Ni}}{\| \mathbf{r}_{Ni} \|^3} \right) \tag{4.7}$$

where $\mathbf{r}_{ij} = \mathbf{r}_i - \mathbf{r}_j$ is the vector representing the relative position of SC j with respect of the SC i in the Hill's reference frame and the Debye exponential term is neglected for the sake of simplicity. In this expression the charges appear as products $q_i q_j$ so that Eq.(4.7) can be rewritten in terms of the charge products. Therefore defining:

$$\mathbf{R}_i = \frac{\kappa_c}{m_i} \left[\frac{\mathbf{r}_{1i}}{\| \mathbf{r}_{1i} \|^3}, .., \frac{\mathbf{r}_{Ni}}{\| \mathbf{r}_{Ni} \|^3} \right] \tag{4.8}$$

and

$$\mathbf{Q} = \begin{pmatrix} Q_{1i} \\ ... \\ Q_{Ni} \end{pmatrix} = \begin{pmatrix} q_1 q_i \\ ... \\ q_N q_i \end{pmatrix} \tag{4.9}$$

the following formulation can be obtained:

$$\mathbf{u}_{el_i} = \mathbf{R}_i \mathbf{Q}.$$

This formulation is particularly attractive because the acceleration experienced by each SC is linear in the charge product vector. When the charge product approach is used, the general optimization problems described in section 4.2 are splitted in two different phases:

- Find the charge products such that the minimum [the most balanced] amount of propellant is used for the given maneuver
- Derive the SC individual charge from the computed charge products.

In the following both the optimization problems in Eq.(4.2) and in Eq.(4.3) are considered with the formulation resulting from the charge product approach. A simple case of two-three SC formation is considered first and then the main problems concerning the generalization of this method to the N SC case are addressed.

4.4.1 Two spacecraft formation example

In this section a simple example in which the swarm is composed only by two SC is considered. In particular it will be shown that for this simple case it is possible to find a solution to both the optimization problems defined in section 4.2. The equation of the

specific force balance for the two spacecraft belonging to the formation projected along the direction connecting them is

$$\begin{cases} \mathbf{u}_{des_1} \cdot \hat{\mathbf{r}}_{12} = \mathbf{u}_{thr_1} \cdot \hat{\mathbf{r}}_{12} - \frac{\kappa_c Q_{12}}{m_1 r_{12}^2} \\ \mathbf{u}_{des_2} \cdot \hat{\mathbf{r}}_{12} = \mathbf{u}_{thr_2} \cdot \hat{\mathbf{r}}_{12} + \frac{\kappa_c Q_{12}}{m_2 r_{12}^2} \end{cases} \tag{4.10}$$

where $r_{12} = ||\mathbf{r}_{12}||$, $\hat{\mathbf{r}}_{12} = \frac{\mathbf{r}_{12}}{r_{12}}$ gives the direction of the line connecting the two SC and $Q_{12} = q_1 q_2$ is the sole charge product. Note that the Debye exponential term is neglected in Eq.(4.10) because the assumption is done that $r_{12} < \lambda_d$. Moreover in the direction orthogonal to $\mathbf{r}_{12}$ the electrostatic actuation can not reduce the specific force to be provided with the thrusting system. Since the charging level of each spacecraft will effect the motion of the other member of the formation, the two spacecraft must find in a coordinated manner the Q_{12} value that will allow the best exploitation of the electrostatic actuation.
If the main objective is to reduce the total fuel required to perform the maneuver at any instant during the acquisition, the resulting optimization problem can be obtained writing Eq.(4.2) with $N = 2$

$$\forall t, \quad \min_{Q_{12}}(J(Q_{12})) = \min_{Q_{12}}(\| \mathbf{u}_{th_1} \|_2 + \| \mathbf{u}_{th_2} \|_2). \tag{4.11}$$

Note that if the problem would have been to find the minimum of $\| \mathbf{u}_{th_1} \|_2^2 + \| \mathbf{u}_{th_2} \|_2^2$ the solution could have been computed using a pseudo inverse calculation of the matrix in Eq.(4.10). For a swarm of two satellites it is possible to solve Eq.(4.11) in an analytical way and therefore to compute the Q_{12} value simply performing algebraic calculations. Expanding the expression of the $||\cdot||_2$ norm the cost function in Eq.(4.11) can be written as

$$\| \mathbf{u}_{th_1} \|_2 + \| \mathbf{u}_{th_2} \|_2 = \sqrt{u_{+_1}^2 + (\mathbf{u}_{des_1} \cdot \hat{\mathbf{r}}_{12} + \frac{\kappa_C Q_{12}}{m_{SC} r_{12}^2})^2} + \sqrt{u_{+_2}^2 + (\mathbf{u}_{des_2} \cdot \hat{\mathbf{r}}_{12} - \frac{\kappa_C Q_{12}}{m_{SC} r_{12}^2})} \tag{4.12}$$

where $u_{+_i} = ||\mathbf{u}_{des_i} - \mathbf{u}_{des_i} \cdot \hat{\mathbf{r}}_{12} \hat{\mathbf{r}}_{12}||$. Setting the following definitions

$$\begin{aligned} A &= \| \mathbf{u}_{des_1} \|^2 \\ B &= \frac{2\mathbf{u}_{des_1} \cdot \hat{\mathbf{r}}_{12}}{m_{SC} {r_{12}}^2} \\ C &= \frac{1}{(m_{SC} {r_{12}}^2)^2} \\ D &= \| \mathbf{u}_{des_2} \|^2 \\ E &= -\frac{2\mathbf{u}_{des_2} \cdot \hat{\mathbf{r}}_{12}}{m_{SC} {r_{12}}^2} \end{aligned} \tag{4.13}$$

Eq.(4.12) can be rewritten as:

$$\| \mathbf{u}_{th_1} \|_2 + \| \mathbf{u}_{th_2} \|_2 = \sqrt{A + BQ_{12} + CQ_{12}{}^2} + \sqrt{D + EQ_{12} + CQ_{12}{}^2} \tag{4.14}$$

where A, B, C, D, E are parameters computed at any time by the SC given the SC relative positioning and the computed $\mathbf{u}_{des}$. Taking the derivative of the last expression with respect to Q_{12} and setting it to zero it is possible to find the extremal point of the function in Eq.(4.12). The solution of the minimization problem is thus found solving the following second order equation:

$$aQ_{12}{}^2 + bQ_{12} + c = 0 \tag{4.15}$$

where

$$\begin{aligned} a &= C(B^2 - E^2) + 4C^2(D - A) \\ b &= 4C(DB - EA) + BE(B - E) \\ c &= B^2D - E^2A. \end{aligned} \tag{4.16}$$

Once the optimal value of Q_{12} is found there are infinite ways to derive the individual charges of each SC. For the two SC case the following simple strategy has been considered:

$$\begin{aligned} q_1 &= \sqrt{Q_{12}} \\ q_2 &= Q_{12}/q_1. \end{aligned}$$

Note that in this way the charge value of the first SC is always positive. In order to test the performances of such a strategy a complete simulation campaign has been performed for a formation of two spacecraft starting from different initial conditions and performing acquisition maneuvers driven by the ES navigation technique. The results have shown that the exploitation of the EA can lead to savings in terms of the total fuel consumption of the swarm up to 80% with respect to the case in which no electrostatic actuators are mounted on board.
As already introduced in section 4.2 in formation flying control a crucial issue is also to perform maneuvers such that the required fuel consumption is balanced for all the satellites belonging to the formation. In this case the new optimization problem to be solved during the maneuver is the one in Eq.(4.3) here again rewritten for $N = 2$

$$\begin{aligned} &\forall t \quad \min_{\mathbf{Q}_{12}}(\| \mathbf{u}_{th_i} \|_2) \\ &with \quad i : \min_{i \in [1,2]}(\Delta v_1(t), \Delta v_2(t)). \end{aligned} \tag{4.17}$$

The solution of this optimization problem can be easily computed with a pseudo-inverse calculation involving only one of the equations in Eq.(4.10).

In a recent work [18] the EA concept has been considered to control the relative position of satellites in a formation. In this work a switching strategy is introduced such that at each time the electrostatic actuation is exploited to control the spacecraft with the highest tracking error. Therefore, according to this scheme the control system attempts at any time to reduce the residual specific force acting only on the spacecraft with the highest tracking errors disregarding the disturbances induced to the other members of the swarm.

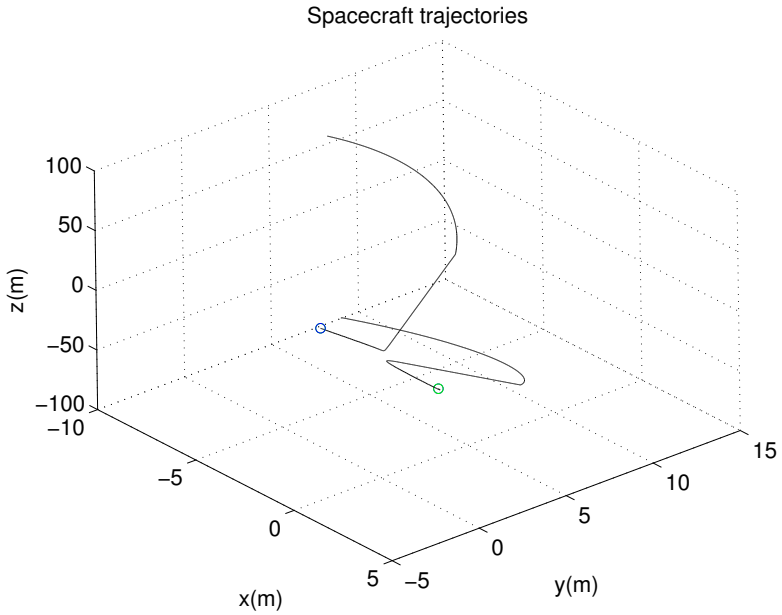

Figure 4.5: Two SC acquisition maneuver: SC trajectories.

All the charging strategies described so far can be compared in order to assess the different performances and to verify pros and cons of each one of them. For this reason in Figure 4.5 the trajectories of two spacecraft performing an acquisition maneuver driven by the ES navigation algorithm are shown. The spacecraft are starting from an initial position of $\mathbf{r}_1 = [-10, 9, -100]m$ and $\mathbf{r}_2 = [-7, 5, 100]m$ with initial velocities $\mathbf{v}_1 = [0, 0, 0.08](m/s)$ and $\mathbf{v}_2 = [0, 0, 0](m/s)$ both with respect to the Hill's reference frame centered in the center of the target formation that is set to be on a GEO orbit. The target configuration is set to $\mathbf{r}_1^{des} = [3, 0, 0]m$ and $\mathbf{r}_2^{des} = [-3, 0, 0]m$ and the acquisition time is approximately $4,5 \cdot 10^4 sec$. The actuation capabilities of the spacecraft are assumed to be limited so that $\| \mathbf{u} \| = 0.005 m/s^2$ and $|Q_{12}| < 4\mu C^2$. Moreover the mass of both the spacecraft is assumed to be $50kg$. The maneuver can be divided in three phases:

- **First actuated phase:** The SC thrusts in order to inject into a natural trajectory

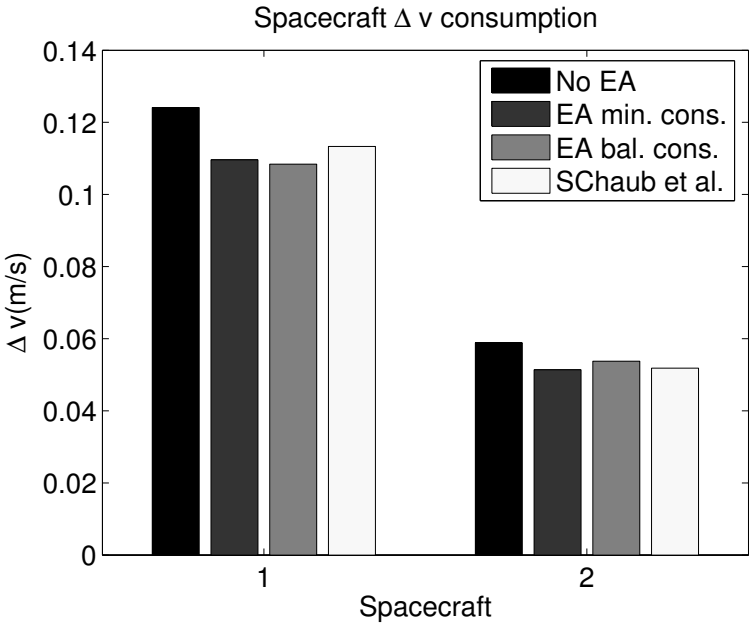

Figure 4.6: Results of the integration of the EA concept with the ES navigation scheme. Note: Minimum consumptions stands for the algorithm in Eq.(4.11) whereas Balanced consumptions stands for the algorithm in Eq.(4.17).

that will bring it to the desired position in a given time.

- **Coasting phase:** The actuators are switched off and the SC follow a natural trajectory.
- **Second actuated phase:** The actuators are switched on again and the SC avoid collision and decide autonomously which position to take in the final configuration.

The desired velocity vector is computed with the the parameters c_j, d_j, b and k_A, k_D listed in Table 4.1:

$b(s^{-1})$	0.0183
$d(s^{-1})$	0.0150
$c(s^{-1})$	$3.8637 \cdot 10^{-5}$
$k_A(m)$	9
$k_D(m)$	9.18

Table 4.1: ES parameters for 2 spacecraft acquisition maneuver.

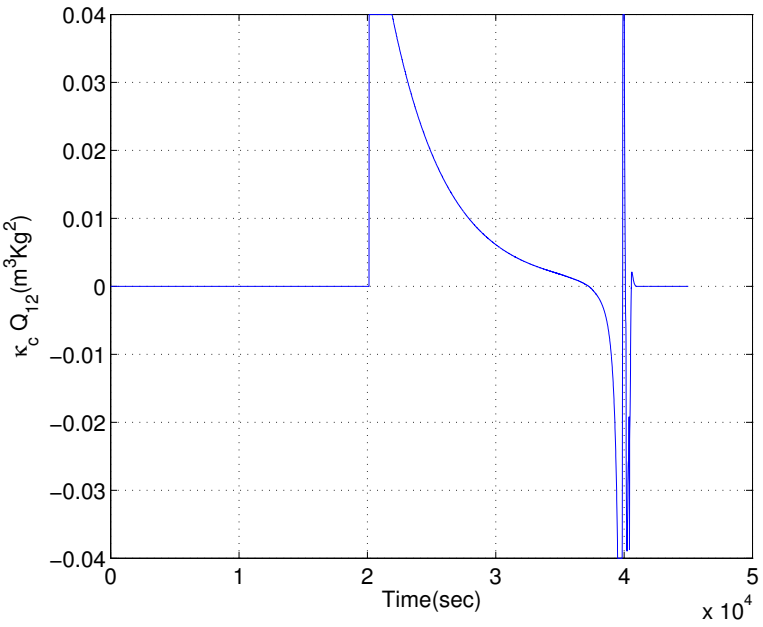

Figure 4.7: Nondimensional charge product for minimum fuel consumption strategy.

For the proposed simulation the exploitation of the EA concept leads to a saving of 13% of the total fuel consumption required for the acquisition maneuver with respect to the situation without electrostatic actuation. If the same simulation is performed exploiting the algorithm proposed in [18] the reduction in terms of total fuel consumption is 7%. Note that in the Δv computation also the maneuvers performed at the very beginning of the simulation are considered. Anyway at the very beginning of the simulation the two spacecraft are too far apart one from each other and no electrostatic actuation can be exploited. When this phase of the acquisition is not considered in the Δv computation the saving induced by the integration of the ES and EA concepts reaches 21% of the total Δv required. The same simulation has been used to test the charging strategy in Eq.(4.17). Since the tracking error of the spacecraft 1 at the very beginning of the simulation is higher with respect to the one of satellite 2 at each time during the maneuver $\Delta v_1 > \Delta v_2$. So according to Eq.(4.17) the swarm will decide during the maneuver to assume the value of Q_{12} such that $\| \mathbf{u}_{th_1} \|_2$ will be minimized at any time. The savings in terms of fuel consumption of satellite 1 induced by the EA concept are 13% whereas the savings for the entire formation are 11%. As expected this strategy attempts to reduce the fuel consumption of satellite 1 rather than the one of the all formation. The bars diagram in Figure 4.6 can be used to verify that the fuel consumption of satellite 1 when the strategy in Eq.(4.17) is used, is lower with respect to the one induced with the other strategies considered in this paper.

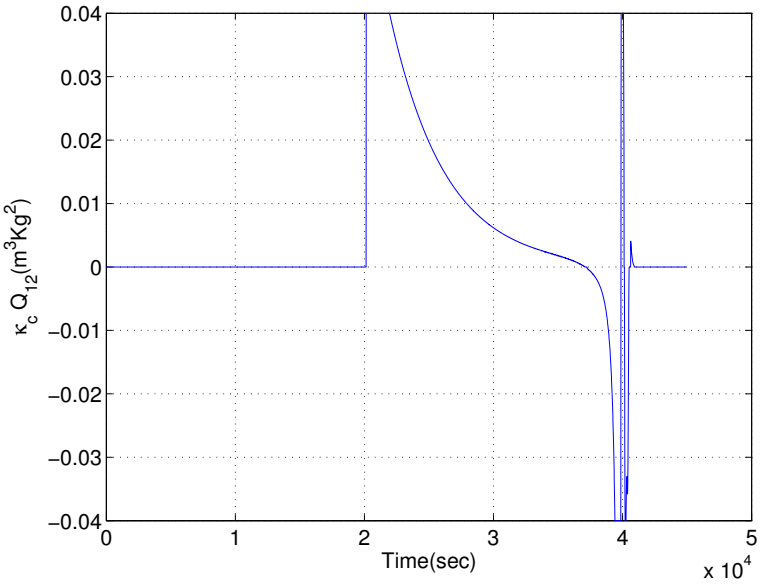

Figure 4.8: Nondimensional charge product for balanced fuel consumption strategy.

In Figure 4.7 and Figure 4.8 the variation in time of the charge product Q_{12} is displayed for both the algorithm in Eq.(4.11) and in Eq.(4.17). In this charts it is possible to observe that a charge saturation level has been included in order to constrain the charge of the SC to lay into a feasible range. The maximum allowed level of charge is set to $2\mu C$. For a spherical SC of radius $0.5m$ this amounts to a voltage level on the SC surface of about $40kV$. Note also that in the first part of the simulation the charge product is set to zero because the EA can not produce, when the SC are far apart one from each other, a force able to influence the motion of the satellites.
In Figure 4.9 the thrusting specific forces required during the acquisition without electrostatic actuation and with electrostatic actuation exploited according to Eq.(4.17) are displayed. From this plot it is possible to see how the Coulomb force acts in order to balance at any time the thrusting control required to each spacecraft. In the upper part of this plot the typical actuation history of an acquisition maneuver driven with the ES path planning strategy is shown. In this chart the three different phase of the maneuver are visible. A zoom of the $||\mathbf{u}_{th}||$ signal between $3.9 \cdot 10^5 sec$ and $4.1 \cdot 10^5 sec$ is also included in Figure 4.9. This time interval is in the third phase of the acquisition maneuver where the SC are close one to each other. Therefore the electrostatic actuation can influence the motion of the satellites and then increase the system efficiency.
As a final remark we point out here that the approach in Eq.(4.17) is again different with respect to the one in [18]. In fact in the simulation of Figure 4.5 satellite 1 has highest tracking error in a phase of the maneuver in which no Coulomb force can be

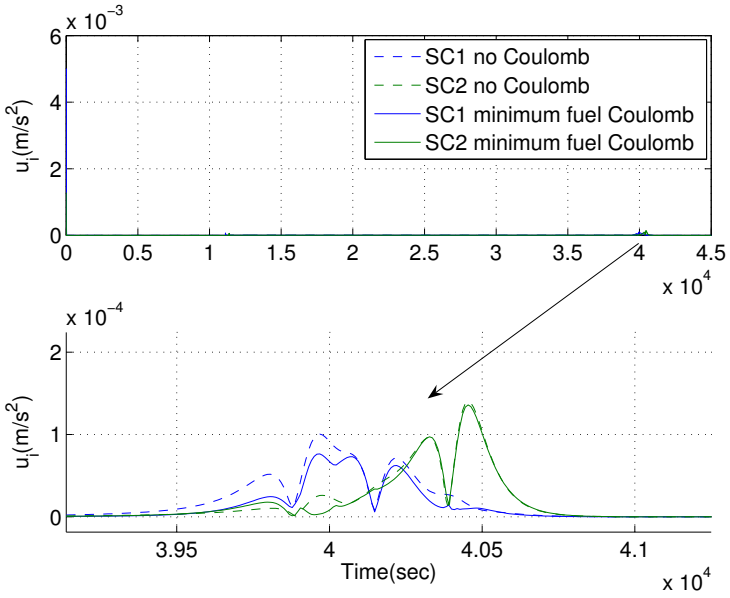

Figure 4.9: Force to be provided with conventional actuation system. Minimum fuel consumption algorithm.

used to actuate the control signal.

4.4.2 Three SC formation example

If the EA is exploited to balance the total fuel consumption, it is possible to solve the optimization problem in Eq.(4.17) also for a swarm of three agents. On the other hand it is not in principle so easy to extend the solution to the problem of Eq.(4.11) proposed for a two SC formation to a three-craft formation. In section 4.4.1 it has been shown that for a two SC formation it is possible to choose the individual charges q_1, q_2 from the sole charge product Q_{12} among infinite possibilities. In the three SC problem the mapping from the charge products to the individual charges is not always possible. Given the charge product vector $\mathbf{Q}$ in fact the individual charges can be obtained by

$$q_i = \sqrt{\frac{Q_{ij}Q_{ik}}{Q_{jk}}}.$$

Therefore the argument of the square root must be positive to have a non-imaginary value of the individual charges. In particular as outlined in [15] rather than ensuring that $\frac{Q_{12}Q_{13}}{Q_{23}} \geq 0$, $\frac{Q_{13}Q_{23}}{Q_{12}} \geq 0$ and $\frac{Q_{12}Q_{23}}{Q_{13}} \geq 0$ at the same time, it is equivalent, and

simpler, to enforce the following constraint:

$$Q_{12}Q_{13}Q_{23} \geq 0. \tag{4.18}$$

Therefore for a three SC formation the solution of the first part of the optimization problem, i.e. to find the optimal value of the charge products, must take into account the constraint in Eq.(4.18).
Whenever the EA is exploited to balance the total fuel consumption, it is always possible to find a vector $\mathbf{Q}$ that satisfies the condition in Eq.(4.18). For the three-craft balanced fuel consumption in fact the optimization problem can be rewritten as

$$\begin{aligned} &\forall t \quad \min_{Q_{ij}Q_{ik}} (\| \mathbf{u}_{th_i} \|_2) \\ &with \quad i : \min_{i\in[1,2,3]} (\Delta v_1(t), \Delta v_2(t), \Delta v_3(t)). \end{aligned} \tag{4.19}$$

The solution of such a problem is a reduced charge product vector with elements Q_{ij}, Q_{ik}. There are infinite ways to derive feasible individual charges from Q_{ij}, Q_{ik}. Following the idea in [18] in this work we use the following approach:

$$\begin{aligned} q_i &= \sqrt{(max(|Q_{ij}|, |Q_{ik}|))}, \\ q_j &= Q_{ij}/q_i, \\ q_k &= Q_{ik}/q_k. \end{aligned}$$

Note that with this approach the q_i charge is always positive whereas the q_j and q_k charges may be positive or negative depending from the sign of Q_{ij} and Q_{ik}.
The analytical solution of the problem in Eq.(4.2) presented in the previous section for a two SC formation can not so easily be extended to the three SC case. Eq.(4.11) written for the three SC case in fact does not always have a feasible solution. In order to generate charge product vectors $\mathbf{Q}$ that allow to derive feasible individual charges it is therefore necessary to include directly into the optimization problem the constraint in Eq.(4.18). In the three SC case Eq.(4.2) becomes

$$\begin{aligned} &\forall t, \quad \min_{\mathbf{Q}}(J(\mathbf{Q})) = \min_{J(\mathbf{Q})}(\| \mathbf{u}_{th_1} \|_2 + \| \mathbf{u}_{th_2} \|_2 + \| \mathbf{u}_{th_2} \|_2) \\ &subject\ to \quad Q_{12}Q_{13}Q_{23} \geq 0 \end{aligned} \tag{4.20}$$

where $\mathbf{Q} = [Q_{12}, Q_{13}, Q_{23}]$ are the charge products associated with the three SC formation. Since the problem in Eq.(4.20) can require an high computational effort to be solved, a simpler optimization problem is considered

$$\begin{aligned} &\forall t, \quad \min_{\mathbf{Q}}(\mathbf{Q}) = \min_{J(\mathbf{Q})}(\| \mathbf{u}_{th_1} \|_2^2 + \| \mathbf{u}_{th_2} \|_2^2 + \| \mathbf{u}_{th_2} \| 6_2^2) \\ &subject\ to \quad Q_{12}Q_{13}Q_{23} \geq 0. \end{aligned} \tag{4.21}$$

Anyway the solution of Eq.(4.21) represents an acceptable approximation of the solution of Eq.(4.20). Without the constraint of Eq.(4.18) the solution of Eq.(4.21) could be computed performing a simple pseudo-inverse calculation. In order to explain in detail how the algorithm proposed to solve the problem in Eq.(4.21) functions we first write in an extended way the balance of specific force for the 3 SS formation

$$\begin{cases} \mathbf{u}_{des_1} = \frac{\kappa_c Q_{12}}{m_1 r_{12}^2}\hat{\mathbf{r}}_{12} + \frac{\kappa_c Q_{13}}{m_1 r_{13}^2}\hat{\mathbf{r}}_{13} + \mathbf{u}_{th_1} \\ \mathbf{u}_{des_2} = -\frac{\kappa_c Q_{12}}{m_1 r_{12}^2}\hat{\mathbf{r}}_{12} + \frac{\kappa_c Q_{23}}{m_1 r_{23}^2}\hat{\mathbf{r}}_{23} + \mathbf{u}_{th_2} \\ \mathbf{u}_{des_3} = -\frac{\kappa_c Q_{13}}{m_1 r_{13}^2}\hat{\mathbf{r}}_{13} - \frac{\kappa_c Q_{23}}{m_1 r_{23}^2}\hat{\mathbf{r}}_{23} + \mathbf{u}_{th_3} \end{cases} \tag{4.22}$$

Let us define the configuration matrix $\mathbf{R}_{ij}$ as

$$\mathbf{R}_{ij} = \begin{bmatrix} \frac{\mathbf{r}_{12}}{\|\mathbf{r}_{12}\|^3}\cdot\hat{\mathbf{i}}_H, & \frac{\mathbf{r}_{13}}{\|\mathbf{r}_{13}\|^3}\hat{\mathbf{i}}_H, & 0 \\ \frac{\mathbf{r}_{12}}{\|\mathbf{r}_{12}\|^3}\cdot\hat{\mathbf{j}}_H, & \frac{\mathbf{r}_{13}}{\|\mathbf{r}_{13}\|^3}\hat{\mathbf{j}}_H, & 0 \\ \frac{\mathbf{r}_{12}}{\|\mathbf{r}_{12}\|^3}\cdot\hat{\mathbf{k}}_H, & \frac{\mathbf{r}_{13}}{\|\mathbf{r}_{13}\|^3}\hat{\mathbf{k}}_H, & 0 \\ \frac{\mathbf{r}_{21}}{\|\mathbf{r}_{21}\|^3}\cdot\hat{\mathbf{i}}_H, & 0, & \frac{\mathbf{r}_{23}}{\|\mathbf{r}_{23}\|^3}\cdot\hat{\mathbf{i}}_H \\ \frac{\mathbf{r}_{21}}{\|\mathbf{r}_{21}\|^3}\cdot\hat{\mathbf{j}}_H, & 0, & \frac{\mathbf{r}_{23}}{\|\mathbf{r}_{23}\|^3}\cdot\hat{\mathbf{j}}_H \\ \frac{\mathbf{r}_{21}}{\|\mathbf{r}_{21}\|^3}\cdot\hat{\mathbf{k}}_H, & 0, & \frac{\mathbf{r}_{23}}{\|\mathbf{r}_{23}\|^3}\cdot\hat{\mathbf{k}}_H \\ 0, & \frac{\mathbf{r}_{31}}{\|\mathbf{r}_{31}\|^3}\cdot\hat{\mathbf{i}}_H, & \frac{\mathbf{r}_{32}}{\|\mathbf{r}_{32}\|^3}\cdot\hat{\mathbf{i}}_H \\ 0, & \frac{\mathbf{r}_{31}}{\|\mathbf{r}_{31}\|^3}\cdot\hat{\mathbf{j}}_H, & \frac{\mathbf{r}_{32}}{\|\mathbf{r}_{32}\|^3}\cdot\hat{\mathbf{j}}_H \\ 0, & \frac{\mathbf{r}_{31}}{\|\mathbf{r}_{31}\|^3}\cdot\hat{\mathbf{k}}_H, & \frac{\mathbf{r}_{32}}{\|\mathbf{r}_{32}\|^3}\cdot\hat{\mathbf{k}}_H \end{bmatrix}$$

where $[\hat{\mathbf{i}}_H, \hat{\mathbf{j}}_H, \hat{\mathbf{k}}_H]$ are the usual versor of the Hill's reference frame. The system in Eq.(4.22) can be simply rewritten as

$$\mathbf{R}_{ij}\mathbf{Q} = \tilde{\mathbf{u}}.$$

where $\tilde{\mathbf{u}}$ contains all the components of the desired control vector

$$\tilde{\mathbf{u}} = \begin{pmatrix} \mathbf{u}_{el_1} \cdot \hat{\mathbf{i}}_H \\ \mathbf{u}_{el_1} \cdot \hat{\mathbf{j}}_H \\ \mathbf{u}_{el_1} \cdot \hat{\mathbf{k}}_H \\ \mathbf{u}_{el_2} \cdot \hat{\mathbf{i}}_H \\ \mathbf{u}_{el_2} \cdot \hat{\mathbf{j}}_H \\ \mathbf{u}_{el_2} \cdot \hat{\mathbf{k}}_H \\ \mathbf{u}_{el_3} \cdot \hat{\mathbf{i}}_H \\ \mathbf{u}_{el_3} \cdot \hat{\mathbf{j}}_H \\ \mathbf{u}_{el_3} \cdot \hat{\mathbf{k}}_H \end{pmatrix}.$$

For a three SC formation this is a system of 9 equations in 3 unknowns. Note that for a three SC formation there exists a proper reference frame for which the number of independent equations can be reduced to 6. This reference frame must have at any instant one of its coordinate planes coincident with the plane of the instantaneous satellite formation. Any possible vector $\mathbf{Q}'$ when multiplied for the matrix $\mathbf{R}_{ij}$ will produce a different value of the known vector $\tilde{\mathbf{u}}'$ representing the accelerations acting on the three SC due to the electrostatic force i.e.

$$\mathbf{R}_{ij}\mathbf{Q}' = \tilde{\mathbf{u}}'.$$

In this formulation the residuals vector $\mathbf{u}_{res} = \tilde{\mathbf{u}} - \tilde{\mathbf{u}}'$ represents the difference between the desired acceleration and the electrostatic one thus the one to be provided with thrusters. It is well known that the vector $\tilde{\mathbf{Q}}$ that minimizes the residuals is the one obtained using the Moore-Penrose matrix

$$\tilde{\mathbf{Q}} = \mathbf{R}_{ij}^{+}\tilde{\mathbf{u}}'.$$

where $\mathbf{R}_{ij}^{+} = (\mathbf{R}_{ij}^{T}\mathbf{R}_{ij})^{-1}\mathbf{R}_{ij}^{T}$. Unfortunately the Moore-Penrose matrix does not provide always a solution that satisfies the constraint in Eq.(4.18). For this reason in this work an iterative algorithm is proposed that exploits a routine aimed at finding the positive solutions of a general least square problem. In recent years many techniques have been developed that allow to solve the least square problem with linear inequality constraint [43]. This problem is stated as follows:
for a given matrix $\mathbf{C} \in R^{(n\times m)}$ *and a vector* $\mathbf{d} \in R^{(n\times 1)}$ *find* $\mathbf{x} \in R^{(m\times 1)}$ *such that*

$$\begin{aligned} &\min_{\mathbf{x}}(||\mathbf{C}\mathbf{x} - \mathbf{d}||) \\ &\textit{subject to} \quad x_i \geq 0. \end{aligned} \tag{4.23}$$

An iterative application of an algorithm providing the solution to this problem can allow to solve also the problem in Eq.(4.21). In particular the nonlinear inequality constraint in Eq.(4.18) is satisfied when $\mathbf{Q}$ has all its elements positive or whenever two out of three elements of $\mathbf{Q}$ are negative. All these situation can be separately recast into the form of Eq.(4.23) simply writing Eq.(4.22) in terms of the modified set of variables

$$\mathbf{Q}_1 = [Q_{12}, -Q_{13}, -Q_{23}] \ , \ \mathbf{Q}_2 = [-Q_{12}, Q_{13}, -Q_{23}] \ , \quad \mathbf{Q}_3 = [-Q_{12}, -Q_{13}, Q_{23}]$$

It is then possible to compute the non negative solution in terms of all the sets of modified variables and then to find the global constrained minimum of the problem in Eq.(4.21) simply taking the solution associated with the minimum amount of fuel consumption.

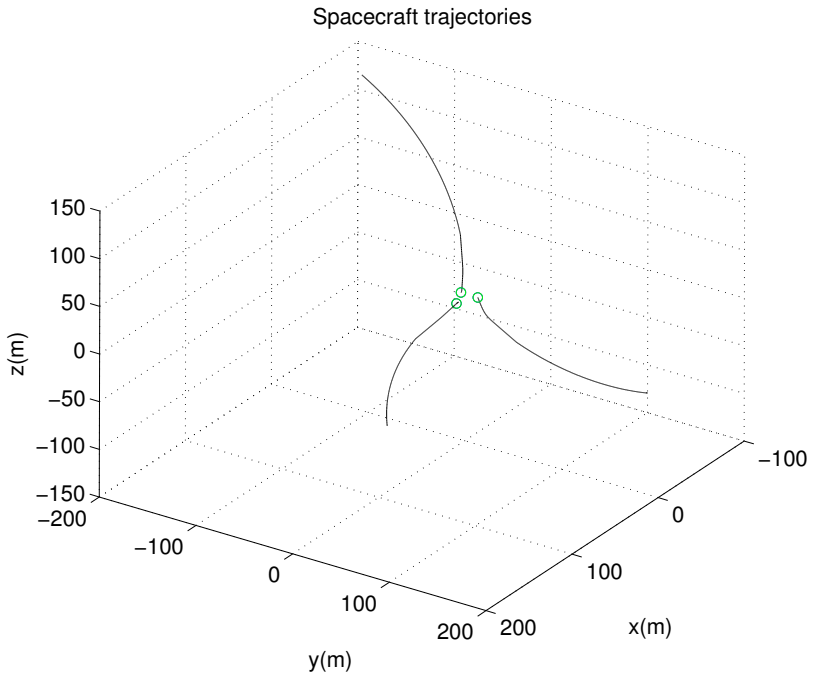

Figure 4.10: Three SC acquisition maneuver: SC trajectories.

In the following the performance of the proposed algorithms are discussed. In Figure 4.10 the trajectories of three spacecraft performing an acquisition maneuver driven by the ES swarm navigation technique are shown. The spacecraft are starting from an initial position of $\mathbf{r}_1 = [161, 9, 63.6, -19.4]m$, $\mathbf{r}_2 = [-72.8, -171.9, 139.5]m$ and $\mathbf{r}_3 = [-89.2, 108.2, -120.1]m$. The SC initial velocities with respect to the Hill's reference frame centered in the center of the target formation and set on a GEO orbit are $\mathbf{v}_1 = [0, 0, 0](m/s)$, $\mathbf{v}_2 = [0, 0, 0](m/s)$ and $\mathbf{v}_3 = [0, 0.12, 0](m/s)$. The target configuration is an equilateral triangle of radius $10m$ centered in the center of the Hill's reference frame.

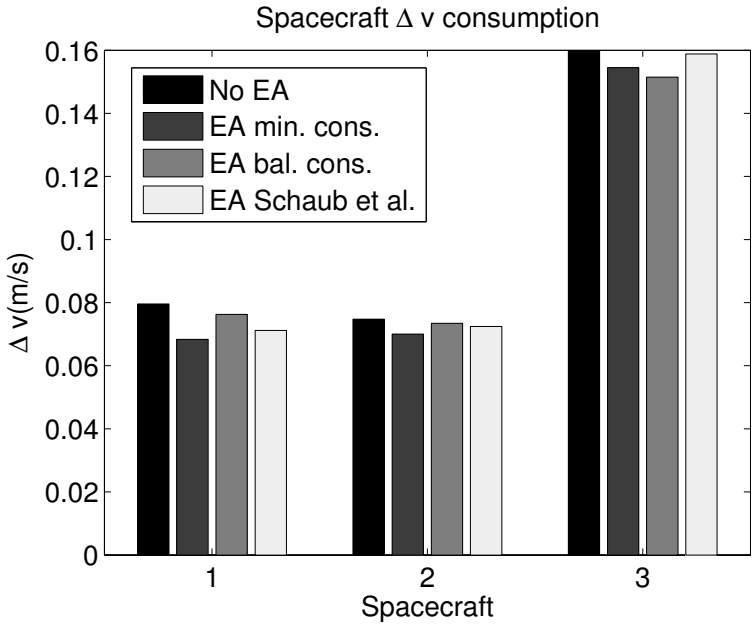

Figure 4.11: Results of the integration of the EA concept with the ES navigation scheme. Note: Minimum consumptions stands for the algorithm in Eq.(4.11) whereas Balanced consumptions stands for the algorithm in Eq.(4.17).

The parameters to be defined in order to apply the ES are listed in Table 4.2. The total

$b(s^{-1})$	0.0011
$d(s^{-1})$	$9.0 \cdot 10^{-4}$
$c(s^{-1})$	$7.2423 \cdot 10^{-6}$
$k_A(m)$	100
$k_D(m)$	102

Table 4.2: ES parameters for 3 spacecraft acquisition maneuver.

formation acquisition time is approximately $6 \cdot 10^4 sec$. The actuation capabilities of the spacecraft are the ones already introduced in section 4.4.1. Following the line already proposed in section 4.4.1 the performance of the proposed strategies are compared with the strategy introduced in [18]. For the proposed simulation the exploitation of EA with the minimum fuel strategy leads to a saving of 8% of the total fuel consumption required for the acquisition maneuver with respect to the situation without electrostatic actuation. If the same simulation is performed exploiting the algorithm proposed in

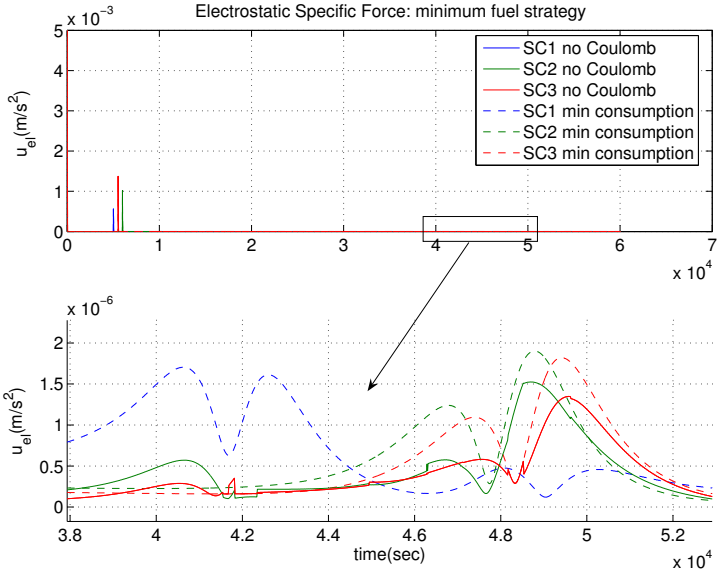

Figure 4.12: Force to be provided with conventional actuation system: minimum fuel consumption algorithm.

[18] the reduction in terms of total fuel consumption is 4%. Again higher savings are obtained as long as the very first phase of the acquisition maneuver is not taken into account in the computation of the fuel consumption (up to 18%). Since again at the beginning of the simulation the tracking error of the spacecraft 3 is higher with respect to the one of the other satellites belonging to the swarm $\Delta v_3 > \Delta v_2$ and $\Delta v_3 > \Delta v_1$. If the strategy of Eq.(4.19) is applied the savings in terms of fuel consumption of satellite 3 induced by the EA concept are 6% (up to 12% when the first phase is neglected) whereas the savings for the entire formation are 5%. The bars diagram in Figure 4.11 can be used to compare the performances of the different strategies. In particular the savings associated with SC 3 due to the minimum fuel strategy are lower (5%) with respect to the one induced by the balanced strategy.
In Figure 4.12 and Figure 4.13 the thrusting specific forces required during the acquisition with and without electrostatic actuation are shown. In Figure 4.12 the forces resulting from the charging strategy in Eq.(4.21) are displayed whereas in Figure 4.13 the ones due to the strategy in Eq.(4.19) are shown. In the upper part of both these plots it is possible to recognize again the usual actuation signal of an acquisition maneuver steered by means of the ES technique. In particular the three SC start the breaking phase already after approximately $5000 sec$. This can be seen from the peaks appearing in the actuation signals of the three SC in both figures Eq.(4.21) and Eq.(4.19). A zoom of the $||\mathbf{u}_{th}||$ signal between $3.8 \cdot 10^5 sec$ and $5.2 \cdot 10^5 sec$ is also included in Figure 4.12. In

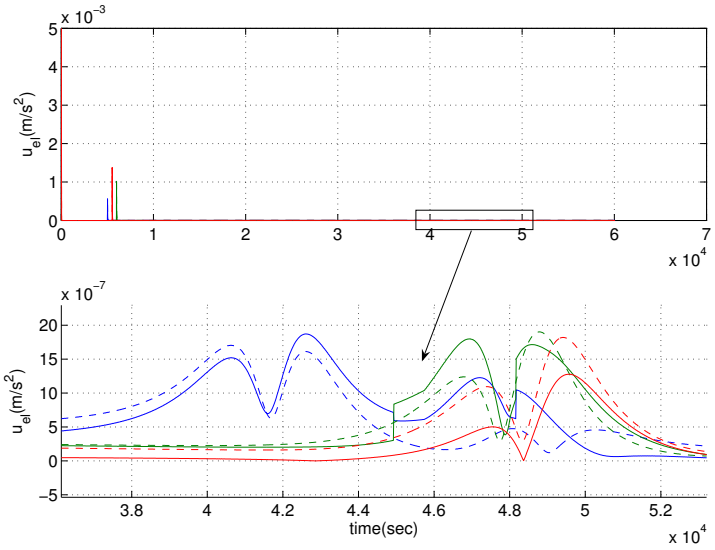

Figure 4.13: Force to be provided with conventional actuation system: balanced fuel consumption algorithm.

this time interval the spacecraft are close to each other and therefore the electrostatic force can have a big influence in the formation fuel consumption. From these plots it is possible to note how the switching algorithm proposed to solve both the optimization problems result in a discontinuos behavior of the thrusting actuation signal.
In Figure 4.7 and Figure 4.15 the variation in time of the three charge products in $\mathbf{Q} = [Q_{12}, Q_{13}, Q_{23}]$ is displayed for both the algorithm in Eq.(4.11) and in Eq.(4.17). In this charts it is again possible to observe that a charge saturation level has been included. Moreover in the proposed simulation the EA is switched on only when the SC are close one to each other. For this reason during the first $6000sec$ of the simulation the charge of each SC is set to zero. At the end of the simulation the charge products converge to the fixed values needed to balance the gravitational and inertial force in the final configuration.
Even if the method used to minimize the total fuel consumption has shown interesting results it is not free from weak points. In particular the main one deals with the time needed to perform the calculation of the desired charges. Every optimization problem in fact requires the on board computer of each SC to solve in an iterative way the problem in Eq.(4.23). This represents a limit of the proposed algorithm because the real capabilities of the EA in principle allows to track in a very fast way the computed charges (as seen in chapter).

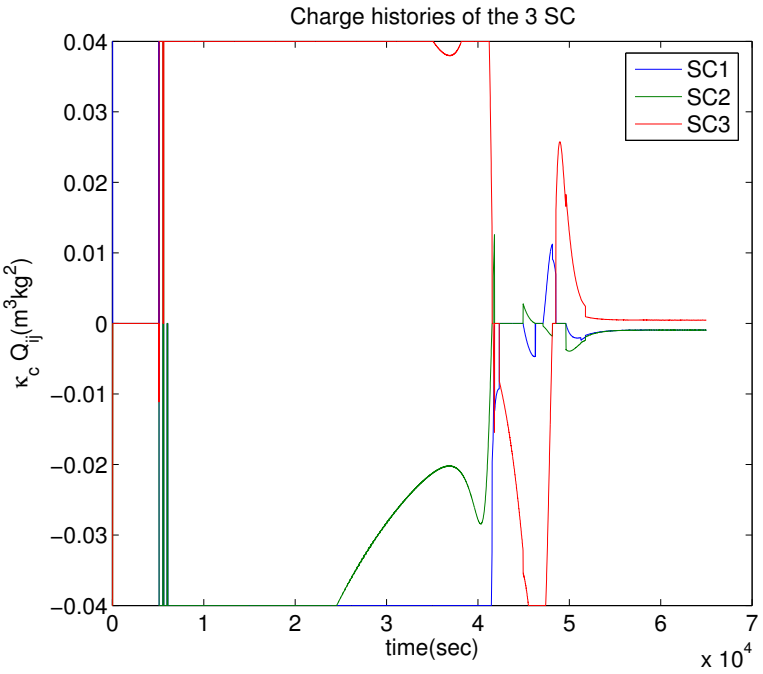

Figure 4.14: Nondimensional charge product for minimum fuel consumption strategy.

4.4.3 Charge product approach: N-SC formation, open problems.

The solution to the balanced fuel consumption proposed for the two-three SC case can be easily extended for a swarm of N SC. On the other hand whenever the charge approach is used for swarms of N spacecraft the solution to the minimum fuel consumption problem gets more and more complicated. In particular other constraints must be added to the optimization problem in order to find a vector of charge products that can be mapped into a corresponding vector of feasible individual charges. The specific force balance of a swarm of N charged SC depends in general form $N(N-1)/2$ charge products. The mapping from $\mathbf{Q}$ to $\mathbf{q}$ is therefore not always possible and equality constraints have to be added to the inequality one defined in Eq.(4.18)

$$Q_{ij}Q_{lm} = Q_{jm}Q_{il} \ , \ \forall \ i,j,l,m \in [1,..,N]. \tag{4.24}$$

The solution of a least square problem with the constraints in Eq.(4.24) can be highly expensive from a computational point of view. For this reason the algorithm proposed to solve the minimum fuel problem for a three SC formation may not be useful for the on line computation of the charges for the N satellites case. A possible extention of the charge product approach to the N SC problem has been proposed in [15] where the charge of the SC are rapidly switched on and off by means of a pulse-width modulation in order to have at any time the possibility to track any possible charge product history.

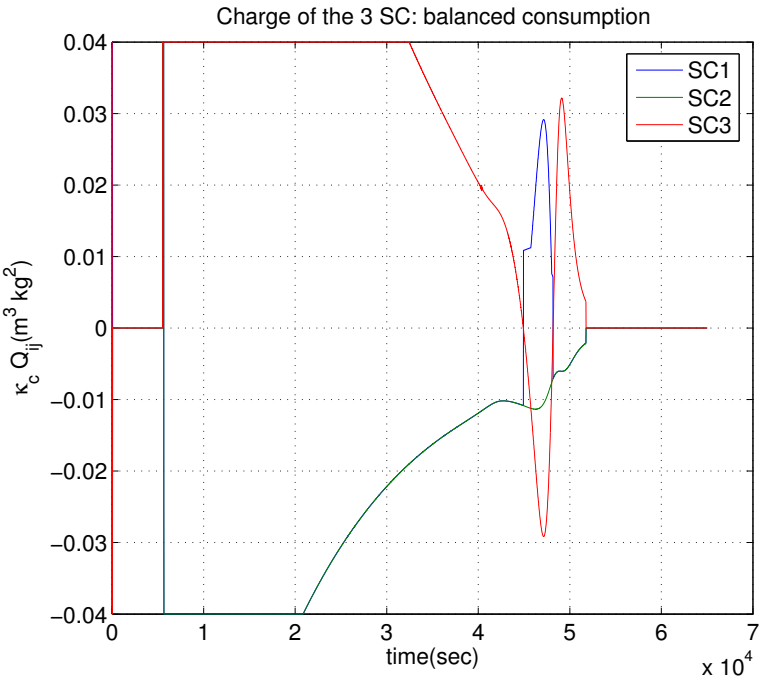

Figure 4.15: Nondimensional charge product for balanced fuel consumption strategy.

An alternative approach to the solution of the N SC problem can be obtained finding at any time the charge product that will control the SC with the highest tracking error. A switching algorithm between the different satellites will allow to control the whole formation. An extensive study of the properties of such a scheme is given again in [18].

4.5 Behavior based charge control

In this section a behavior based approach is used to solve the problem in Eq.(4.2). Let us consider a swarm of N SC performing a general maneuver. As shown in chapter active emission of charged particles is the most appealing candidate to produce the variation of the charge on the SC surface. Let us introduce the following feedback law

$$\mathbf{I} = \kappa_I(\mathbf{q}_{des} - \mathbf{q}) \tag{4.25}$$

where $\mathbf{q} = [q_1, .., q_N]$ is the charges vector containing the charges of the N SC and $\mathbf{q}_{des} = [q_{des_1}, .., q_{des_N}]$ is the vector containing the charge values that each SC instantaneously wants to acquire. The vector $\mathbf{I} = [I_1, .., I_N]$ contains the current emitted by each satellite to assume its desired charge. There are different options to define the desired charge of each SC in the swarm. In this work a behavior based approach is introduced. According

to this approach each SC individually assumes the charge that reduces its individual fuel expenditure.
At a certain instant in time $\hat{t}$ the $i-$th SC state with respect to the rest of the swarm can be described by two vectors, the instantaneous configuration and the instantaneous maneuver vector.

- The $i-$th SC instantaneous configuration is defined by the inter-SC relative position vectors $\mathbf{r}_{ij}(\hat{t}) = \mathbf{r}_i(\hat{t}) - \mathbf{r}_j(\hat{t})$ and by the instantaneous charge vector $\mathbf{q}(\hat{t}) = [q_1(\hat{t}), .., q_N(\hat{t})]$. These informations can be lumped together in a single matrix called the swarm instantaneous configuration matrix

$$\mathbf{C}_i = \mathbf{R}_i \mathbf{q} \tag{4.26}$$

  where $\mathbf{R}_i$ is defined according to Eq.(4.8)

- The $i-$th SC instantaneous maneuver vector $\mathbf{u}_{des_i}(\hat{t}) \in R^{(3\times 1)}$ is the vector containing the instantaneous specific force that the SC has to provide in order to track the planned motion.

When the swarm instantaneous configuration and maneuver are available the actual state of the $i-$th SC is fully known. These informations can then be used to compute the $\mathbf{q}_{des}$ vector at any time

$$q_{des_i} = \mathbf{C}_i^{+} \mathbf{u}_{des_i} \tag{4.27}$$

where $\mathbf{C}_i^{+} = (\mathbf{C}_i^T \mathbf{C}_i)^{-1} \mathbf{C}_i$ represents the Moore-Penrose inverse of the instantaneous configuration matrix.
A simple geometrical interpretation of the charging strategy in Eq.(4.27) is given in the following. At the instant $\hat{t}$ the $i-$th SC control system outputs the instantaneous maneuver vector $\mathbf{u}_{des_i}$. Given the charges of the other SC belonging to the formation and the geometric instantaneous configuration, the $i-$th SC can evaluate the direction along which the electrostatic force acts

$$\hat{\mathbf{u}}_{el_i} = \mathbf{R}_i \mathbf{q}. \tag{4.28}$$

The charging strategy in Eq.(4.27) requires to assume that value of the charge so that the electric force acting on the SC is the projection of the instantaneous maneuver vector on the direction individuated by Eq.(4.28)

$$q_{des_i} = \mathbf{u}_{des_i} \cdot \mathbf{R}_i \mathbf{q} / |\mathbf{R}_i \mathbf{q}|^2. \tag{4.29}$$

This is clearly the charge that will minimize the residual specific force to be provided with thrusters. According to this strategy the $i-$th SC gets as input the charge of the other SC belonging to the formation and evaluates its own desired charge trying to minimize an individual cost function.

Before testing the performance of the developed charging strategy it is interesting to highlight what is the information exchange between the SC introduced by the proposed algorithm. In order to evaluate the desired charge each SC needs in principle the information about the instantaneous swarm geometrical configuration and about the charge vector $\mathbf{q}$. These information are then processed on board with the instantaneous maneuver vector $\mathbf{u}_{des_i}$ to derive the value of the desired charge.
The algorithm proposed in this work can be compared with the one introduced in [18]. As already mentioned througout this chapter in this work the charge product formulation is exploited to derive the charge vector that minimizes the residual acceleration acting on the SC with the highest tracking error. Whenever the algorithm in [18] has to be implemented on board two different strategies could be exploited:

- **Centralized strategy:** The computation of the charge products and of the individual charges is performed on board a sole satellite called chief craft. This SC receives from the other SC the information about the swarm component tracking errors and instantaneous maneuver vectors, computes the charges vector and transmit it to the satellites belonging to the formation. This approach enjoys the advantage that it can rely on a simple communication architecture. On the other hand the main drawback of such approach is that the chief craft represents a single failure point of the all system.

- **Distributed strategy:** The calculation of the charge products and of the associated individual charges is performed on board each satellite. For this reason each SC must have available on board the information about the other SC tracking errors, the inter-SC relative positions and the instantaneous maneuver vector of the SC with highest tracking error. In particular the exchange of this information between the SC will require a particular attention. In fact in principle the $i-$th SC does not need to collect the information about the instantaneous maneuver vector of all the other SC. A possible strategy would then be a two step communication algorithm where first the tracking errors informations are exchanged and then each SC uses this information to downlink the instantaneous maneuver of the SC with highest tracking error.

This considerations allow to conclude that in general the approach introduced in this work requires a simpler communication architecture to be established between the members of the swarm.
In the following the performances of the proposed charging strategy are assessed by means of simulations. The dynamical system considered in the simulation is

$$\dot{\mathbf{q}} = \kappa_I(\mathbf{q}_{des} - \mathbf{q}) \tag{4.30}$$

where $\dot{\mathbf{q}}$ is the vector containing the time derivatives of the charges of all the SC. Note that in this system a simplification is done since all the environmental charges described in chapter are not considered.

The parameter κ_I can be chosen in order to achieve different charging strategies. In particular if one wants to keep the rate of charge almost constant in time an adaptive gain can be introduced that becomes smaller [bigger] as long as the difference between q_i and q_{des_i} becomes bigger [smaller]. Moreover typically the charge on the SC can only vary within a certain range. For this reason a saturation cycle has been included in the proposed charging strategy so that the current emitted by the SC is suddenly switched off as long as the value of the charge exceeds the saturation value of $2\mu C$.
In the remaining of this chapter two different simulation set up are considered to test the behavior based charging strategy. First we consider a static condition that mimics a station keeping problem. In this set up the SC are frozen in a given configuration and therefore the instantaneous maneuver of each SC is constant so that $\mathbf{u}_{des_i}$ perfectly counteracts the inertial and gravitational force acting on the SC. Then we consider a dynamic situation where the SC perform a given maneuver steered by the ES path planning technique. In this case a time varying $\mathbf{u}_{des_i}$ is generated. A simulation campaign has been performed in order to verify to which extent the proposed charging strategy is able to track the time varying instantaneous maneuver.

4.5.1 Test of the behaviour based charge feedback for static formations

In this section the performance of the proposed charge feedback is tested for static formations i.e. for configurations in which the swarm is frozen in a virtual structure. In such a condition the instantaneous maneuver is constant in time being the constant force needed to counteract the static contribution of the gravitational and inertial force present in the non inertial frame. At the beginning of the simulation the charge of the satellites are randomly chosen. In Figure 4.16 the results of a simulation performed for a four SC formation are shown. In this chart the variation of the charges on the SC during the simulation are presented. The positions of the SC in the formation are listed in Table 4.3 together with the initial condition on the SC charges. A picture representing the static formation considered in this simulation is shown in Figure 3.5(b). The dynamical system converges to a stationary solution and the steady state charges are equivalent to the equilibrium ones found in chapter 3 for the same formation.

	Position(m)	Charge (μC)
SC1	$[20.89, 0, -14.04]$	-2.8
SC2	$[-14.04, 0, -20.89]$	-2.5
SC3	$[-20.89, 0, 14.04]$	2.0
SC4	$[14.04, 0, 20.89]$	2.2

Table 4.3: Initial conditions and parameters for a 4 SC static formation.

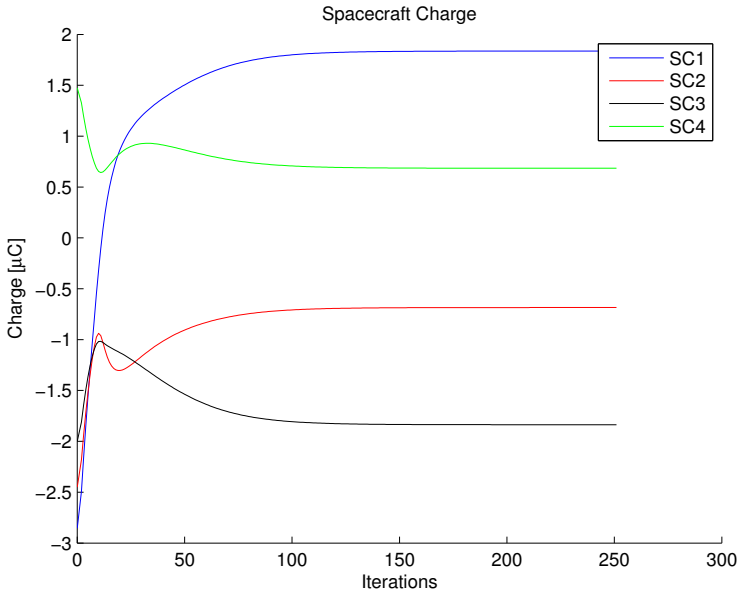

Figure 4.16: Charge variation in time for a static 4 SC formation.

In Figure 4.17 the charges histories for a formation of six satellites are shown. The formation in this simulation forms an hexagon in the Hill's $x - z$ plane. The positions of the SC in the formation as long as the initial condition on the charges are presented in Table 4.4.

	Position(m)	Charge (μC)
SC1	$[10, 0, 0]$	-2.8
SC2	$[5, 0, 8.66]$	2.5
SC3	$[-5, 0, 8.66]$	2.0
SC4	$[-10, 0, 0]$	-1.5
SC5	$[-5, 0, -8.66]$	1.0
SC6	$[5, 0, -8.66]$	1.5

Table 4.4: Initial conditions and parameters for a six SC static formation.

Also in this simulation the system converges to a set of stationary charges. Moreover it is possible to verify that the value of the charges is the one that can be obtained solving the minimization problem defined in Eq.(4.2). The stability of the dinamical system in Eq.(4.30) has been assessed performing similar simulations for a large amount of formations. Although the closed loop system in Eq.(4.30) has shown good stability properties, a singularity problem occurs when all the SC assume zero charge at the same time. In this eventuality the direction of application of the electrostatic force can not be defined and $\mathbf{q}_{des}$ is always zero. Although this represents a problem connected with the proposed feedback a simple singularity escape procedure can be implemented to avoid the occurrence of such an eventuality.

4.5.2 Test of the behaviour based charge feedback for swarm maneuvering

In this section the charge control strategy in Eq.(4.25) is tested with a time varying instantaneous maneuver signal. In particular the task of this section is to verify that the proposed feedback can be used to integrate the EA into the ES swarm navigation technique. For this reason the feedback defined in Eq.(4.25) is used to solve the problem in Eq.(4.2) for some acquisition or reconfiguration maneuvers.
In section 4.4.1 and 4.4.2 the charge product algorithm has been introduced and its performance for different simulation maneuvers has been tested. In these sections it has been shown that the EA can be used to reduce the fuel consumption associated to a typical acquisition maneuver driven by the ES technique. The fuel savings triggered by the use of EA is clearly dependent from the maneuver that is performed. In addition to the test of the charge feedback in Eq.(4.25) in this section it is also shown how it is possible to tune the ES parameter such that the path planning technique automatically generates trajectories for which EA causes high savings in terms of fuel consumption.
From a control authority point of view a conventional actuator has a saturation level that is independent from any other variable so that each SC can rely on the same amount

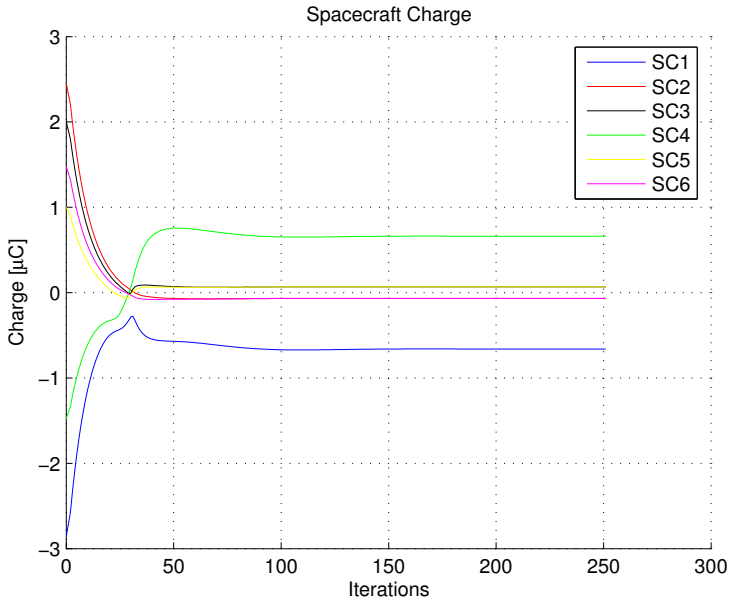

Figure 4.17: Charge variation in time for a static 6 SC formation.

of thrust in all the working condition. On the other hand the EA has a saturation level that is dependent on the inter SC distance i.e. high electrostatic force can be obtained only when the SC are close one to each other. This is sketched in Figure 4.18. A path planning technique able to maximize the possible advantage triggered by the EA must require high changes in velocities, i.e. forces, only in conditions where the SC are close one to each other.

For a given formation in space the ES technique defines a set of acquisition maneuvers parameterized by the values of the parameters k_A, k_D, d_j, c_j and b. As already mentioned in the previous chapters for many interesting formations the ES formula establishes a reduced number of relations between these parameters so that, most of the times, the choice of some of them is completely left to the system designer.

By varying the values of the d_j, c_j and b parameters it is possible to change the magnitude of $\mathbf{v}_{des}$. If the SC are starting the maneuver from a rest condition the asymptotic stability of the Q-guidance feedback allows to conclude that the error on velocity will be in a worst case scenario of the order of magnitude of $\mathbf{v}_{des}$. Moreover given the aggregation properties of the swarm during the reconfiguration maneuver, the motion of the swarm will be confined in a certain volume of characteristic length l. A first simple rule to generate trajectories suitable for the introduction of the EA is therefore to set the d_j, c_j and b so that:

$$\kappa v_g \sim \frac{\kappa_c \overline{q_i}^2}{l^2}. \tag{4.31}$$

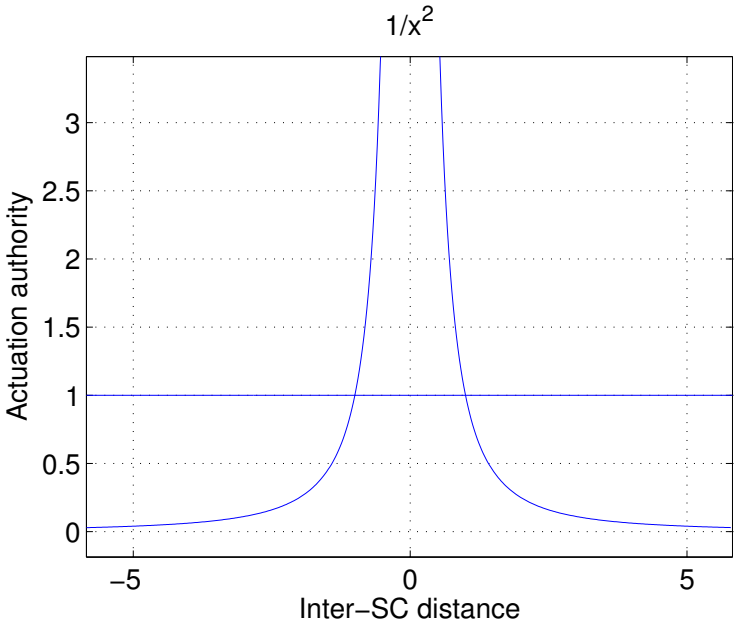

Figure 4.18: Actuation saturation vs. inter SC distance for conventional and electrostatic actuation

Moreover the parameters k_A, k_D link the desired velocity to the inter-SC distance and the distance between the SC and the target positions. These can be tuned to require high acceleration only when the SC are close one to each other.
Following these simple guidelines some test simulations have been derived for the feedback in Eq.(4.25). Some of these simulations are presented here to show both the performance of the behaviour based feedback law and the effect of the application of these simple guidelines in the ES path planning technique.

Two SC tether reconfiguration maneuver

A first simple simulation is presented in Figure 4.19. Here a swarm of two satellites in a tether configuration performs a reconfiguration maneuver that reduces the inter-SC distance. The trajectories of the two SC are shown in Figure 4.19(a). The main simulation data are listed in Table 4.5

$b(s^{-1})$	0.0011
$d(s^{-1})$	$9.0 \cdot 10^4$
$c(s^{-1})$	$7.2423 \cdot 10^{-6}$
$k_A(m)$	100
$k_D(m)$	102

Table 4.5: Simulation parameter for the 2 SC tether reconfiguration maneuver.

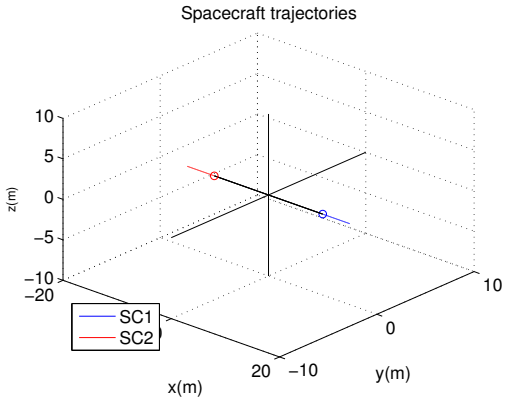

(a) Electrostatic tether reconfiguration: SC trajectories.

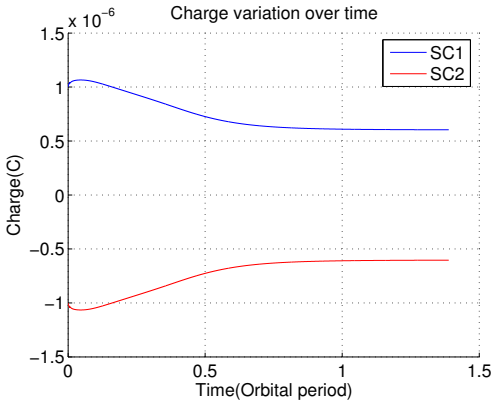

(b) Electrostatic tether reconfiguration: SC charge histories.

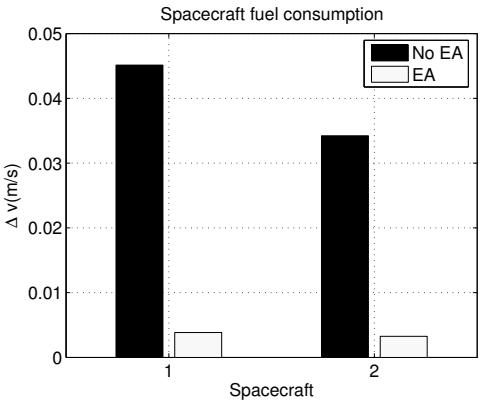

(c) Electrostatic tether reconfiguration: SC fuel consumption.

Figure 4.19: Electrostatic tether reconfiguration.

The SC start from an initial position respectively of $\mathbf{r}_1 = [15, 0, 0]m$ and $\mathbf{r}_2 = [-15, 0, 0]m$ and from zero initial charge. The total maneuver time is 1.5 orbital periods. Note that the magnitude of the parameters in Table 4.5 gives reason of the characteristic time scale

of the instantaneous maneuver variation. On the other hand the parameter κ_I describes the characteristic time scale of the dynamical system in Eq.(4.30). An appropriate tuning of these parameters allows to separate in time the two processes so that the time interval in which a significative change in the instantaneous maneuver take place is always bigger with respect to the convergence time of the charge dynamical system. This fact is evident from the graph in Figure 4.19(b) where the variation in time of the SC charge is displayed. In this graph no transient dynamics appears so that the SC have at any instant the desired level of charge.
During the maneuver the absolute value of the charges decreases. This is due to the fact that the attractive electrostatic force acting between the two SC counteracts the gravitational and inertial force that diminishes as long as the SC are getting closer to the center of the Hill's frame.
In Figure 4.19(c) the Δv required to perform the maneuver with and without the exploitation of the EA are displayed. For this particular maneuver 97% of the Δv required to the whole swarm can be provided with EA.

Three SC deployment maneuver

In Figure 4.20 the trajectories of a three SC formation performing a deployment maneuver are shown. The initial positions of the SC are shown in Table 4.6 whereas the parameters of the ES technique are listed in Table 4.7.

	Position(m)	Charge (μC)
SC1	$[20.89, 0, -14.04]$	-2.8
SC2	$[-14.04, 0, -20.89]$	-2.5
SC3	$[-20.89, 0, 14.04]$	2.0

Table 4.6: Initial conditions for a 3 SC deployment maneuver.

$b(s^{-1})$	$5.5 \cdot 10^{-5}$
$d(s^{-1})$	$5.2 \cdot 10^{-5}$
$c(s^{-1})$	$8.89 \cdot 10^{-11}$
$k_A(m)$	30
$k_D(m)$	20

Table 4.7: Simulation parameter for the 3 SC deployment maneuver.

The SC are supposed to reach a final configuration forming an equilateral triangle of size $10m$. In Figure 4.20(a) and in Figure 4.20(b) the three dimensional and planar view of the SC trajectories during the maneuver are shown whereas in Figure 4.21 the variation in time of the SC charge are displayed.

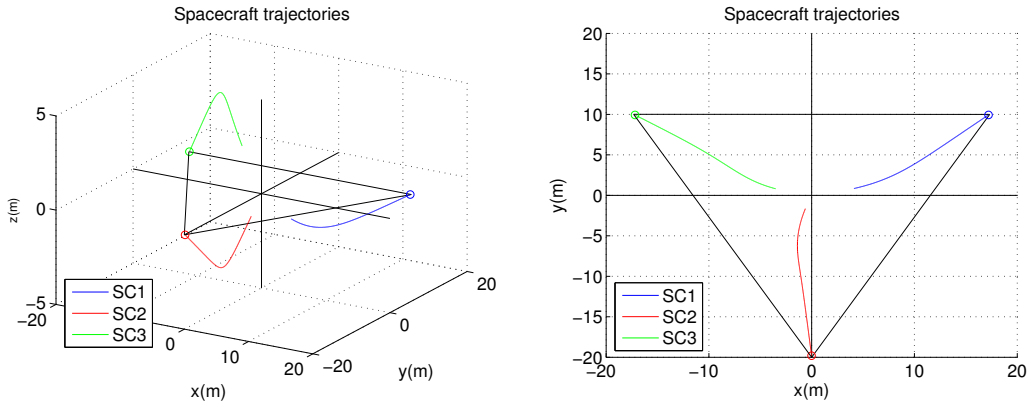

(a) Trajectories of the three SC deployment: 3D view

(b) Trajectories of the three SC deployment: planar view.

Figure 4.20: 3SC deployment maneuver: SC trajectories.

At the very beginning of the simulation the SC are at rest condition and must acquire a certain radial velocity to reach the final desired position. Therefore in the first 150 seconds all the SC assume a positive charge so that the electrostatic repulsion force can provide a considerable part of the initial instantaneous maneuver. This is shown in Figure 4.21(a). After $250s$ the satellites must start the deceleration process. For this reason attractive electrostatic forces must be established. In particular two SC assume charges of opposite sign and approximately same order of magnitude (blue and green line in Figure 4.21(a)) whereas the third one (red line) assumes a very small negative charge. The SC marked with the blue and the green line move along the Hill's x axis (see Figure 4.20(b)). For this reason they have to counteract the gravitational and inertial effect that would make their trajectories divergent. On the other hand the satellite marked with red line moves along the Hill's y axis where it experience only the Coriolis force that pushes it towards the direction of the negative x. The attraction between the SC in green and blue line allows to avoid the two SC to diverge. On the other hand the attraction between the red and the blue counteracts the Coriolis force acting on the red SC. Note that in the time interval between $150s$ and 0.5 orbital periods the SC marked with blue and green are charged at different magnitudes. This asymmetric condition is beneficial because it allows to influence also the motion of the third SC. The same result can not be obtained using the charge product approach.

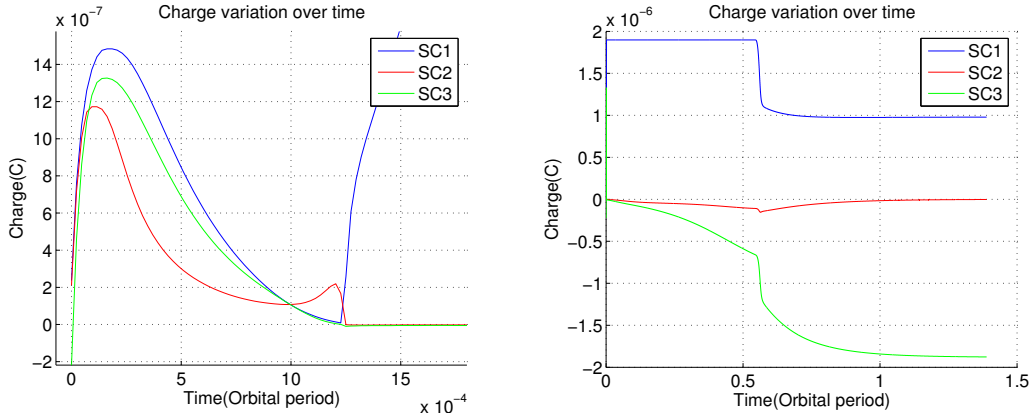

(a) Three SC deployment charge histories: zoom at the beginning of the maneuver.

(b) Three SC deployment charge histories.

Figure 4.21: 3SC deployment maneuver: charge variation.

In Figure 4.22 the Δv required to perform the maneuver with and without EA are displayed. The approach proposed in this work is also compared with the one in [18]. The proposed charge control algorithm yields a saving in terms of Δv required to perform the maneuver of 81% with respect to the case in which no EA is considered. A lower performance is obtained with the algorithm from [18].

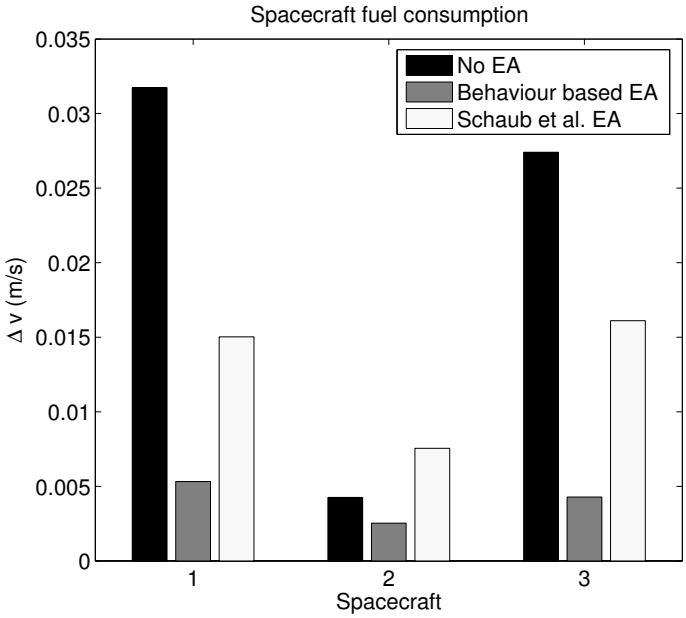

Figure 4.22: Fuel consumption of the three SC deployment maneuver.

Four SC reconfiguration maneuver

In Figure 4.23 a four SC reconfiguration maneuver performed with the aid of EA is considered. The SC positions at $t = 0$ are shown in Table 4.8 whereas the characteristic parameters of the ES technique are listed in Table 4.9.

	Position(m)	Charge (μC)
SC1	$[5.0, 0, 3.53]$	0.3
SC2	$[-5.0, 0, 3.53]$	0.2
SC3	$[0, 5.0, -3.53]$	0.1
SC4	$[0, 5.0, 3.53]$	0.1

Table 4.8: Initial conditions and parameters for a 4 SC reconfiguration maneuver.

$b(s^{-1})$	$1.833 \cdot 10^{-4}$
$d(s^{-1})$	$5.0 \cdot 10^{-5}$
$c(s^{-1})$	$4.066 \cdot 10^{-8}$
$k_A(m)$	28
$k_D(m)$	30

Table 4.9: Simulation parameter for the 4 SC deployment maneuver.

In this particular simulation a swarm of four SC starts from a tetrahedron configuration and acquires a square formation in the Hill's $x - y$ plane. The trajectories followed by the SC during this maneuver are shown in Figure 4.23(a). Note that the radius of the target formation is bigger with respect to the characteristic length of the initial configuration. For this reason at the very beginning of the simulation the SC must have a radial component of the velocity. Therefore in the first $200s$ all the SC assume a positive value of the charge so that the resulting repulsive force provides the desired radial acceleration (see Figure 4.23(b)).

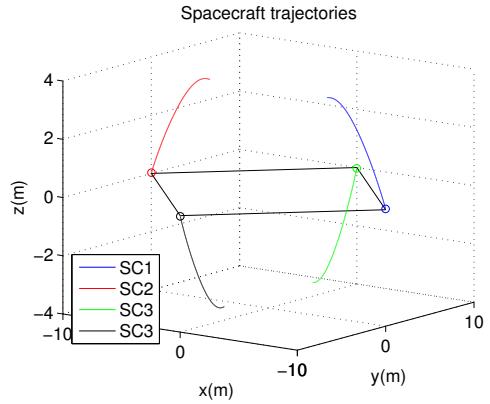

(a) Electrostatic 4 SC formation reconfiguration: SC trajectories.

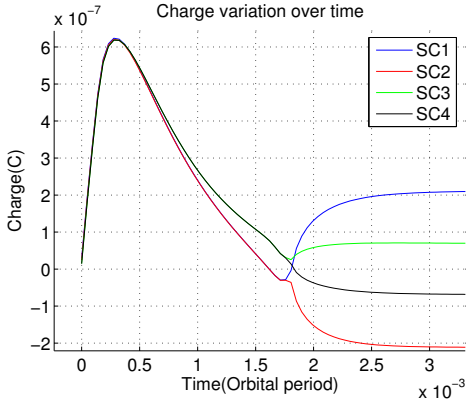

(b) Electrostatic 4 SC formation reconfiguration: SC charge histories at the beginning of the simulation.

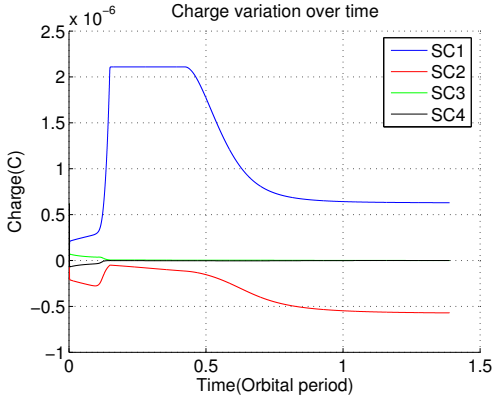

(c) Electrostatic 4 SC formation reconfiguration: SC charge histories.

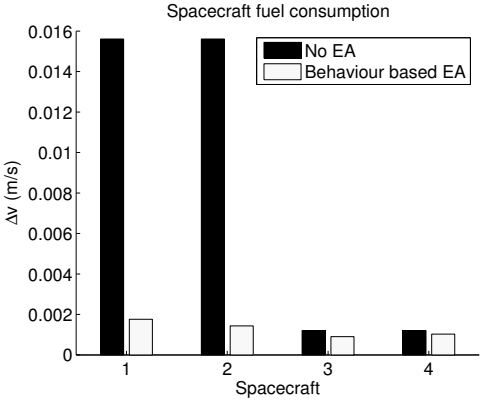

(d) Electrostatic 4 SC formation reconfiguration: SC Δv.

Figure 4.23: Electrostatic 4 SC formation reconfiguration.

The SC marked with blue and red line move along the Hill's x axis and therefore they have to counteract the gravitational and inertial force that otherwise will make them drift apart one from each other. For this reason, as shown in Figure 4.23(c), the blue and the red SC assume charges of opposite sign so that an attractive force is established between them. Moreover the other two SC, moving along the Hill's y axis, have a nearly zero value of the charge. At the end of the simulation both the position of the SC and the charges converge to a stationary solution. The SC acquire the final configuration and the charges assume the values such that the electrostatic force counteracts the inertial and gravity ones. In Figure 4.23(d) the bar diagram representing the Δv associated to the maneuver of all the SC is shown. For the reconfiguration maneuver described in this simulation the use of EA yields a saving in terms of Δv of 80% with respect to the case where no EA is mounted on board the satellites. Moreover from this chart is possible

to notice how the proposed approach is highly beneficial to redistribute also the fuel consumption between the SC belonging to the formation.

Six SC reconfiguration maneuver

In this section we consider again the problem of six SC reconfiguration maneuver already introduced in section 3.7 where the possibility of using compatible configurations as stand-by positions has been explored. In this simulation set up a swarm of six SC starts from an hexagonal formation in the $y-z$ plane and has to maneuver in order to acquire an octahedron configuration. For the proposed target formation the ES and EA are fully compatible in the sense introduced in section 3.2. The initial SC positions are given in Table 4.10 and the selected parameters for the ES navigation technique are displayed in Table 4.11.

	Position(m)	Charge (μC)
SC1	$[10.0, 0, 0]$	0.28
SC2	$[5, 0, 8.66]$	0.24
SC3	$[-5, 0, 8.66]$	0.14
SC4	$[-10.0, 0, 0]$	0.14
SC5	$[-5, 0, -8.66]$	0.28
SC6	$[5, 0, -8.66]$	0.24

Table 4.10: Initial conditions and parameters for a 6 SC reconfiguration maneuver.

$b(s^{-1})$	0.0011
$d(s^{-1})$	$2.0 \cdot 10^{-4}$
$c(s^{-1})$	$6.89 \cdot 10^{-7}$
$k_A(m)$	28
$k_D(m)$	30

Table 4.11: Simulation parameter for the 6 SC deployment maneuver.

In particular the parameters in Table 4.11 have been chosen following the guidelines described at the beginning of this section. The main objective is again to increase as much as possible the advantage of having the EA mounted on board. The trajectories followed by the SC during the reconfiguration maneuver are shown in Figure 4.24(a). These trajectories are different for the one displayed in Figure 3.10 showing how a

variation in the parameters displayed in Table 4.11 has a big influence on the planned trajectories. In Figure 4.24(b) the charge histories for the six SC are displayed.

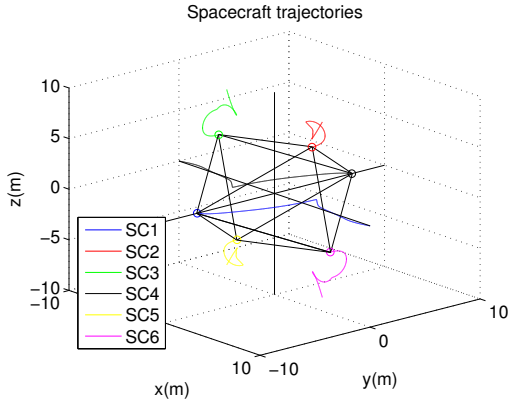

(a) Electrostatic 6 SC formation reconfiguration: SC trajectories.

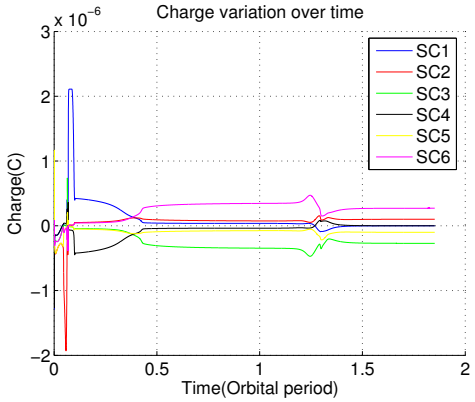

(b) Electrostatic 6 SC formation reconfiguration: SC charge histories.

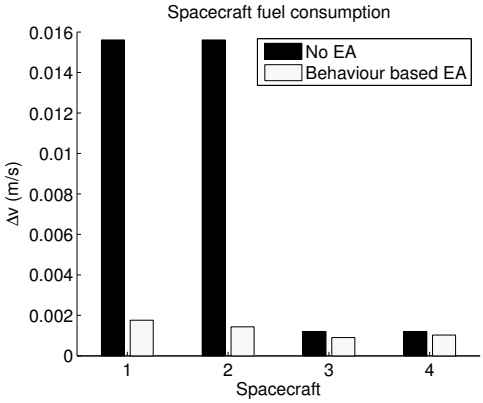

(c) Electrostatic 6 SC formation reconfiguration: SC Δv for EA optimized trajectories.

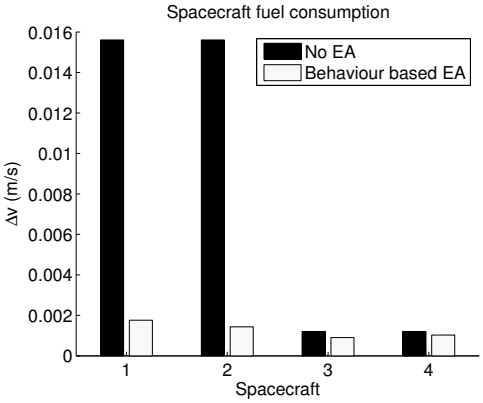

(d) Electrostatic 6 SC formation reconfiguration: SC Δv for EA non optimized trajectories.

Figure 4.24: Electrostatic 6 SC formation reconfiguration.

Moreover in Figure 4.24(c) and in Figure 4.24(d) a comparison of the Δv savings associated to the different maneuvers shown in Figure 4.24(a) and in Figure 3.10 are displayed. The Δv saving for the all formation reaches 65% when the parameters in Table 4.11 are carefully tuned whereas is just 9% when the path planning technique is not tuned for the introduction of the EA.

4.6 Conclusion

In this section it has been shown that it is possible to exploit the electrostatic interaction between the SC to increase the efficiency of the ES path planning technique also for

acquisition or reconfiguration maneuvers. In particular it has been demostrated that the electrostatic force can be used to reduce the fuel expenditure of the whole swarm associated to a given maneuver or to balance the fuel consumption between the SC in the formation. These results can be achieved relying on two different charging strategies here introduced namely charge product and behavior based charge control.
The charge product approach provides a good solution for the N-SC balanced consumption problem. On the other hand a computationally affordable solution for the minimum fuel problem can be obtained only for formations with a reduced number of SC. In particular for a two SC formation an analytical solution has been found that allows to compute the optimal charges of the formation in a fast and efficient way.
The behavior based charge control provides a solution for the minimum fuel consumption problem in the general case of an $N-$craft formation. The method developed has been tested under different possible simulations and it has shown good performances in terms of reduction of Δv of the whole swarm.

5 Conclusion and Recommendations

In this work the feasibility and applicability of the concept of Satellitron Satellites (SS), i.e. a swarm of satellites controlled by a hybrid thrusting electrostatic actuation system has been assessed.
To this end in the first part of this study it has been verified that the exploitation of inter-spacecraft electrostatic forces can be used to control the spacecraft relative positions in certain orbits. Then a scheme for a possible Hybrid Propulsion System has been developed following *ad hoc* defined requirements. The candidate propulsion system consists of the combined use of the Radiofrequency Ion Thruster engine (RIT) and an electron gun. The devices are operated simultaneously to control the spacecraft charge via the emission of two fluxes. Depending on the desired charge each device can work either to drive the spacecraft to the desired potential (charging current) or to counteract any overcharging natural effects (stabilising current). The approach has been chosen in a trade off of simplicity and applicability. With the application of Hydrogen as ion-delivering gas, the mass flow efficiency is in advance to conventional ion thrusting for most of the intended force range.
In the second phase of the work the electrostatic actuation concept has been integrated into a swarm navigation technique. The dynamics of such a system is highly coupled and nonlinear since any change in charging or position of each SC affects the forces acting upon every other satellite belonging to the swarm. For this reason a decentralized navigation scheme has been considered in this work in order to avoid a too complex inter SC comunication scheme. The Equilibrium Shaping navigation technique has been selected to control the maneuvers of the SS swarm for its high level of decentralization and robustness.
First the compatibility between the equilibrium shaping and the electrostatic actuation concepts has been addressed. With this intention the formations that can be acquired autonomously relying upon the equilibrium shaping path-planning technique and then maintained with high efficiency only relying upon the electrostatic actuation have been found. For these formations the integration between the two concepts is already satisfactory because the resulting system enjoys a high level of autonomy (ensured by the equilibrium shaping path planning technique), and is also fuel efficient. The results showed that there exist particular formations for which the two concepts are fully compatible both in a GEO environment and around the Earth-Sun L1 Lagrangian point.
Exploiting the results on the compatibility the electrostatic interaction between the SC has been considered to increase the efficiency of acquisition or reconfiguration maneu-

vers. In particular it has been demostrated that the electrostatic force can be used to reduce the fuel expenditure of the whole swarm associated to a given maneuver or to balance the fuel consumption between the SC in the formation. These results can be achieved relying on two different charging strategies here introduced namely charge product and behavior based charge control. The charge product approach can solve the N-SC balanced consumption problem but it fails in providing a computationally affordable solution for the minimum fuel problem.
On the other hand the behavior based charge control provides a solution for the minimum fuel consumption problem in the general case of an $N-$craft formation. This method allows a more efficient exploitation of the electrostatic actuation and requires a minimum amount of inter SC communication. The developed charging strategy has been tested under different possible simulations and it has shown good performances in terms of reduction of Δv of the whole swarm.
In the future the following investigations are recommended for the further development of the concepts introduced in this work:

- Development of a more detailed plasma-SC interaction model in order to have a better estimate of the worst case scenarios expecially for high SC voltages.
- Feasibility study of feedback charging control which requires the measurement of plasma environment parameters and spacecraft charge.
- Improvement of the charge product algorithm for the minimum fuel consumption problem.
- Stability analysis of the behaviour based charge control.
- Optimization of the equilibrium shaping technique for the combined use with the electrostatic actuation.

Bibliography

[1] J. Lawton, B. Young, and R. Beard. A decentralized approach to elementary formation maneuvers. In *IEEE International Conference on Robotics and Automation*, 2000.

[2] E. Frazzoli. Quasi-random algorithms for real-time spacecraft motion planning and coordination. *Acta-Astronautica*, 53(4-10):485–495, August-November 2003.

[3] EADS-Astrium. The apies mission. Feasibility Study A0/1-3846/02/NL/JA, ESA, 2004.

[4] S.A. Curtis, J. Mica, J. Nuth, G. Marr, M. Rilee, and M. Bath. Ants (autonomous nano-technology swarm): An artificial intelligence approach to asteroid belt resource exploration. In *51st International Astronautical Congress, Rio de Janeiro, Brazil*, 2000.

[5] M. Campbell. Planning algorithm for multiple satellite clusters. *Journal of Guidance Control and Dynamics*, 26(5):770–780, 2003.

[6] V. Gazi. Swarm aggregations using artificial potentials and sliding mode control. In *Proceedings of the 42nd IEEE Conference on Decision and Control*, 2003.

[7] M. Ayre, D. Izzo, and L. Pettazzi. Self assembly in space using behaviour based intelligent components. In *TAROS, Towards Autonomous Robotic Systems*, 2005.

[8] D. Izzo and L. Pettazzi. Equilibrium shaping: Distributed motion planning for satellite swarm. In *iSAIRAS, International Symposium of Artificial Intelligence, Robotics and Automation in Space*. ESA, 2005.

[9] L. Pettazzi, M. Ayre, and D. Izzo. Self-assembly in space using behaviour based intelligent component. Technical Report ACT-RPT-LP-6000-SASUBBIC05, ESA-ACT, 2004.

[10] K Sato. Dead-lock motion path planning using the laplace potential field. *Advanced Robotics*, 17(5):449–461, 1993.

[11] G. Schoner and M. Dose. A dynamics systems approach to task level systems integration used to plan and control autonomous vehicle motion. *Robotics and Autonomous Systems*, 10:253–267, 1992.

[12] L.B. King, G.G. Parker, and JH. Satwik, D. Chong. Spacecraft formation flying using inter-vehicle coulomb forces. Technical report, NIAC, 2002.

[13] L.B. King, G.G. Parker, and JH. Satwik, D. Chong. A study of inter-spacecraft coulomb forces and implications for formation flying. *Journal of Propulsion and Power*, 19(3):497–505, 2003.

[14] J. Berryman and H. Schaub. Static equilibrium configurations in geo coulomb spacecraft formations. In *15 ASS/AIAA Space Flight Mechanics Meeting*. ASS/AIAA, 2005.

[15] J. Berryman and H. Schaub. Analytical charge analysis for 2- and 3-craft coulomb formations. In *ASS/AIAA Astrodynamics Specialists Conference*. ASS/AIAA, 2005.

[16] H. Joe, H. Schaub, and G.G. Parker. Formation dynamics of coulomb satellites. In *6th International Conference on Dynamics and Control of Systems and Structures in Space*, 2004.

[17] H. Schaub and M. Kim. Differential orbit element constraints for coulomb satellite formations. In *ASS/AIAA Astrodynamics Specialists Conference*. ASS/AIAA, 2004.

[18] H. Schaub. Stabilization of satellite motion relative to a coulomb spacecraft formation. In *14 ASS/AIAA Space Flight Mechanics Meeting*. ASS/AIAA, 2004.

[19] Kenneth Moe, Mildred M. Moe, and Steven D. Wallace. Simple instruments for continous measyrement of trapped particles. In *ESA Symposium on Environment Modelling for Space-based Applications*, number SP-392, pages 87–92, 1996.

[20] A.C. Tribble. *The Space Environment*. Princeton University Press, 1995.

[21] C.K. Purvis, H.B. Garrett, A.C. Whittlesey, and N.J. Stevens. Design Guidelines for Assessing and Controlling Spacecraft Charging Effects, 1984. NASA Technical Paper 2361.

[22] R. Grard, K. Knott, and Pedersen. Spacecraft Charging Effects. *Space Science Reviews*, 34:289–304, 1983.

[23] Heidelberg Dust Research Group - Dust in the Earth's Magnetosphere, 2006.

[24] H.E Garret and S.E. DeForest. An analytical simulation of the Geosynchronous environment. *Journal of Spacecraft and Rockets*, 22.

[25] R.C. Olsen. A Threshold effect for Spacecraft charging. *Journal of Geophysical research*, 88:493–499, 1983.

[26] W. Riedler, K. Torkar, F. Rüdenauer, M. Fehringer, A. Pedersen, R. Schmidt, Gradr. R.J.L., H. Arends, B.T. Narheim, J. Troim, R. Torbert, R.C. Olsen, E. Whipple, R. Goldstein, N. Valavanoglou, and Hua Zhao. Active Spacecraft Potential Control. *Space Science Reviews*, 79:271–302, 1997.

[27] B.K Dichter, K.P Ray, M.S. Gussenhofen, E.G. Holeman, D.E. Delorey, and E.G. Mullen. High Voltage Frame and Differential Charging Observed on a Geosynchronous Spacecraft. In *6th Spacecraft Charging Technology Conference*, pages 329–333, September 2000.

[28] S.T. Lai. A critical overview on spacecraft charging mitigation methods. *IEEE Transactions on Plasma Science*, 31(6):1118–1124, 2003.

[29] K. Torkar, W. Riedler, C.P. Escoubet, M. Fehringer, R. Schmidt, R.J.L. Grard, H. Arends, F. Rüdenauer, W. Steiger, B.T. Narheim, K. Svenes, R Torbert, M.é Andre, A. Fazakerley, R. Goldstein, R.C. Olsen, A. Pedersen, E. Whipple, and H. Zhao. Active spacecraft potential control for Cluster - implementation and first results. *Annales Geophysicae*, 19:1289–1302, 2001.

[30] M. Schlotterer, D. Bindel, and S. Theil. Internal Report: Compilation of μ-Propulsion Thrusters for Attitude and Orbit Control of Spacecraft. Technical report, ZARM - Center of Applied Space Technology and Microgravity, 2006.

[31] D. Feili. Personal Conversation, May-July 2006.

[32] D. Feili, H.W. Loeb, K.H. Schartner, St. Weis, D. Kirmse, and B. K. Meyer. Testing of new μN-RITs at Giessen, 2003.

[33] ACT Homepage - Section of Dual Stage 4 Grid Ion Thruster, 2006.

[34] Kimball Physics Inc. Homepage, 2006.

[35] R.C. Olsen. Experiments In Charge Control at Geosynchronous Orbit - ATS-5 and ATS-6. *Journal of Spacecraft and Rockets*, 22.

[36] R. Storn and K. Price. Differential evolution- a simple and efficient adaptive scheme for global optimization over continuous spaces. Technical Report TR-95-012, ICSI-University of Berkley, March 1995.

[37] Bong Wie. *Space Vehicle Dynamics and Control*. AIAA Education Series. American Institue of Astronautics and Aeronautics, 1998.

[38] Arun Natarajan and Hanspeter Schaub. Linear dynamics and stability analysis of a coulomb tether formation. *Journal of Guidance, Control, and Dynamics*, 29(4):831–839, July–Aug. 2006.

[39] Shuquan Wang and Hanspeter Schaub. One-dimensional 3-craft coulomb structure control. In *7th International Conference on Dynamics and Control of Systems and Structures in Space*, pages 269–278, Greenwich, London, England, July 19–20 2006.

[40] Arun Natarajan, Hanspeter Schaub, and Gordon G. Parker. Reconfiguration of a 2-craft coulomb tether. In *AAS Space Flight Mechanics Meeting*, Tampa, FL, Jan. 22–26 2006. Paper No. AAS-06-229.

[41] Lyon B. King Gordon G. Parker and Hanspeter Schaub. Steered spacecraft deployment using interspacecraft coulomb forces. In *American Control Conference*, Minneapolis, Minnesota, June. 14–16 2006. Paper No. WeC10.5.

[42] R.H Battin. *An Introduction to the Mathematics and Methods of Astrodynamics*. AIAA Education Series, 1987.

[43] C.L. Lawson and R.J. Hanson. *Solving Least-Square Problems*. Prentice-Hall, 1974.